1999

Durability and mode-I fracture of fiber-reinforced plastic (FRP)/wood interface bond

Brent Stephen Trimble
West Virginia University

Durability and Mode-I Fracture of Fiber-Reinforced Plastic (FRP)/Wood Interface Bond

Brent Stephen Trimble

Thesis
submitted to the
College of Engineering and Mineral Resources
at West Virginia University
in partial fulfillment of the requirements
for the degree of

Master of Science
in
Civil and Environmental Engineering

Dr. Julio F. Davalos, Ph.D., Chair
Dr. Pizhong Qiao, Ph.D., P.E., Co-Chair
Dr. Karl Barth, Ph.D.

Morgantown, West Virginia
1999

Keywords: Durability, Mode-I Fracture, FRP Composite, Interface Bond, Wood, Adhesive, Moisture Effect

ABSTRACT

Durability and Mode-I Fracture of Fiber-Reinforced Plastic (FRP)/Wood Interface Bond

Brent Stephen Trimble, BSCE

Advisor: Dr. Julio F. Davalos, and Co-Advisor: Dr. Pizhong Qiao

Fiber-reinforced plastic (FRP) composites are being used for reinforcement of wood, concrete, and steel. Current research on wood reinforcement has focused on the use of fiber-reinforced strips or fabrics bonded to wood members. Although significant increases in stiffness and strength have been achieved by this reinforcing technique, there is a concern about the reliable performance of the FRP-wood interface bond, which can be susceptible to delamination. An inadequate interface bond strength and integrity can lead to premature failure of a reinforced wood member.

The objective of this study is to develop a qualification program to evaluate the service performance and fracture of composite/wood bonded interfaces. The proposed method is used for two types of FRP wood interface: FRP strips (plates) bonded to wood (used commercially for glulam timber beams) and wood cores wrapped with FRP by filament winding (being investigated for reinforced railroad wood crossties and utility wood poles). First, the service performance and durability of FRP-wood interface bond is evaluated using a modified ASTM delamination test. Second, the apparent shear strengths of interface bond under both dry and wet conditions are obtained from modified ASTM block shear tests. Finally, a simplified design of an innovative contoured double cantilever beam (CDCB) specimen is developed, and this specimen is used to evaluate Mode-I fracture of interface bonds; interface fracture toughness data are experimentally obtained for dry, wet and 3-cycle aging conditions.

This study presents a combined experimental and analytical program to evaluate the potential in-service performance and the fracture toughness of FRP-wood interface bonds. It is shown that the modified ASTM D2559 standard test can be effectively used to study the effect of several parameters. Then for the best combination of parameters, the average interface shear strengths can be obtained from block-shear tests of ASTM D905 for hybrid laminates under dry and wet conditions. The contoured double cantilever beam (CDCB) specimen proposed in this study is an efficient tool to evaluate mode-I fracture toughness of hybrid interfaces, such as FRP-wood, and the fracture toughness data obtained can be used to predict whether or not a bonded interface will delaminate under general moisture, temperature, and service loads conditions. The guidelines presented in this study are useful for designing bonded joints, evaluating the in-service durability of bonded interfaces, and obtaining fracture toughness data for FRP-wood material combinations.

ACKNOWLEDGMENTS

I would like to express my gratitude to my advisor Dr. Julio F. Davalos, for his guidance and inspiration towards the completion of this research work. My Co-Advisor, Dr. Pizhong Qiao for his time, effort, and dedication with the work performed in this research. Dr. Karl Barth for his constructive comments and review. Thanks is also due to Dr. Elemer M. Lang, Dr. Ben E. Dawson-Andoh, and Jeff Slahor for their cooperation and involvement with the experimental work performed in this research.

The valuable help provided by laboratory Technicians; Dave Turner, Dana Humberson, Paul Frum, Frank Amons, and Paul Ludrosky was vital to the completion of this research.

I would like to thank Kira Kaleps of Industrial Fiberglass Specialties, Inc. , and Raymond Bender of Indspec Chemicals for their help and assistance with this research along with the production of materials.

The contributions of Truss-Joist McMillan and Creative Pultrusions are acknowledged; these industries provided materials used in this study as well as technical advice.

I would like to recognize the funding and sponsorship of this research provided by the USDA/CSREES/NRICGP program and West Virginia University.

A special thanks to my Family and Friends for all of their support, advice, and STRESS RELIEF!

TABLE OF CONTENTS

TITLE PAGE i
ABSTRACT ii
ACKNOWLEDGMENTS iii
TABLE OF CONTENTS iv
LIST OF TABLES x
LIST OF FIGURES xiv

CHAPTER 1: INTRODUCTION 1
1.1 Introduction 1
1.2 Objective 2
1.3 Scope of Study 2
1.4 Literature Review 4
1.4.1 Durability studies 4
1.4.1.1 Introduction 4
1.4.1.2 Previous work on durability tests 5
1.4.1.3 Coupling agents used to promote bonding 10
1.4.2 Block-Shear tests 11
1.4.3 Mode-I fracture tests 14

CHAPTER 2: DELAMINATION OF INTERFACE BOND 19
2.1 Introduction 19
2.2 Materials 19
2.2.1 Red Maple (Acer Rubrum) 22
2.2.2 Pultruded Phenolic FRP Laminate 22
2.2.3 Filament Wound Epoxy FRP Composite 23
2.2.4 Coupling agents 24
2.2.5 Adhesives 26

2.3 Manufacturing of Delamination Specimens ……. 26
2.3.1 Phenolic FRP-Wood ……..…. 26
2.3.2 Epoxy FRP-Wood ……. 27
2.4 Modified ASTM D 2559 Delamination Test ……... 27
2.5 Number of Test Samples …….. 29
2.5.1 Phenolic FRP-Wood …….. 29
2.5.2 Epoxy FRP-Wood ……. 30
2.6 Test Results …….. 30
2.6.1 Phenolic FRP-Wood …….. 30
2.6.1.1 Effect of HMR coupling ……. 30
2.6.1.2 Effect of clamping pressure …… 32
2.6.1.3 Effect of assembly time …….. 33
2.6.2 Epoxy FRP-Wood ……. 34
2.6.2.1 Effect of HMR/RF coupling agents ……... 34
2.6.2.2 Effect of confinement ……. 35
2.7 Conclusions …….. 36
2.7.1 Phenolic FRP-Wood interface ……... 36
2.7.2 Epoxy FRP-Wood interface …….. 37

CHAPTER 3: SHEAR STRENGTH OF INTERFACE BOND …… 38
3.1 Introduction …….. 38
3.2 Materials ……... 38
3.3 Manufacturing of Block-Shear Test Samples …….. 41
3.3.1 Phenolic FRP-Wood …….. 41
3.3.2 Epoxy FRP-Wood ……. 42
3.4 Experimental Design and Testing …… 43
3.5 Test Results …….. 44
3.5.1 Phenolic FRP-Wood …….. 44
3.5.2 Epoxy FRP-Wood ……. 51
3.6 Discussion of Test Results ……... 59
3.6.1 Phenolic FRP-Wood …….. 59

3.6.2 Epoxy FRP-Wood ……. 60
3.7 Conclusions …….. 61
3.7.1 Phenolic FRP-Wood …….. 61
3.7.2 Epoxy FRP-Wood ……. 62

CHAPTER 4: DESIGN APPROACH FOR CDCB SPECIMENS …… 63
4.1 Introduction …….. 63
4.2 Design of CDCB Specimens by the Rayleigh-Ritz Method ……..... 66
4.3 Simplified Design Procedure and Parametric Study ……..... 74
4.3.1 Two-Step design procedure ……... 74
4.3.2 Parametric study …… 75

CHAPTER5: FRACTURE TOUGHNESS OF DRY/WET FRP-WOOD BONDED INTERFACE …… 84
5.1 Introduction …….. 84
5.2 Materials ……... 85
5.2.1 Wood materials ……. 85
5.2.2 FRP materials …… 86
5.2.3 Material characterization ……... 86
5.3 Contour Shapes of the Designed CDCB Specimens ……..... 88
5.3.1 Wood-Wood …….. 89
5.3.2 Phenolic FRP-Phenolic FRP ……..… 90
5.3.3 Epoxy FRP-Wood ……..… 91
5.3.4 Compliance rate change of CDCB specimens …….. 92
5.4 Experimental Compliance Calibration of the CDCB Specimens ……. 92
5.5 Finite Element Modeling of the CDCB Specimens ……..… 99
5.6 Experimental Evaluation of Fracture Toughness ……... 101
5.6.1 Material and specimen preparation ……. 101
5.6.1.1 Wood-Wood specimens ……... 102
5.6.1.2 Phenolic FRP-Wood specimens ……...… 103
5.6.1.3 Epoxy FRP-Wood specimens ……... 104

5.6.2 Testing procedure ……... 105
5.6.3 Fracture Failure Mode: Pattern of crack initiation and arrest…….. 105
5.6.4 Mode-I fracture toughness for Wood-Wood bonded interface ...… 107
5.6.4.1 Wood-wood dry condition ……...… 107
5.6.4.2 Wood-wood wet condition ……... 110
5.6.4.3 Discussion for wood-wood samples ……. 114
Critical leads and Fracture Toughness ……. 114
Brittleness Index ……...… 114
5.6.5 Mode-I fracture toughness for Phenolic FRP-Wood
bonded interface …….. 116
5.6.5.1 Phenolic FRP-wood dry condition ……... 116
5.6.5.2 Phenolic FRP-wood wet condition ……... 122
5.6.5.3 Discussion for Phenolic FRP-wood samples ……... 127
5.6.6 Mode-I fracture toughness for Epoxy FRP-Wood
bonded interface …….. 128
5.6.6.1 Epoxy FRP-wood dry condition ……... 128
5.6.6.1.1 HMR coupling agent for dry condition ……. 128
5.6.6.1.2 RF coupling agent for dry condition ……. 132
5.6.6.1.3 Discussion for Epoxy FRP-wood dry samples .. 135
5.6.6.2 Epoxy FRP-wood wet condition …….. 136
5.6.6.2.1 HMR coupling agent for wet condition ……. 136
5.6.6.2.2 RF coupling agent for wet condition ……. 142
5.6.6.2.3 Discussion for Epoxy FRP-wood wet samples . 147
5.6.7 Review and comparison of critical loads and fracture
toughness ……..… 148
5.6.8 Fracture toughness predictions by the
Jacobian Derivative Method (JDM) …… 149
5.7 Conclusions …… 149

CHAPTER 6: FRACTURE TOUGHNESS OF AGED PHENOLIC FRP-WOOD
BONDED INTERFACE ……... 151

6.1 Introduction …… 151
6.2 Materials ……. 152
6.2.1 Wood materials ……... 152
6.2.2 FRP materials …….. 152
6.2.3 Material characterization ……. 152
6.2.3.1 Testing of small coupon samples ……. 153
6.2.3.2 Testing of samples cut from CDCB specimens ……... 154
6.3 Contour Shapes of the Designed CDCB Specimens …….. 155
6.4 Experimental Evaluation of Fracture Toughness ……... 158
6.4.1 Testing procedure …… 158
6.4.2 Mode-I fracture toughness for Phenolic FRP-wood aged bonded interface …….. 159
6.4.2.1 Cycle 1 conditioning …… 159
6.4.2.2 Cycle 2 conditioning …… 162
6.4.2.3 Cycle 3 conditioning …… 165
6.4.2.4 Discussion for Phenolic FRP-wood aged samples ……... 169
6.5 Conclusions …… 170

CHAPTER 7: CONCLUSIONS AND RECOMMENDATIONS ……... 172
7.1 Importance of FRP-Wood Bonded Interface Performance …… 172
7.2 Guidelines for FRP-Wood Bonded Interface Performance Evaluations …… 172
7.3 Overall Conclusions of this Research …… 174
7.4 Specific Findings of this Research ……. 174
7.4.1 Results of each test method ……. 174
7.4.1.1 Delamination tests …… 174
7.4.1.2 Block-Shear tests …….. 175
7.4.1.3 Fracture mechanics tests ……... 176
7.4.2 Correlation of test methods ……. 177
7.5 Recommendations for Future Work ……... 178

REFERENCES ……. 180
APPENDIX A …….. 184
APPENDIX B …….. 188
VITA …… 192

LIST OF TABLES

Table 2.1 Delamination of Phenolic FRP-Wood and wood-wood bonded interface with PRF adhesive (pressure: p = 200 psi; Open/Closed assembly time: t = 5/30 min) …….. 31

Table 2.2 Delamination of Phenolic FRP-Wood and wood-wood bonded interface with RF adhesive (pressure: p = 180 psi; Open/Closed assembly time: t = 5/30 min) …….. 32

Table 2.3 Delamination of Phenolic FRP-wood bondline under three pressure conditions (with RF adhesive and without HMR primer) …….. 33

Table 2.4 Delamination of Phenolic FRP-wood bondline under Open/Closed assembly times (with RF adhesive and without HMR primer) …….. 34

Table 2.5 Delamination of Epoxy FRP-wood bonded interface by ASTM D 2559 .. 35

Table 2.6 Delamination of Epoxy FRP-wood confined samples by ASTM D 2559 . 36

Table 3.1 Shear strengths and percent material failures for wood-wood samples at 12% MC …….. 45

Table 3.2 Shear strengths and percent material failures for Phenolic FRP-wood samples at 12% MC …… 46

Table 3.3 Shear strengths and percent material failures for wood-wood samples at saturation MC (more than 100% MC) …… 47

Table 3.4 Shear strengths and percent material failures for Phenolic FRP-wood samples at saturation MC (more than 100% MC) …….. 48

Table 3.5 Shear strength and percent material failure of wood-wood and Phenolic FRP-wood interface block-shear specimen ……. 49

Table 3.6 Moisture effects on mean shear strength for wood-wood and Phenolic FRP-wood specimens …….. 50

Table 3.7 Moisture effects on percent material failure for wood-wood and Phenolic FRP-wood specimens …….. 51
Table 3.8 Shear strengths and percent material failures for Epoxy FRP-wood/HMR samples at 12% MC …… 52
Table 3.9 Shear strengths and percent material failures for Epoxy FRP-wood/RF samples at 12% MC …… 53
Table 3.10 Shear strengths and percent material failures for Epoxy FRP-wood/HMR samples at saturation MC (more than 100% MC) …….. 54
Table 3.11 Shear strengths and percent material failures for Epoxy FRP-wood/RF samples at saturation MC (more than 100% MC) …….. 55
Table 3.12 Shear strength and percent material failure of Epoxy FRP-wood interface block-shear specimens …… 56
Table 3.13 Moisture effects on shear strength for Epoxy FRP-wood specimens …… 57
Table 3.14 Coupling agents (primer) effects on shear strength for Epoxy FRP-wood specimens ……... 57
Table 3.15 Moisture effects on percent material failure for Epoxy FRP-wood specimens ……... 58
Table 3.16 Coupling agents (primer) effects on percent material failure for Epoxy FRP-wood specimens ……. 59

Table 4.1 Linearlized slopes with constant *dC/da* ……. 82
Table 4.2 Linearlized *dC/da* for constant slope, *k* ……. 83

Table 5.1 Material properties of Red Maple under dry and wet conditions ……..… 87
Table 5.2 Material properties of LVL under dry and wet conditions ……. 87
Table 5.3 Material properties of Phenolic FRP ……..… 87
Table 5.4 Material properties of Epoxy FRP ……..… 87
Table 5.5 Compliance rate change of linear tapered specimens …… 92
Table 5.6 Crack loads of CDCB specimens with wood-wood/dry interface …….... 109
Table 5.7 Crack loads of CDCB specimens with wood-wood/wet interface …..… 113
Table 5.8 Critical initiation and arrest loads for wood-wood interface bonds ……. 115

Table 5.9 Fracture toughness of wood-wood interface bonds ……..… 115
Table 5.10 Crack loads of CDCB specimens with Phenolic FRP-wood/dry interface ……...119
Table 5.11 Crack loads of CDCB specimens with Phenolic FRP-wood/wet interface …….. 125
Table 5.12 Critical initiation and arrest loads for Phenolic FRP-wood interface bonds …… 127
Table 5.13 Fracture toughness of Phenolic FRP-wood interface bonds ……...… 127
Table 5.14 Crack loads of CDCB specimens with Epoxy FRP-wood/HMR/Dry interface …… 130
Table 5.15 Crack loads of CDCB specimens with Epoxy FRP-wood/RF/Dry interface …… 134
Table 5.16 Critical initiation and arrest loads for Epoxy FRP-wood/Dry interface bonds …… 135
Table 5.17 Fracture toughness of Epoxy FRP-wood/Dry interface bonds ……. 135
Table 5.18 Crack loads of CDCB specimens with Epoxy FRP-wood/HMR/Wet interface …… 138
Table 5.19 Crack loads of CDCB specimens with Epoxy FRP-wood/RF/Wet interface …… 144
Table 5.20 Critical initiation and arrest loads for Epoxy FRP-wood/Wet interface bonds …… 147
Table 5.21 Fracture toughness of Epoxy FRP-wood/Wet interface bonds …… 147
Table 5.22 Comparison of critical initiation and arrest loads …… 148
Table 5.23 Comparison of fracture toughness …… 148

Table 6.1 Material properties of Red Maple under cyclic conditioning …….. 154
Table 6.2 Material properties of LVL under cyclic conditioning …… 154
Table 6.3 Material properties of Phenolic FRP under normal conditions …… 154
Table 6.4 Compliance rate change of linear tapered specimens ……..… 156
Table 6.5 Crack loads of CDCB specimens with Cycle 1 aged Phenolic FRP-wood interface …… 161

Table 6.6 Crack loads of CDCB specimens with Cycle 2 aged Phenolic FRP-wood interface …… 164
Table 6.7 Crack loads of CDCB specimens with Cycle 3 aged Phenolic FRP-wood interface …… 167
Table 6.8 Critical initiation and arrest loads for aged Phenolic FRP-wood interface bonds ……..… 169
Table 6.9 Fracture toughness of aged Phenolic FRP-wood interface bonds …… 170

LIST OF FIGURES

Figure 2.1 Experimental program for Phenolic FRP-wood ASTM D 2559 delamination tests 20

Figure 2.2 Experimental program for Epoxy FRP-wood ASTM D 2559 delamination tests 21

Figure 2.3 Manufacturing of Phenolic FRP-wood delamination specimens 22

Figure 2.4 Lay-up of pultruded Phenolic FRP laminate 23

Figure 2.5 Manufacturing of Epoxy FRP-wood sample by filament winding process 25

Figure 2.6 Epoxy FRP-wood and wood-wood samples for ASTM D 2559 delamination tests 28

Figure 3.1 Experimental program for Phenolic FRP-wood ASTM D 905 standard tests 40

Figure 3.2 Experimental program for Epoxy FRP-wood ASTM D 905 standard tests 40

Figure 3.3 Modified ASTM D 905 Phenolic FRP-wood specimen for block-shear test..... 42

Figure 3.4 Modified ASTM D 905 Epoxy FRP-wood specimen for block-shear test 43

Figure 3.5 Shear strength for wood-wood and Phenolic FRP-wood specimens 49

Figure 3.6 Material failure for wood-wood and Phenolic FRP-wood specimens 50

Figure 3.7 Shear strength comparison for Epoxy FRP-wood specimens 56

Figure 3.8 Material failure comparison for Epoxy FRP-wood specimens 58

Figure 4.1 Geometric parameters of the contour of the CDCB specimen 65

Figure 4.2 CDCB actual and transformed cross sections 69

Figure 4.3 Slope vs Crack length (b = 0.750 in) …….. 76
Figure 4.4 Slope vs Crack length (b = 1.000 in) …….. 77
Figure 4.5 Slope vs Crack length (b = 1.250 in) …….. 78
Figure 4.6 *dC/da* vs Crack length (b = 0.750 in) ……. 79
Figure 4.7 *dC/da* vs Crack length (b = 1.000 in) ……. 80
Figure 4.8 *dC/da* vs Crack length (b = 1.250 in) ……..…… 81

Figure 5.1 Lay-up of Linear Veneered Lumber (LVL) ……... 85
Figure 5.2 Contour shapes for CDCB wood-wood specimens …… 89
Figure 5.3 Contour shapes for CDCB Phenolic FRP-Phenolic FRP specimens ……. 90
Figure 5.4 Contour shapes for CDCB Epoxy FRP-wood specimens …….. 91
Figure 5.5 Experimental set-up for calibration and Mode-I fracture tests …….. 94
Figure 5.6 Compliance vs crack length for wood-wood/Dry specimen …….. 95
Figure 5.7 Compliance vs crack length for wood-wood/Wet specimen …….. 96
Figure 5.8 Compliance vs crack length for Phenolic FRP-Phenolic FRP/Dry specimen ……..… 97
Figure 5.9 Compliance vs crack length for Phenolic FRP-Phenolic FRP/Wet specimen ……. 98
Figure 5.10 Finite element modeling and displacement contour of half of CDCB specimen ……...… 100
Figure 5.11 Contour shapes for CDCB wood-wood specimens for Mode-I fracture tests ……..… 102
Figure 5.12 Contour shapes for CDCB Phenolic FRP-wood specimens for Mode-I fracture tests ……. 103
Figure 5.13 Contour shapes for CDCB Epoxy FRP-wood specimens for Mode-I fracture tests ……. 104
Figure 5.14 Typical crack pattern for contoured double-cantilever beam test …… 106
Figure 5.15 Fracture of wood-wood/Dry interface for CDCB specimen …… 108
Figure 5.16 Load vs crack-opening displacement for specimen WWD1 …… 108
Figure 5.17 Fracture of wood-wood/Wet CDCB specimen …… 111
Figure 5.18 Fractured surface of wood-wood/Wet specimen …….. 111

Figure 5.19 Load vs crack-opening displacement for specimen WWW7 ……... 112
Figure 5.20 Fracture test of Phenolic FRP-wood/Dry interface (Specimen WFD3) ... 117
Figure 5.21 Fracture surfaces of Phenolic FRP-wood/Dry specimen (WFD3) ……... 117
Figure 5.22 A close-up observation of fiber bridging along the interface (WFD6) … 118
Figure 5.23 Load vs crack-opening displacement for specimen WFD4 ……. 118
Figure 5.24 Fracture test of Phenolic FRP-wood/Wet (specimen WFW2) ……..… 123
Figure 5.25 Fractured faces of Phenolic FRP-wood/Wet specimen (WFW2) …...… 123
Figure 5.26 A close-up look of fiber bridging in Phenolic FRP-wood/Wet specimen (WFW2) ……...… 124
Figure 5.27 Load vs crack-opening displacement for specimen WFW2 ……. 124
Figure 5.28 Fractured faces of Epoxy FRP-wood/HMR/Dry specimen (HMR-DRY 7) ……..… 129
Figure 5.29 Load vs crack-opening displacement for specimen (HMR-DRY 4) …… 129
Figure 5.30 Fractured faces of Epoxy FRP-wood/RF/Dry specimen (RF-DRY 1) … 133
Figure 5.31 Load vs crack-opening displacement for specimen (RF-DRY 7) …… 133
Figure 5.32 Fractured faces of Epoxy FRP-wood/HMR/Wet specimen (HMR-WET 7) ……. 137
Figure 5.33 Load vs crack-opening displacement for specimen (HMR-WET 4) …… 137
Figure 5.34 Fractured faces of Epoxy FRP-wood/RF/Wet specimen (RF-WET 2) … 143
Figure 5.35 Load vs crack-opening displacement for specimen (RF-WET 7) …… 143

Figure 6.1 Contour shapes for CDCB Phenolic FRP-wood aged specimens …… 157
Figure 6.2 Fractured faces of Phenolic FRP-wood cycle 1 specimen (Day 1-2) ….. 160
Figure 6.3 Load vs crack-opening displacement for specimen (Day 1-7) ……. 160
Figure 6.4 Fractured faces of Phenolic FRP-wood cycle 2 specimen (Day 2-2) ….. 163
Figure 6.5 Load vs crack-opening displacement for specimen (Day 2-4) ……. 163
Figure 6.6 Fractured faces of Phenolic FRP-wood cycle 3 specimen (Day 3-1) ….. 166
Figure 6.7 Load vs crack-opening displacement for specimen (Day 3-4) ……. 166

CHAPTER 1

INTRODUCTION

1.1 Introduction

Fiber-reinforced plastic (FRP) composites are being used for reinforcement of wood, concrete, and steel. Current research on wood reinforcement has focused on the use of fiber-reinforced plastic (FRP) composites bonded to wood members. Although significant increases in stiffness and strength have been achieved by this reinforcing technique, there is a concern about the reliable performance of the wood-FRP interface bond, which can be susceptible to delamination. Inadequate interface bond strength and integrity can lead to delamination and premature failure of a hybrid wood-FRP composite. It has been shown that delamination of bonded interfaces can be described by fracture mechanics models (Davalos, Raman and Qiao 1997), and although three distinct modes of fracture can be defined, an interface bond is generally less resistant to crack extension (delamination) under the action of normal load than under shear load; therefore, Mode-I (opening mode) fracture is often more critical than other modes of fracture. In this study, a newly developed Contoured Double Cantilever Beam (CDCB) specimen (Davalos, Raman and Qiao 1997) is used to evaluate the fracture toughness of wood-FRP bonded interfaces. The manufacturing of CDCB specimens is a difficult and time-consuming effort, and therefore, preliminary tests to establish the performance of the bonded interfaces are first conducted following ASTM D 2559 and D 905 standards.

1.2 Objective

The objective of this study is to characterize the service performance of the interface bond by modified standard tests and a fracture mechanics approach to provide fracture toughness data for bonded wood-composite interfaces. The proposed method is used for two types of reinforcement: FRP plates bonded to wood (used commercially for glulam timber beams) and wood cores wrapped with FRP by filament winding (used for proposed hybrid railroad crossties and utility poles). Modified ASTM standard D 2559 and D 905 tests are used to study the performance of the bond under moisture and/or mechanical loads, and then CDCB specimens are tested to evaluate the fracture toughness of the bonded wood-composite interfaces. The present qualification approach can be extended for evaluation of other materials, such as concrete and steel.

1.3 Scope of Study

In this study, the following tasks are conducted: First, the performance of the adhesive interface is evaluated by modified standard ASTM D 2559 and D 905 tests. The potential in-service delamination is evaluated by a 3-cycle test (modified ASTM D 2559) of repeated wetting and drying, and the wet and dry interface strengths are evaluated through block-shear tests (modified ASTM D 905). Several key parameters are studied, such as coupling agents (primers) to promote bonding, surface texture of composite, open/closed assembly time, and clamping pressure. Next, a simplified and modified Rayleigh-Ritz method is developed and used to design a Contoured Double Cantilevered Beam (CDCB) specimen. Using the CDCB specimen under Mode-I fracture, fracture toughness data are obtained for dry, wet and each cycle of the simulated three-cycle aging testing of ASTM D 2559.

The performance of bonded interfaces is evaluated and the fracture toughness of these bonded interfaces under dry, wet and each cycle of the simulated aging cycles are evaluated. The details of this research include:

- Study on bonding parameters for optimum performance under delamination by ASTM D 2559 tests (Chapter 2);
- Measurement of average dry and wet bond shear strength and percent material failure by ASTM D 905 block-shear tests (Chapter 3);
- Simplified design approach for CDCB specimens by the Rayleigh-Ritz method (Chapter 4);
- Material characterization of wood and FRP composites (Chapter 5);
- Design of CDCB specimens for dry and wet wood-wood and FRP-wood interfaces by the Rayleigh-Ritz method (Chapter 5);
- Compliance calibration of CDCB specimens (Chapter 5);
- Finite element modeling of CDCB specimens (Chapter 5);
- Testing of CDCB specimens and evaluation of fracture toughness for dry and wet conditions designed by the Rayleigh-Ritz method (Chapter 5);
- Design of CDCB specimens for each cycle of the simulated aging cyclic conditions for FRP-wood bonded interfaces designed by the Rayleigh-Ritz method (Chapter 6);
- Testing of CDCB specimens and evaluation of fracture toughness for each cycle of aging cyclic conditions (Chapter 6).

Based on the research performed in this study, recommendations and guidelines for wood-FRP bonded interface evaluations are provided.

1.4 Literature Review

Corresponding to the scope of this study, a literature review on current studies of durability, block-shear, and fracture tests is presented in this section.

1.4.1 Durability studies

1.4.1.1 Introduction

One of the most noticeable problems with adhesive bonding is that of durability. The service life of a finished product must always be considered; therefore, after the mechanical and physical properties of an adhesive are determined, the environmental factor usually draws the second wave of concern (Cagle 1968). Predicting the performance of an adhesive bond cannot be accomplished with any great degree of accuracy until it has been tested through simulated service conditions. There are several exposure conditions that are available to help in determining the durability of an adhesive bond. These include: temperature effects, moisture exposure, salt spray, fluid immersion, and general weathering. While each of these conditions can measure some aspects of bond interface performance, it is difficult to predict the long term performance. Therefore, it is common to modify an existing standard test to help match the weathering that the structure will undergo throughout its expected service-life. Upon review of the available standard tests, it must be decided on if each standard is evaluating the adhesive itself or of the complete adhesive bonded product.

Durability tests for adhesive bonding are available for the bonding of many different products. These include such adherends as concrete, timber, metals and fiber reinforced plastics (FRP).

1.4.1.2 Previous work on durability tests

The following is a review of studies that have been conducted by researchers on the durability of adhesive bonds:

Dewimille and Bunsell (1983) studied the effect of accelerated aging on glass fiber-reinforced epoxy resins. E-glass fiber-reinforced epoxy resin pultruded bars, of diameter 32 mm, were aged in distilled water under a wide range of temperatures. The water immersion tests were conducted within a temperature range from 22°C to 100°C. The immersion times varied from several days in boiling water to three years in water at ambient temperature. Following the immersion tests, the samples were then checked for the development of damage and overall specimen condition. This was accomplished by the use of a scanning electron microscope and mechanical torsion tests. The authors concluded that accelerated aging tests on composites can produce a wide variety of damage and degradation mechanisms. It was observed that the use of higher temperatures to speed up the degradation process, does not give the same results as that of longer tests at ambient temperatures. Therefore, when developing an accelerated aging test, the conditioning should be done to parallel the actual conditions that will be seen in service. Therefore, great care should be exercised when developing an accelerated aging test.

Russell and Street (1985) researched mixed-mode delamination fracture of unidirectional graphite/epoxy, under the affect of moisture and temperature. Four types of unidirectional composite fracture specimens were adopted to measure the combined Mode-I/Mode-II interlaminar fracture. They included: Double Cantilever Beam, Cracked Lap Shear, End-Notched Flexural, and Mixed-Mode Flexural Specimens. The fracture specimens were tested over a temperature range of -50°C to 100°C for both dry and water saturated conditions. Concluding the testing, it was found that the delamination fracture energy G_C was more sensitive to temperature than to moisture.

Chajes et al. (1995) evaluated the durability of concrete beams reinforced with external composite fabrics. The concrete beams were immersed in a calcium chloride solution and subjected to two different environmental tests: under freeze/thaw condition and under wet/dry condition. The freeze/thaw conditioning followed the general procedures of ASTM C 672-84 (1990). The cycles consisted of immersing the samples in a calcium chloride solution and exposing them to 16 hours in a freezer at -17°C followed by eight hours at room temperature. Twelve of the samples underwent 50 cycles, whereas another twelve underwent 100 cycles. The wet/dry conditioning samples were also immersed into a calcium chloride solution. They then were bathed for 16 hours and then dried at room temperature for eight hours. As in the freeze/thaw cycles, twelve samples were subjected to 50 cycles and twelve samples were subjected to 100 cycles. After conditioning, the samples were loaded to failure in four-point bending. The tests showed that chloride exposure in both of the conditioning environments caused degradation of the beam strength. The wet/dry conditioning was noted to be more severe than the freeze/thaw cycles.

Prokopski (1996) researched the influence of moisture content on the fracture toughness of pine and common oak. Both species of wood were tested in Mode-I fracture at moisture contents of 6%, 9%, and 12%, respectively. The testing apparatus used was in accordance with ASTM E 399-83 (1983). The Stress Intensity Factor, K_{IC}, was found for each species at each moisture content. The values of K_{IC} [$MN/m^{3/2}$] for Pine at 6, 9, and 12% MC are 3,469, 2,569, and 2,306 respectively; for Common Oak, they are 3,498, 4,649, and 5,381. It is observed that the K_{IC} of Pine decreased with an increase in the moisture content; whereas, the K_{IC} of Common Oak increased with an increase in moisture content.

Sellers and Miller (1997) conducted cyclic delamination tests on three different adhesive systems for chromated copper arsenate (CCA) treated lumber. The adhesives consisted of a commercial resorcinol formaldehyde adhesive, a commercial emulsion-isocyanate adhesive and a laboratory modified resorcinol adhesive mixture. CCA southern pine lumber was used to produce glulam beams of which delamination test billets were

produced. The glulam billets were cut into specimens for the cyclic delamination test (T-110) according to the Inspection Manual AITC 200-92 (1996) for Structural Glued Laminated Timber. The delamination tests were repeated for three cycles instead of the normal one or two cycles. The three cycles included: (I) water submerged vacuum/pressure (25 in Hg for 30 minutes/75 psi for 2 hours), (II) dry for approximately 10 hours at 160°F, (III) repeat the above two cycle steps. The three adhesive types all failed differently throughout the delamination tests. According to AITC T-110, the maximum delamination allowed is 5 and 10 percent of the glueline after one and two cycles, respectively. Of the three adhesive systems, the RF passed all three cycles with a delamination of less than 5 percent. The modified RF passed two of the three with a failure of 7 percent after the third cycle. The emulsion-isocyanate adhesive failed all three cycles with respective bondline delamination of 5.9, 7.9 and 11.7 percent. Future studies were proposed with the ASTM D 2559 (1992) cyclic delamination test for a more rigorous testing procedure for evaluating the wet use of adhesives.

Devalapura et al. (1998) studied the performance of glass fiber reinforced plastics (GFRP) using accelerated test methods. This was a three phase project with phase I consisting of testing of FRP rods made of different glass fibers exposed to acidic environments with elevated temperatures and stresses. Phase II consisted of similar testing in alkaline environments which was used to simulate GFRP exposure to concrete. Phase III was conducted to correlate accelerated testing to real-time application conditions. The FRP rods were pultruded by Owens Corning and produced out of either 2400 or 4800 TEX glass of ECR, Advantex, E/NA and E/Europe. All rods were produced with Polyester (E 701) resin. The 6.4 mm (0.25 inch) by 610 mm (24 inch) FRP rods were then conditioned depending upon which Phase they were to be tested for. Phase I rods were conditioned in a 1 Normal solution of either hydrochloric or sulfuric acid. While conditioning, they were oven kept at 60°C (140°F). The Phase II rods were conditioned at the same temperature as those of Phase I, but the acid solutions were replaced with a saturated cement extract of approximately pH 11. All sets of rods were conditioned for approximately 90 days. After conditioning, the cooled and towel dried rods were then stress rupture tested. It was concluded, that based on Phase I and Phase II results, it is possible to design an

environmental and temperature accelerated stress rupture test that can predict the life cycle performance of GFRC/concrete systems. It was seen that the conditioning of the specimens prior to stress testing has proven to significantly accelerate the failure without affecting the failure modes of the tests. It was concluded that GFRC/concrete exposed to both alkaline and acid environments retain significant load bearing capacities for extended life cycles under conditions harsher than expected in field service.

Kshirsagar, et al. (1998) evaluated the durability of fiber-reinforced composite wrapping for the rehabilitation of concrete piers. To estimate the dependability of a woven glass-fabric/epoxy composite wrap upon aging, compression tests were conducted on 102 mm x 203 mm standard concrete cylinders wrapped with FRP. The cylinders were wrapped both before and after exposure to accelerated aging conditions. The fiber material was a woven sheet of a hybrid E-glass and polyaramid called SEH-51 (Knytex). The resin was the TYFO™ S Epoxy, which is a two-component, solvent-free, moisture insensitive epoxy matrix material. The aging conditions that were employed on the cylinders consisted of 1000 hours of immersion in one of the following solutions: I) Alkaline solution of pH 9.4 and a temperature of 22.8°C (73°F); II) Alkaline solution of pH 12.4 and a temperature of 22.8°C (73°F); III) Alkaline solution of pH 12.4 and a temperature of 65.5°C (150°F); IV) Water of neutral pH and a temperature of 65.5°C (150°F); V) Dry heat at a temperature of 65.5°C (150°F); VI) Freeze-thaw cycles with a temperature range of -29°C to 49°C and a relative humidity of 100% (Approximately 17 freeze-thaw cycles were applied). The cylinders were then tested under compression after the 1000 hours of conditioning. After testing, it was seen that a detrimental effect on the cylinder compressive strength was observed only in the cases of exposure to a combination of moisture and high temperatures.

Soudki, et al. (1998) researched the durability of repaired concrete beams with carbon fiber reinforced polymer (CFRP) laminates subjected to wet/dry cycles. The research consisted of 11 concrete beams for testing. Of the 11 beams, eight were cracked under expected service loads and the remaining beams were left un-cracked to be used as control specimens. The eight cracked beams were repaired with two types of CFRP

laminates: Tonen sheets and Sika laminates. The three control beams were kept at room temperature and the eight beams were subjected to wetting and drying cycles of 50, 100, 200 and 300. These cycles were conducted using a deicing solution of 2% NaCl. Each wet-dry cycle consisted of two days: Wetting the beam for one day and then drying the beam with blow heaters for one day. Following completion of the wet-dry cycles, each of the beams were subjected to a 4-point bending failure. After a total of 50 and 100 cycles, three different nondestructive tests were performed: electrical potential measurement, corrosion rate measurements, and chloride content analysis. The corrosion measurements showed that there was virtually no corrosion activity in the specimens, while the chloride analysis revealed that the chloride levels in the beams were above the possible corrosion threshold level.

Nanni et al. (1998) conducted research on the acceleration of FRP-rebar bond degradation. Throughout the testing, two types of machined FRP rods were used: glass vinyl ester and carbon vinyl ester. These 12.7 mm FRP rods were then cast into concrete cubes where they were used for pullout tests. The pullout tests were conducted under two different accelerated testing schemes: mechanical and environmental. The mechanical testing consisted of sustained loading of approximately 170 to 340 N. The sustained loading conditioning lasted between 7 and 224 days at 30, 50, and 65% loading levels with respect to the ultimate bond strength. The environmental conditioning entailed exposure of the FRP rods to a saturated calcium hydroxide solution, which had a pH of 12-13, at 26, 60 and 80°C, respectively. It was concluded from this study that there was no acceleration of the FRP-concrete bond degradation from the sustained loading, but the exposure to alkaline environments did accelerate the degradation of the FRP-concrete bond. Also it was noted that the carbon vinyl ester rods were more resistant to the environmental conditioning than the glass vinyl ester rods.

Ghasemzadeh et al. (1998) studied the durability of glass-epoxy-wood hybrid composites. Red oak, neat resin, glass fiber epoxy, and wood-GFRC block shear samples were manufactured in accordance with ASTM D 905 (1989). Before testing, the specimens underwent an accelerated aging process. The accelerated aging process

consisted of cycles of a vacuum/pressure soak in water, followed by a freeze/thaw cycle. The aging process consisted of six-cycles of the following: (I) vacuum soaking in room-temperature water at 635 mm (25 inches) Hg vacuum for 30 minutes, (II) pressure soaking in room-temperature water at 6.9 E ^{5} N/m^{2} (100 psi) pressure for 30 minutes, (III) freezing at -22°C (-8°F) for 2.5 hours, (IV) oven drying at 66°C (150°F) for 1 hour. Following conditioning and block shear testing, it was concluded that the composite and hybrid samples showed exceptional durability throughout the accelerated aging cycle; whereas, the red oak samples were degraded with respect to the bondline shear strength.

1.4.1.3 Coupling agents used to promote bonding

Currently there are several coupling agents or primers available which can improve the bond durability of metals, plastics and advanced composite materials.

Vick (1996) studied the effect of using hydroxymethylated resorcinol (HMR) primer for improved adhesion of epoxy and other thermosetting adhesives. The research was conducted to determine if HMR could be used to enhance adhesion of various epoxy formulations to softwood and hardwood species along with wood in fiber-reinforced plastic composites. The test specimens were subjected to the cyclic delamination protocol of ASTM D 2559 (1992), and the effectiveness of the HMR primer was evaluated. The tested epoxy adhesives were extraordinarily resistant to delamination; whereas, the phenol-resorcinol, emulsion polymer/isocyanate and polymeric isocyanate adhesives also met the ASTM standard. Through the testing, it was shown that the capability of epoxies with HMR primer to adhere to both wood and plastics presents an opportunity for making highly durable composites from FRP and wood.

Indspec Chemical Corporation (1989) recommends using a resorcinol-formaldehyde (RF) resin adhesive solution as a primer when bonding materials other than wood. Penacolite® Adhesive G-1131 (Indspec Chemical Corporation, Pittsburgh, PA) technical bulletin advises that when bonding non-porous materials, priming with a dilute

solution of Penacolite® Adhesive G-1131 (100 parts by weight of mixed adhesive plus 15 parts denatured alcohol) will promote bonding. After drying of the RF primer, the materials can then be bonded with a regular mix of Penacolite® Adhesive G-1131.

1.4.2 Block-shear tests

Okkonen and River (1988) examined the factors affecting shear strength measurement with the ASTM D 143-83 (1983) and ASTM D 905-49 (1986) block shear tests. Both of these test are commonly used for the shear strength testing of both solid wood and adhesively bonded wood joints. The research was conducted with samples of southern pine, douglas-fir, white oak, and hard maple (both solid and bonded with phenol-resorcinol formaldehyde adhesive). The comparison factors included: specimen shape (Single- or double-notched), shear tool (with or without offset), specimen size (full or reduced) and grain orientation (radial or tangential). The greatest difference observed was that of the offset. When tested with no offset, the shear strengths were often higher (50 to 60%) than those with the offset. The reduced size specimens also gave consistently higher shear strength values. The specimen shape and grain orientation, caused movements in the shear strengths, but they gave inconsistent results, and therefore a definite conclusion was not drawn. The authors concluded that all factors had statistically significant effects on shear strength and there were significant interactions among the factors. Therefore, comparisons of the strength of solid wood and adhesively bonded joints should be approached with caution.

Janowiak et al. (1992) used the findings of Okkonen and Rivers (1988) to study the strength properties of exterior adhesives on preservative-treated hardwoods. The hardwoods that were tested include: chestnut oak, red maple and yellow poplar. The preservatives consisted of chromated copper arsenate (CCA) and pentachlorophenol (penta). Resorcinol formaldehyde (RF), phenol-resorcinol formaldehyde (PRF), and phenol-formaldehyde (PF) formulations were used for the adhesive bonding of the samples. The samples were then bonded into billets according to ASTM D 905 (1980). The samples tested included both 12% MC along with water vacuum pressure soaked

samples (VPS). The following steps were used for the conditioning cycles: I) water bath under 25 in Hg for 15 minutes; II) water bath pressure of 65 psi for 2 hours; III) repeat steps I and II; IV) dry specimens for 91.5 hours to achieve 12% equilibrium moisture content (EMC); V) steps I through III were repeated; VI) specimens were then dried according to step IV. The conditioned samples, prior to drying, were observed to have obtained moisture contents exceeding 100 percent. The results for the red maple ASTM D 905 samples showed that the shear strength values of the VPS samples were 91 percent of the shear strength of the control samples which were bonded with RF at 12 % MC. The percentages of wood failure actually increased and were 75% and 78% for the control and the VPS samples, respectively. It was concluded from the study that no single adhesive would provide a constant level of performance for all hardwood species. The ASTM D 905 test results showed that the RF adhesive was found most often to yield the highest shear strengths out of all the adhesives that were tested.

Gardner et al. (1994) researched adhesive bonding of pultruded fiber reinforced plastic to wood. Modified ASTM D 905 shear block tests (1989) were performed on combinations of yellow poplar and polyester- or vinylester-pultruded composite bonded with adhesives. The following adhesives were selected for the study: resorcinol-formaldehyde (RF: INDSPEC, Pencolite G-1131), emulsion polymer isocyanate (EPI: Ashland, Isoset WD3-C120/CX 47) and epoxy (Magnolia Plastics Magnobond 56). Specimens were bonded at ambient conditions using a glue spread rate of 244 g/m^2. Open assembly time was less than 5 minutes, and the closed assembly time was approximately 20 minutes followed by C–clamping and curing for 24 hours. Samples were then tested under two conditions: dry (at 12 percent wood moisture content) and wet (where specimens were subjected to a vacuum-pressure-soak test: 40 minutes vacuum, 51 cm Hg/40 minutes pressure, 620 kPa, and followed by testing the samples wet). Additional testing was conducted on glueline integrity by conditioning the samples with a modified ASTM D 1101 (1992). The modified ASTM D 1101 consisted of a 5 cycle vacuum-pressure-soak-dry testing procedure (40 minutes vacuum, 51 cm Hg/40 minutes pressure, 620 kPa). The research concluded that the RF adhesive performed significantly better in both the dry and wet conditions than the other two adhesives for production of FRP-wood

composites. Following the 5-cycle test the RF adhesive appeared to perform quite well considering the severity of the induced stresses from these cycles. The 5-cycleconditioned samples were not tested for actual strength properties, but were tested only to make an assessment of the bond integrity with the RF adhesive. The researchers concluded that FRP composites can be successfully adhesive bonded to wood. All of the studied epoxies indicated to be suitable for interior uses; whereas, RF adhesive showed promise for external use with polyester and vinylester FRP composites.

Abdel-Magid et al. (1996) conducted ASTM D 905 (1989) tests on samples of both carbon/phenolic and glass/phenolic composite sheets bonded to Eastern Hemlock using phenol-resorcinol formaldehyde (PRF) adhesive. The FRP-wood shear samples were produced using varying spread rates, assembly times and surface preparations. The results of the shear block tests showed that the use of phenolic resin and PRF adhesive with the glass composite resulted in bond strengths that were comparable to the overall shear strength of the wood. The same was not true for the carbon composite. The carbon FRP did not have a surface mat, which might be the cause of the lower bond strength. Optimal performance was achieved when the FRP composites were sanded with an 80 to 100 grit size, with an open assembly time of 20-30 minutes, a closed assembly time of 10 minutes and a curing period in excess of 24 hours under pressure at ambient temperature..

Sellers and Miller (1997) conducted block-shear tests on three different adhesive systems for chromated copper arsenate (CCA) treated lumber. The adhesives consisted of a commercial resorcinol formaldehyde adhesive, a commercial emulsion-isocyanate adhesive and a laboratory modified resorcinol adhesive mixture. CCA southern pine lumber was used to produce glulam beams of which compression block shear (T-107) billets were cut according to the Inspection Manual AITC 200-92 for Structural Glued Laminated Timber (1996). The block shear specimens were then tested in dry form (11% MC). The results for all three of the adhesive systems were relatively uniform, ranging from 9,984 to 10,600 kPa. The AITC standard for southern pine at 11% MC of 9,310 kPa was passed by all three adhesive systems. The AITC minimum of 70 percent wood failure was also passed by all three adhesive systems with a range from 87 to 91 percent wood

failure. Therefore, all three adhesive types passed the AITC T-107 block shear tests for dry conditions.

GangaRao (1997) conducted studies on both sawn and laminated wood beams wrapped with fiber reinforced plastic composites. Northern red oak beams (4" x 4" x 60" and 7" x 9" x 108") wrapped with a woven E-glass fabric were tested. An epoxy adhesive along with a resorcinol formaldehyde (RF) primer was used for the bonding process. An accelerated aging cycle was performed on the samples to simulate approximately 25 years of external exposure. The accelerated aging cycle consisted of six-cycles, and each of the six cycles followed four steps: I) vacuum soaking in water at 20 to 25 in. Hg for 30 minutes; II) pressure soaking in water at 100 to 110 psi for 30 minutes; III) freezing samples at -15°F for 2 hours; and IV) oven-drying at 250°F for 8 hours. After the aging cycles were completed, the samples were tested according to ASTM D 905 (1989) to determine the wood-composite bond shear strength. From the block shear test results, it indicated that the most desirable primer/adhesive combination was one with a relatively low viscosity, such as resorcinol formaldehyde which filled the wood pores and created a bondable surface for the glass fiber. After review of the results, modifications were made to the accelerated aging test. The modifications included room temperature curing under 200 psi pressure for 12 hours, followed by 1 hour at 150°F and an additional hour at 210°F.

1.4.3 Mode-I fracture tests

It has been shown that delamination of bonded interfaces can be described by fracture mechanics models (Davalos, Raman and Qiao 1997), and although three distinct modes of fracture can be defined, an interface bond is generally less resistant to crack extension (delamination) under normal (mode-I) load than under shear load, and therefore, Mode-I (opening mode) fracture may be more critical than other modes of fracture. In this section, mode-I fracture tests for interface bonds of hybrid materials and interfacial fracture of composite materials are reviewed.

Mostovoy et al. (1967) discussed the use of a crack-line-loaded specimen for measuring plane-strain fracture toughness. By using a crack-line loaded specimen, the opportunity was presented to collect crack arrest as well as crack initiation toughness data. By modifying the Double Cantilever Beam (DCB) specimen, it was possible to produce a Contoured Double Cantilevered Beam (CDCB), which could produce a linear compliance change with respect to crack length (constant *dC/da* throughout the specimen). When using the CDCB specimen, the crack extension force became proportional to the square of the cracking load, and was independent of the crack length, thus greatly simplifying fracture mechanics testing. The shape or contour of the specimen was determined by the material properties and sample dimensions along with the type of testing that was conducted.

Marcus and Sih (1969) used modified contoured double cantilevered beam specimens of titanium alloys, to experimentally establish the linear dependency of compliance with respect to crack length. The samples were produced from several titanium alloys and had an overall length of 5.50 inches. Testing involved the measurement of crosshead displacement as a function of load for various crack lengths. Plots were then made of displacement vs crack length. The plots and testing data showed that the modified DCB samples had a linear dependence of compliance with crack length within the crack range from 1.50 to 3.50 inches. The load to restart the crack within this crack range was also a constant.

Gallagher (1971) studied experimentally the stress intensity factors for the CDCB specimens, and concluded that the compliance rate and thus the stress intensity level of the specimen remained relatively constant for a range of crack length.

Ebewele et al. (1979) used the CDCB specimens to investigate the effects of bondline thickness, wood anisotropy, and cure time on the fracture toughness of phenolic-wood adhesive joints. They concluded that fracture toughness increased initially with respect to the bondline thickness and then jumped considerably and finally droped sharply. Also the grain orientation and curing time also had dramatic effects on fracture energy.

Fracture tests of wood adhesives were conducted by Scott, River, and Koutsky (1991). CDCB test specimens were employed for the Mode-I fracture tests. The specimens consisted of aluminum contours with thin yellow birch substrates. Aluminum was used for the contours to reduce the variability that is typically present with wood contours. This research concluded that after the CDCB samples were calibrated (constant *dC/da* was known), they could be used to obtain the fracture toughness of wood-adhesive bonds.

Fonselius and Riipola (1992) also used DCB specimens to study the Mode-I fracture of wood. They observed that the grain orientation of the specimens was of great importance to fracture toughness, and the moisture content of the specimens did not affect the fracture toughness values in the range of 10-20% M.C.

River and Okkonen (1993) conducted wood CDCB Mode-I fracture tests on adhesive joints. Experiments showed that the compliance and crack length relationship of straight-tapered CDCB specimens generally increased significantly at larger crack lengths. In an attempt to reduce the accelerated increase and linearize the compliance rate change (*dC/da*), concave- and convex-contoured beam designs were employed and tested. First, a convex contour was used and tested, but it also caused an accelerated increase of *dC/da*. Next, a concave contour was tried, which resulted in a decelerated rate of *dC/da*. Finally after a trial-and-error process, a concave contour was recommended to provide a linear *dC/da* for a large range of crack lengths.

A numerical model based on strength of material approach was developed by Penado (1993) for the compliance and energy release rate of the DCB specimen with crack extension within an adhesive layer. It was shown that for a DCB specimen for composite adherends, shear deformation must be taken into account in addition to “elastic foundation” boundary effects.

Davalos, Madabhusi-Raman and Qiao (1997) employed contoured DCB specimens to study Mode-I fracture of bonded interface between hybrid materials (e.g., FRP-Wood). The CDCB specimens were designed for a constant rate of compliance change with respect to crack length by the Rayleigh-Ritz method. Experimental calibration tests, Finite Element modeling, and Rayleigh-Ritz modeling were used to verify the linearity of the compliance crack-length relationship, and a relatively linear compliance rate change (*dC/da*) was achieved over a certain range of crack length. Following verification, linear-tapered CDCB specimens for wood-wood and wood-FRP bonded interfaces were tested under Mode-I to determine critical loads for crack initiation and arrest, from which the critical strain energy release rates (fracture toughness) were obtained. The critical strain energy release rates were verified by the Jacobian Derivative Method (JDM), a finite element post-processing algorithm. This study concluded that the proposed modeling techniques and testing methods can be efficiently used for the evaluation and investigation of Mode-I fracture toughness (G_{Ic}) for hybrid adherends such as FRP-wood interface bonds.

The double cantilever beam (DCB) specimen has been extensively used to determine the interlaminar fracture toughness of composite materials. Russell (1983) studied the factors that affect the fracture toughness of composite materials. DCB specimens were used for Mode-I fracture tests. Mode-I fracture tests were conducted under varying temperature conditions (-50°C, 20°C, and 100°C), and it was reported that G_C decreased with an increase in temperature. It was also noted that fiber bridging often occurred during testing. The fiber bridging resulted in large increases in G_C, especially following conditioning in wet or hot environments. The fiber bridging caused an increase in G_C because of the peeling and straining that the bridged fibers underwent during testing. Using the DCB specimens, the effect of stacking sequence on energy release rate distribution was theoretically investigated by Davidson et al. (1996). Martin (1997) used the DCB specimens to obtain the interlaminar fracture toughness of woven composites, and the initial crack insert on effect of fracture toughness was studied. Most recently, Ozdil and Carlsson (1999) conducted a combined experimental and analytical study on quasi-unidirectional and angle-ply laminate DCB fracture specimens. In their study, the

DCB specimen was analyzed as two Bernoulli-Euler laminated beams joined at the mid-plane by a Winkler elastic foundation to accommodate transverse elasticity of uncracked region of the specimen. The fracture toughness obtained experimentally was largest for the unidirectional composite and decreased with increased angle in the angle-ply laminate. Also, the angle-ply laminates displayed more yarn debonding and bridging.

CHAPTER 2

DELAMINATION OF INTERFACE BOND

2.1 Introduction

This chapter discusses delamination studies of adhesively bonded FRP-wood interfaces using a modified ASTM D 2559 test method (See Figure 2.1 and Figure 2.2 for details). Two types of FRP-wood interfaces were studied: FRP strips (plates) bonded to wood (used commercially for glulam timber beams) and wood cores wrapped with FRP by filament winding (being investigated for reinforcement of railroad wood crossties and wood utility poles). The following factors related to the performance of bonded interfaces were investigated: (1) the influence of coupling agents, (2) the influence of clamping pressure, and (3) the influence of open/closed assembly time.

In this chapter, a modified ASTM D 2559 delamination test method was used to screen the best combination of parameters to achieve an adequate performance of the FRP-wood interface. The materials, test methods, and details of specimen preparation, along with test results and recommendations for bonding are provided within this chapter.

2.2 Materials

In this study, the wood material used was Red Maple, and the reinforcing material consisted of either E-glass fiber rovings embedded in a Phenolic resin matrix (see Figure 2.3), or E-glass fiber rovings filament wound in an Epoxy matrix (see Figure 2.5). The Phenolic fiber reinforced plastic (Phenolic FRP) composite material was produced by the

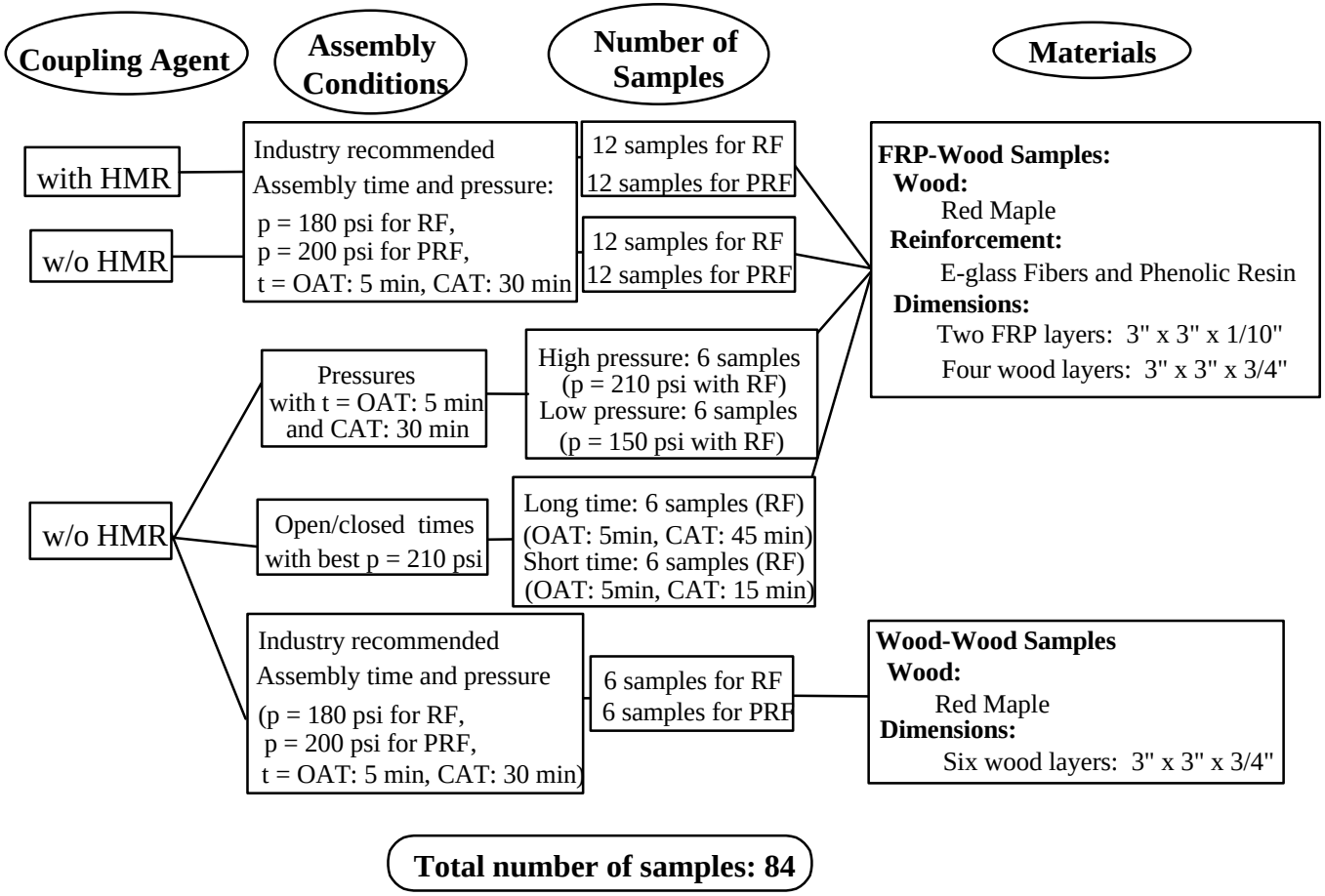

Figure 2.1. Experimental program for Phenolic FRP-wood ASTM D 2559 delamination tests

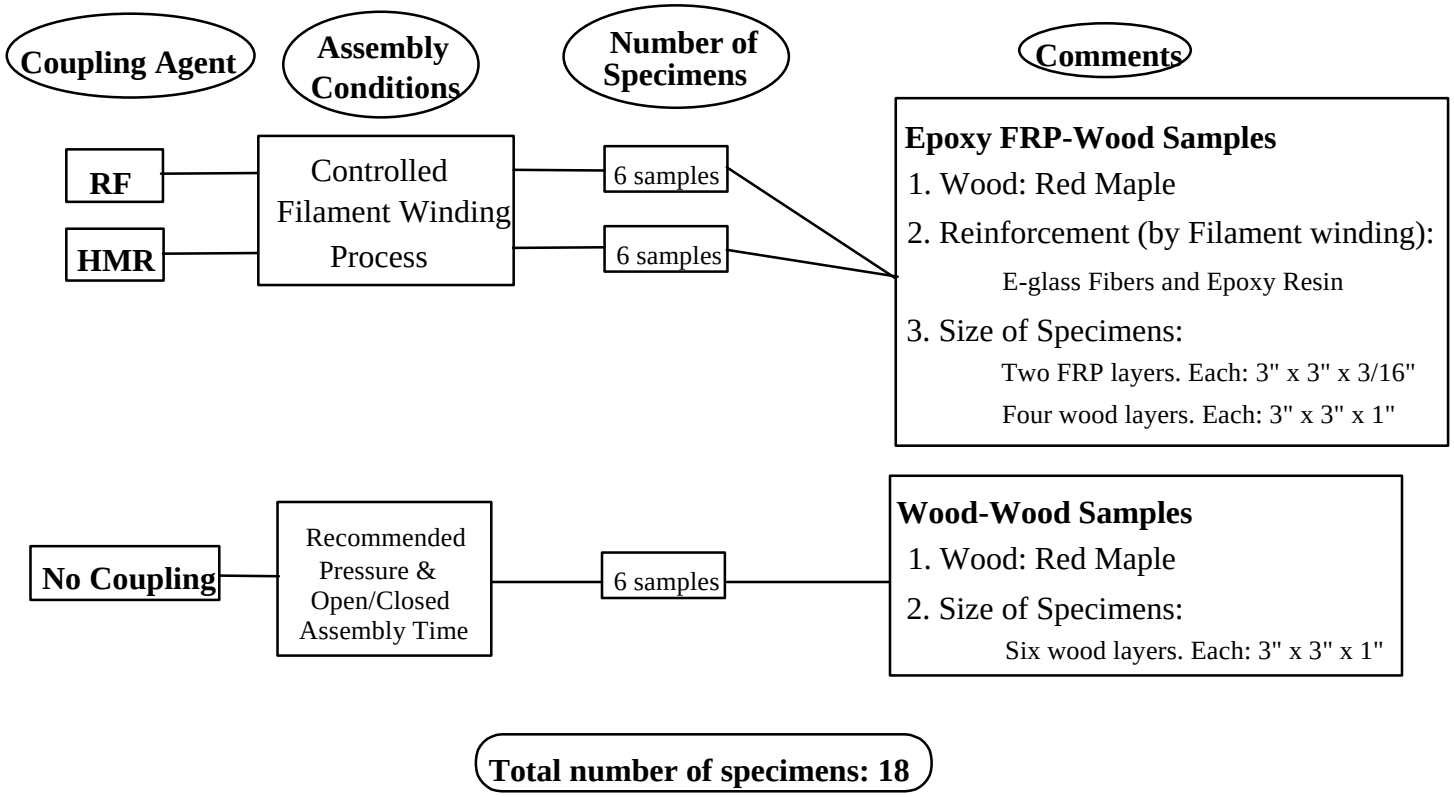

Figure 2.2. Experimental study program for Epoxy FRP-wood ASTM D 2559 delamination tests

pultrusion process; whereas the Epoxy fiber reinforced plastic (Epoxy FRP) composite material was produced by the filament winding process. Pultrusion and filament winding are both well controlled and relatively low cost manufacturing processes that are used in the production of FRP composites. For the Phenolic FRP composite, two types of commercial wood adhesives were used: Resorcinol Formaldehyde (RF, Penacolite® G-1131) and Phenol modified Resorcinol Formaldehyde (PRF, Penacolite® R-400) adhesives from Indspec Chemical Corporation, Pittsburgh, PA.

2.2.1 Red maple (Acer Rubrum)

Red Maple, a hardwood species, was chosen as the wood material, and the samples were cut from 2-in nominal lumber. The finished dimensions of each piece of wood for manufacturing the delamination specimens were 0.75 in thick, 3.0 in wide, and 24 in long, and when possible, the annual growth rings of the laminae were placed with alternated directions through the cross section of the laminate (see Figure 2.3).

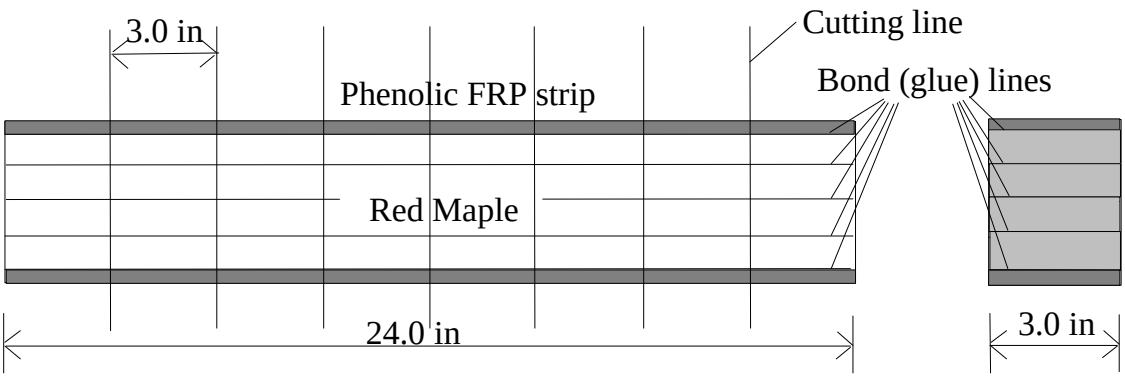

Figure 2.3. Manufacturing of Phenolic FRP-wood delamination specimens

2.2.2 Pultruded Phenolic FRP laminate

Pultruded Fiber-reinforced Phenolic Plastic (Phenolic FRP) laminate was chosen as the composite strip to be bonded to the Red Maple hardwood. The composite material used consisted of E-glass fiber rovings embedded in a Phenolic resin matrix. Pultruded

Phenolic FRP sheets of size 1/10” x 3½” x 5’ were manufactured by Creative Pultrusions, Inc. The sheets were cut into strips of finished dimensions 1/10” x 3.0” x 24.0”. The lay-up of the Phenolic FRP laminate is shown in Figure 2.4. The Continuous Strand Mat (CSM) layer on both outside surfaces is intended to provide a desirable surface texture for bonding, which is important to attain a good adhesive bond interface. The FRP surfaces were sanded lightly with a belt-sander and 100 grit sandpaper to remove the top glossy resin surface and provided a smooth surface for bonding. After sanding, all surfaces of the Phenolic FRP were blown clean with compressed air and then cleaned with a solvent.

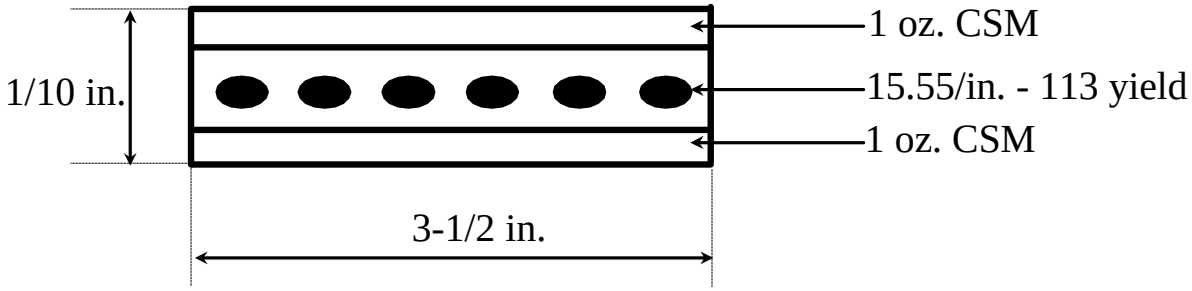

Total # of 113 yield rovings = 54

Fiber Weight Fraction = 70.05%; Fiber Volume Fraction = 50.98%

Figure 2.4. Lay-up of pultruded Phenolic FRP laminate

2.2.3 Filament wound Epoxy FRP composite

Filament wound Fiber-reinforced Epoxy Plastic (Epoxy FRP) was produced using E-glass fiber rovings in an Epoxy matrix. Red Maple was used as the mandrel during the filament winding process; therefore the Red Maple and Epoxy FRP were bonded during production of the composite. The Epoxy FRP wrap was applied at approximately +/-45^{o}, by the filament winding process, to achieve an Epoxy FRP thickness of approximately 3/16”. To produce the Red Maple mandrel, a Resorcinol Formaldehyde (RF) adhesive was used (Penacolite Adhesive G-1131, Indspec Chemical Corporation) for the wood-wood face bonding of four boards (1” x 4” x 36”) to produce a laminated beam (4” x 4” x 36”). Recommendations given by the adhesive manufacturer were followed to bond wood-wood:

pressure of 180 psi and assembly time of 5 min for open and 30 min for closed time. Two distinct coupling agents were used to coat the wood substrate: Resorcinol Formaldehyde (RF) and Hydroxymethylated Resorcinol (HMR; Vick 1996). A schematic figure of the Epoxy FRP-wood beam sample produced by filament winding process is shown in Figure 2.5. Twelve beam samples (4" x 4" x 36") with a 3/16" thick Epoxy FRP layer were manufactured by Industrial Fiberglass Specialties, Inc., Dayton, OH.

2.2.4 Coupling agents

The coupling agent hydroxymethylated resorcinol (HMR), as reported by Vick (1996), was used as a primer on the wood surface, because of the potential for improving the bond performance significantly. This HMR coupling agent was prepared as 5%-solids aqueous solution by reacting formaldehyde with resorcinol (Vick 1996). The ingredients were reacted for 4 hours at room temperature before application to the wood surface. The HMR primer was spread with a brush at approximately 0.03 lb/ft^2 (0.15 kg/m^2), and the primed surfaces were dried for 24 hours at 73^{o}C and 78.0% relative humidity before proceeding with the bonding process.

Indspec Chemical Corporation recommended using a resorcinol-formaldehyde (RF) resin adhesive solution as a primer for the bonding of materials other than wood. Penacolite® Adhesive G-1131 (Indspec Chemical Corporation, Pittsburgh, PA) technical bulletin (October, 1989) advised that when bonding non-porous materials, priming with a dilute solution of Penacolite® Adhesive G-1131 (100 parts by weight of mixed adhesive plus 15 parts denatured alcohol) would promote bonding. The RF primer was spread with a brush at approximately 0.03 lb/ft^2 (0.15 kg/m^2), and the primed surfaces were dried for 24 hours at 73^{o}C and 78.0% relative humidity before proceeding with the bonding process.

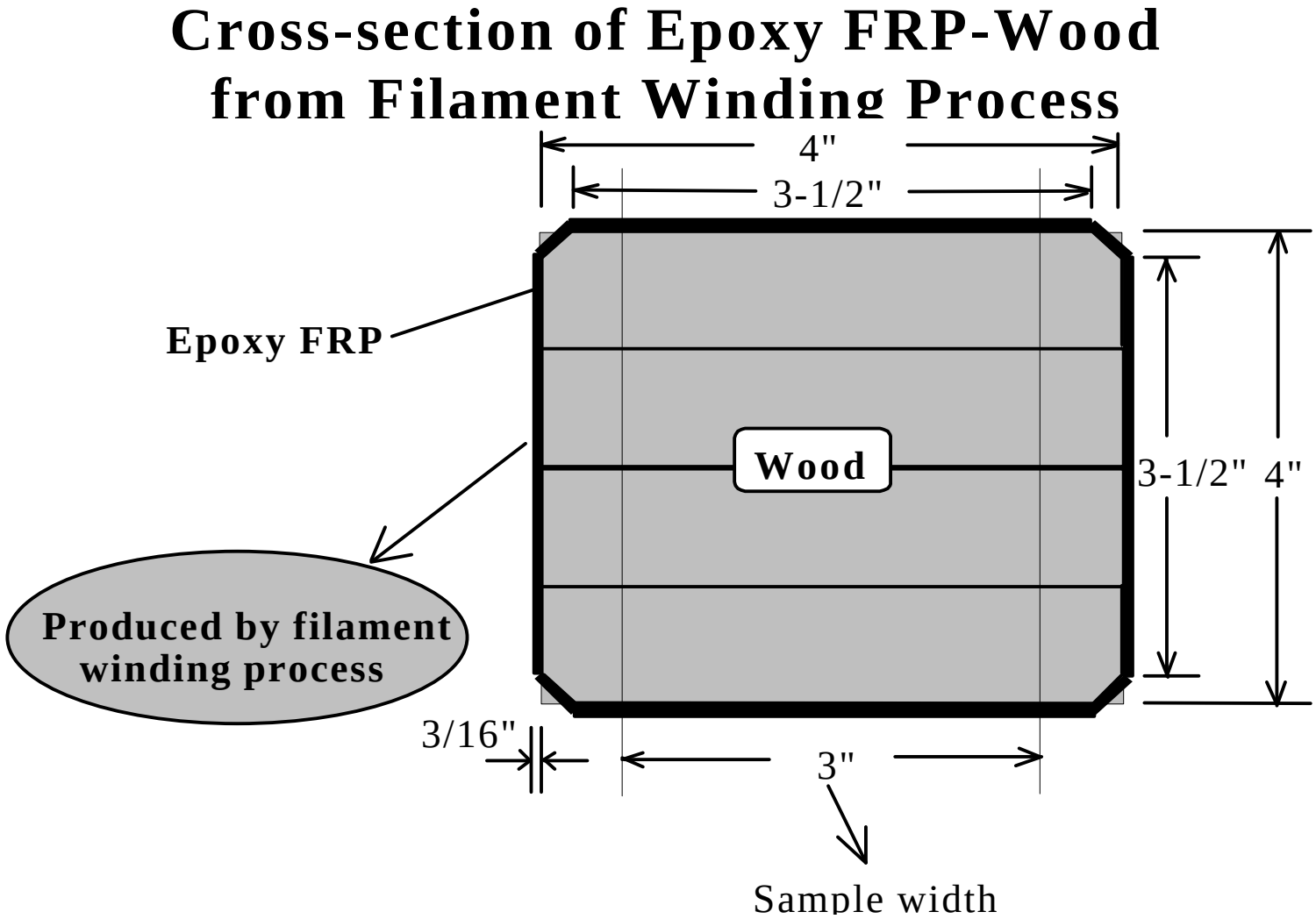

Figure 2.5. Manufacturing of Epoxy FRP-wood sample by filament winding process

2.2.5 Adhesives

Two types of adhesives were used for face bonding of wood-wood and also Phenolic FRP-wood: Resorcinol Formaldehyde (RF) and Phenol-modified Resorcinol Formaldehyde (PRF) adhesives from Indspec Chemical Corporation. Both RF and PRF adhesives are capable of curing at room temperature and providing strong water-proof bonds. The RF adhesive is a two component resorcinol-formaldehyde resin, and consists of resorcinol-formaldehyde polymer (G-1131-A), which is a liquid resin, and paraformaldehyde (G-1131-B), which is a powdered hardener. These two parts of A and B are mixed in the ratio of 5 to 1 by weight. The PRF adhesive is a new phenol-modified resorcinol formaldehyde adhesive system, and is made by mixing Penacolite Resin (R-400), Hardeners (H-30M), and water in the ratio of 100:18:22 by weight. These adhesives are neutral and inert, and they provide resistance to deterioration or disintegration on aging.

2.3 Manufacturing of Delamination Specimens

2.3.1 Phenolic FRP-Wood

Each laminated Phenolic FRP-Wood assembly for the delamination test consisted of four pieces of Red Maple and two pieces of Phenolic FRP: four wood pieces (each 3/4” x 3” x 24”) were placed at the center of the lamination, and the Phenolic FRP strips (each 3/16” x 3” x 24”) were located at the top and bottom of the lamination (see Figure 2.3). Wood-wood assemblies for the delamination test were made by bonding six wood pieces (each 0.75” x 3” x 24”). All wood boards were conditioned to an equilibrium moisture content (MC) of about 12% before bonding.

The adhesive, either RF or PRF, was applied only on one face of each lamina, either wood or Phenolic FRP, with an electronic spreading roller to maintain a constant spread rate of 0.006 to 0.008 lb/ft^2 as recommended by industry. As indicated in Figure 2.1, either

six wood boards or four pieces of wood and two of Phenolic FRP were bonded under different manufacturing combinations of coupling agent, clamping pressure and assembly time. Each of the laminated wood-wood and Phenolic FRP-wood beam-type members were cut into six 3-inch long samples, and these samples were tested following the ASTM D 2559 guidelines.

2.3.2 Epoxy FRP-Wood

Delamination samples obtained from the Epoxy FRP-wood specimens, were bonded by the resin used in the filament winding process to produce the Epoxy FRP composite. As stated earlier, the laminated Red Maple beams were used as the mandrel for filament winding. Delamination samples both with HMR and RF coupling agents were cut from the Epoxy FRP-wood beams (Figure 2.5), and the final dimensions of the samples were 3" x 3" x 4-3/8"(Figure 2.6). For completeness and comparative purposes, all-wood samples (see Figure 2.6) were also tested. In addition, six confined samples with cross sections shown in Figure 2.5 (two treated with HMR and four with RF) were also tested for delamination under the effects of confinement provided by the Epoxy FRP.

2.4 Modified ASTM D 2559 Delamination Test

The ASTM standard test D 2559 was developed for specification of adhesives for structural laminated wood products for use under exterior (wet use) exposure condition. Modified test samples were used to evaluate the delamination percentages of wood-wood and FRP-wood bondlines and the performance of FRP-wood interfaces under the standard test conditions specified in ASTM D 2559. The ASTM D 2559 standard was modified by the reduction of the dimensions of the sample. Following the ASTM specifications, the specimens were subjected to the following three wet-dry cycles: 1) vacuum/pressure (25 in Hg for 5 minutes/75 psi for 60 minutes) soaking [repeat once] followed by oven dry (150°F for 22 hours); 2) steam/pressure (212°F for 90 minutes/75 psi for 40 minutes) soaking

Modified ASTM D2559 Samples

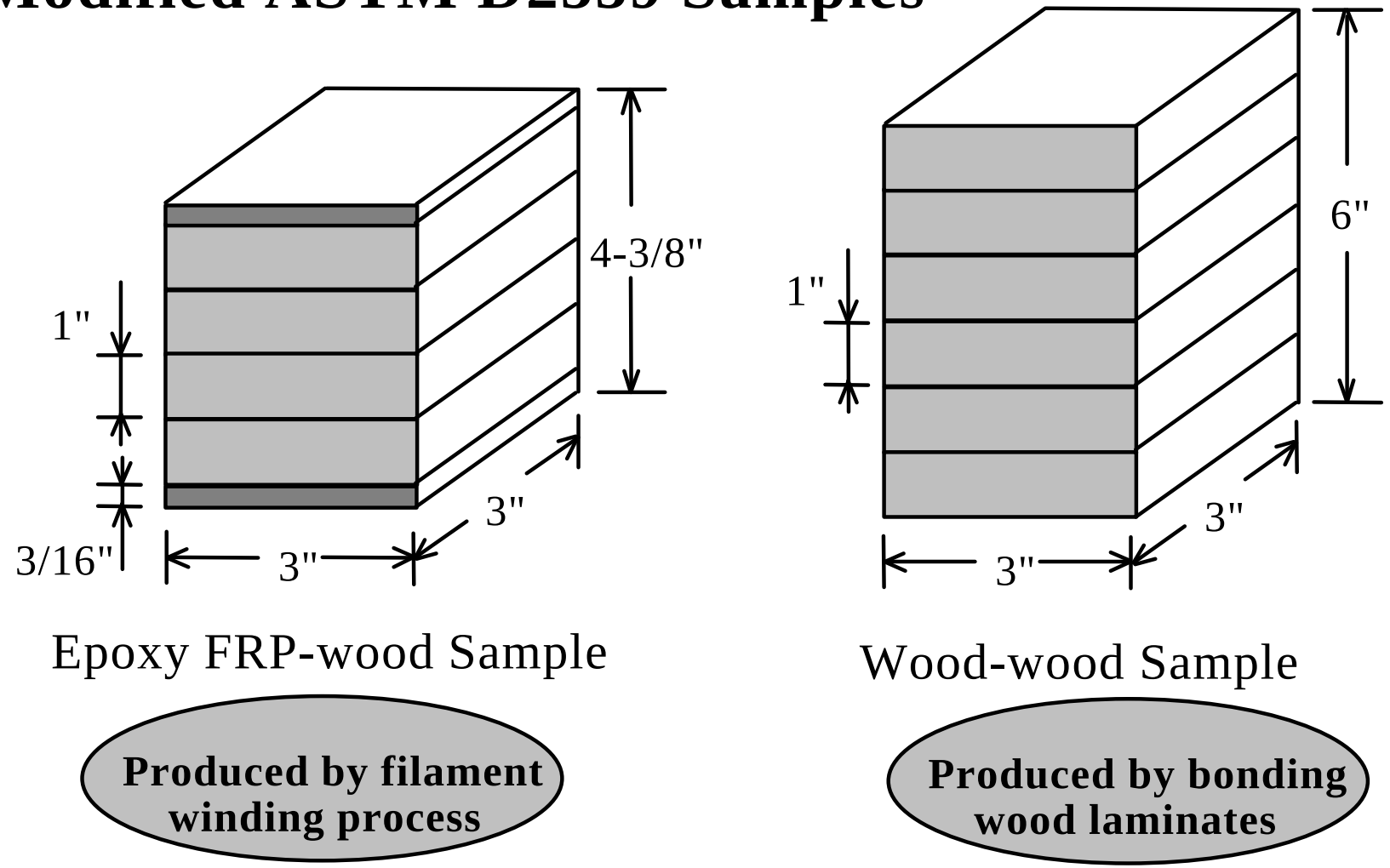

Figure 2.6. Epoxy FRP-wood and wood-wood samples for ASTM D 2559 delamination tests

followed by oven dry (150°F for 22 hours); 3) vacuum/pressure (25 in Hg for 5 minutes/75 psi for 60 minutes) soaking [repeat once] followed by oven dry (150°F for 22 hours).

The total time required for each complete test was three days, and immediately after the last cycle, the bondline delamination was measured on all end-grain surfaces with the aid of a microscope. The delamination is measured as a ratio of the length of delaminated (debonded) end-grain to total end-grain bondline length for each specimen. As specified by the ASTM standard for wood-wood delamination samples, the average delamination for each manufacturing condition shall not exceed 5% for softwoods and 8% for hardwoods. Due to the materials used in this study (Red Maple and FRP composites), the 8% delamination limit for hardwoods was used to evaluate the bond performance for each manufacturing combination.

2.5 Number of Test Samples

2.5.1 Phenolic FRP-Wood

The wood-wood samples were used as a control group for the Phenolic FRP-wood samples. Since the wood-wood assemblies were bonded with proven commercial adhesives (RF and PRF) and expected to perform well, only six samples were used for each of the two wood adhesive types. In contrast, a larger variability of results was expected with the Phenolic FRP-wood samples, and for this reason 12 samples were initially used to evaluate the effect of HMR coupling. The favorable results obtained for Phenolic FRP-wood samples without the need to use HMR coupling provided confidence to reduce the number of samples to six for the study of clamping pressure and open/closed assembly time, and also only the RF adhesive was used to evaluate these two bonding parameters.

2.5.2 Epoxy FRP-Wood

The wood-wood samples that were used as a control group for the Phenolic FRP-wood samples were also used as the control group for the Epoxy FRP-wood samples. Six samples each treated with HMR and RF coupling agents were cut and tested from the Epoxy FRP-wood beams. In addition, six confined cross section samples (two treated with HMR and four with RF) were also tested for delamination under the confinement effects of the Epoxy FRP wrap.

2.6 Test Results

In this section, the results obtained following the modified ASTM D 2559 tests are discussed for both the Phenolic FRP-wood and Epoxy FRP-wood samples.

2.6.1 Phenolic FRP-Wood

In this section, the test results on effect of primer and influence of assembly time and pressure are presented.

2.6.1.1 Effect of HMR coupling

As shown by Vick (1996), the HMR coupling agent may improve the durability of bonded interfaces and reduce the delamination along the bondlines. In this study, two adhesive systems (PRF and RF adhesives) were used to evaluate the HMR (Hydroxymethylated Resorcinol primer) effects on bondline delamination for samples manufactured following recommendations by the adhesive manufacturer for clamping pressure (p = 200 psi for PRF and p = 180 psi for RF adhesives) and open/closed assembly time (t = 5/30 min). The results of the ASTM D 2559 tests for both RF and PRF adhesives with and without the HMR coupling agent, respectively, are shown in Tables 2.1 and 2.2.

Six wood-wood control samples without HMR and 12 Phenolic FRP-wood samples, for each HMR-treated Phenolic FRP and non-HMR Phenolic FRP, were used for each adhesive type.

As shown in Table 2.1 and Table 2.2 for PRF and RF respectively, the wood-wood bondline for samples without (w/o) HMR treatment of the Phenolic FRP surface had less average delamination percentages when compared to the ones primed with (w) HMR treated Phenolic FRP surfaces. By examining the test samples immediately after each test cycle, we observed that in general the wood-wood bondlines immediately below and above the primed wood-FRP bondlines were subjected to larger delamination than the wood-wood bondline at the middle of the specimen. This may be due to the enhanced performance of the HMR-primed Phenolic FRP-wood bondline inducing residual stresses to the adjacent wood substrate, and increasing the delamination of the wood-wood bondline. It is significant that for the HMR-primed samples bonded with RF there was no delamination at the wood-FRP bondlines.

Table 2.1. Delamination of Phenolic FRP-wood and wood-wood bonded interface with PRF adhesive (pressure: p = 200 psi; Open/Closed Assembly Time: t = 5/30 min)

Percent Average Delamination					
Specimens	Wood-Wood	Phenolic FRP-wood			
Coupling Agent	w/o. HMR (6 samples)	w. HMR on wood adjacent to FRP strips (12 samples)		w/o. HMR on wood adjacent to FRP strips (12 samples)	
Bond line	Wood-wood	Wood-FRP	wood-wood	Wood-FRP	wood-wood
Delamination	**3.20**	**3.21**	**8.90**	**2.25**	**0.74**

Table 2.2. Delamination of Phenolic FRP-wood and wood-wood bonded interface with RF adhesive (pressure: *p* = 180 psi; Open/Closed Assembly Time: t = 5/30 min)

Percent Average Delamination					
Specimens	Wood-Wood	Phenolic FRP-wood			
Coupling Agent	w/o. HMR (6 samples)	w. HMR on wood adjacent to FRP (12 samples)		w/o. HMR on wood adjacent to FRP (12 samples)	
Bond line	Wood-wood	Wood-FRP	wood-wood	Wood-FRP	wood-wood
Delamination	**4.00**	**0.00**	**6.53**	**2.44**	**1.46**

Although both adhesives provided similar delamination percentages for samples without HMR, the information provided by the adhesive manufacturer indicates that the RF adhesive is more suitable for bonding hardwoods (Red Maple) than the PRF adhesive; therefore, only the RF adhesive was used to bond samples and study the subsequent parameters given in Figure 2.1. Since the samples without HMR coupling performed within acceptable delamination limits (Phenolic FRP-wood delamination < 3.0%), the subsequent specimens to study clamping pressures and open/closed assembly times were manufactured without the HMR coupling agent.

2.6.1.2 Effect of clamping pressure

Under fixed assembly time (open/closed assembly times are 5 min and 30 min, respectively), the clamping pressure effect was studied for three levels of applied pressure: low (p = 150 psi), intermediate (p = 180 psi) and high (p = 210 psi). Since the intermediate pressure of 180 psi was already evaluated as part of the study of the HMR coupling agent (see Table 2.2), only the low and high pressure levels were evaluated using six samples for each condition. As shown in Table 2.3, the samples assembled under high clamping pressure of 210 psi exhibited less delamination than those assembled under low and

intermediate pressure conditions. Therefore, a pressure of 210 psi was used for the follow-up assembly time study.

Table 2.3. Delamination of Phenolic FRP-wood bondline under three pressure conditions (with RF adhesive and without HMR primer)

Percent Average Delamination			
Pressure *p* (psi)	Open/closed assembly time *t* (min)	FRP-wood Bondline	wood-wood bondline
150.0 (low)	5.0/30.0	0.31	8.08
180.0 (intermediate)	5.0/30.0	2.44	1.46
210.0 (high)	**5.0/30.0**	**0.00**	**1.42**

2.6.1.3 Effect of assembly time

Following the clamping pressure study, the effect of assembly time was investigated. In Table 2.4, under the preferred constant pressure of 210 psi, samples were manufactured with constant open assembly time of 5.0 min and three different closed assembly times of 15 min (short), 30 min (intermediate) and 45 min (long). Six samples were used for each condition. Note that the intermediate closed assembly time (t = 5/30 min) was already evaluated above (see Table 2.3). The samples with long assembly time period (*t* = 5/45 min) showed the largest delamination percentage, especially for the bondlines along the wood-wood interfaces. Both the specimens with short and long assembly times exhibited larger delaminations than the ones with intermediate assembly time. As a conclusion, the specimens with high pressure (*p* = 210 psi) and intermediate open/closed assembly time (*t* = 5/30 min) provided the best results.

Table 2.4. Delamination of Phenolic FRP-wood bondline under open/closed assembly times (with RF adhesive and without HMR primer)

Percent Average Delamination			
Pressure *p* (psi)	Open/closed assembly time *t* (min)	Wood-FRP Bondline	wood-wood bondline
210.0	5.0/15.0 (short)	1.32	5.22
210.0	**5.0/30.0 (intermediate)**	**0.00**	**1.42**
210.0	5.0/45.0 (long)	1.93	14.76

2.6.2 Epoxy FRP-Wood

This section discusses the effects of the HMR and RF coupling agents on Epoxy FRP-wood laminated samples (D 2559) and confined samples by the FRP wrap.

2.6.2.1 Effect of HMR/RF coupling agents on ASTM D 2559 samples

The results on the ASTM D 2559 tests of the Epoxy FRP-wood interface bond with both HMR (Epoxy FRP-Wood/HMR) and RF (Epoxy FRP-Wood/RF) coupling agents are shown in Table 2.5. It indicates that a good performance of the Epoxy FRP-wood interface bond with HMR coupling agent was achieved; no delamination was observed along the Epoxy FRP-wood bondline with HMR coupling agent. For the Epoxy FRP-wood interface bond with the RF coupling agent, a large delamination percentage along the Epoxy FRP-wood bondline occurred at the end of each cycle of the ASTM D 2559 test. In particular, the delamination increased significantly after the second cycle (steam/pressure-soaking and drying), and the average delamination percentage was around 44.2% at the end of three-cycle test.

Table 2.5. Delamination of Epoxy FRP-wood bonded interface by ASTM D 2559

Average Delamination Percentage (%)				
Coupling Agents	Resorcinol Formaldehyde (RF)		Hydroxymethylated Resorcinol (HMR)	
Bondline	FRP-wood	Wood-wood	FRP-wood	wood-wood
Cycle 1	24.58	0.00	0.00	0.00
Cycle 2	43.45	1.19	0.00	0.43
Cycle 3	44.16	1.48	0.00	0.62

The results of the ASTM D 2559 tests for the control wood-wood (Red Maple) samples, given previously in Table 2.2, indicated that a satisfactory performance of wood-wood interface bond by RF adhesives (Penacolite G-1131) was achieved. The average delamination percentage of wood-wood bondline was around 4.0%, which satisfied the standard requirement (5% for softwoods and 8% for hardwoods).

2.6.2.2 Effect of HMR/RF coupling agents on confined samples

The experimental results of the samples with uncut edges (confined samples, see Figure 2.5) are shown in Table 2.6. It shows that the Epoxy FRP-wood interfaces with RF coupling agent had significant delamination in relation to the ones with HMR coupling agent. Due to the confined effect, larger residual stresses were introduced along the Epoxy FRP-wood interfaces during the wetting-drying cycle of the test, and an increased delamination percentage is observed when compared to the unconfined samples (from 44.2% to 76.9% for Epoxy FRP-Wood/RF samples). There is no visible delamination along the Epoxy FRP-wood bond line for both unconfined and confined samples with HMR coupling agent (Epoxy FRP-Wood/HMR).

Table 2.6. Delamination of Epoxy FRP-wood confined samples by ASTM D 2559

Average Delamination Percentage (%)				
Coupling Agents	Resorcinol Formaldehyde (RF) (4 samples)		Hydroxymethylated Resorcinol (HMR) (2 samples)	
Bond line	FRP-wood	Wood-wood	FRP-wood	wood-wood
After the 3rd cycle	76.89	2.93	0.00	4.99

2.7 Conclusions

The performance of the FRP-wood interface bond under simulated exterior or wet-use exposure conditions (three wet-dry cycles) was evaluated using modified ASTM D 2559 Delamination Test, and some important conclusions are presented in this section for Phenolic and Epoxy based FRP-wood samples.

2.7.1 Phenolic FRP-wood interface

The Phenolic FRP-wood interface bond was primed with HMR coupling agent, as developed and reported by Vick (1996). The HMR was applied to the wood surfaces adjacent to Phenolic FRP strips before bonding, and the effect of HMR primer on the delamination performance of bonded interfaces was studied. The specimens without HMR primer showed a small percent delamination (< 3.0%) for Phenolic FRP-wood interfaces, and in general, the specimens without HMR exhibited less delamination of wood-wood interfaces, particularly at layers adjacent to the Phenolic FRP. For face-bonding of Phenolic FRP-wood laminates, the manufacturing parameters related to clamping pressure and open/closed assembly time can be easily controlled. The study of these parameters indicated that specimens manufactured with high pressure (p = 210 psi) and intermediate open/closed assembly times (t = 5/30 min) showed the least delamination along both the wood-wood and Phenolic FRP-wood bondlines; therefore, for the RF adhesive used to

bond the Red Maple wood and phenolic FRP composite in this study, the combination of 210 psi for clamping pressure and 5/30 min open/closed assembly time is recommended.

2.7.2 Epoxy FRP-wood interface

The Epoxy FRP-wood interface bond performance under exterior or wet-use exposure conditions (three wet-dry cycles) was evaluated to study the effect of coupling agents (primers) to promote bonding. The Epoxy FRP-wood interface bond was generated during the filament winding process; therefore, the open/closed assembly time and clamping pressure along the Epoxy FRP-wood interface can not be controlled. The influence of two different coupling agents on bond strength was investigated. As indicated in Tables 2.5 and 2.6, the Epoxy FRP-wood interface with HMR coupling agent performed well under cyclic wetting and drying delamination tests; whereas, the interface with RF coupling agent failed to pass the delamination test. It is recommended that the HMR coupling agent be applied to the Red Maple wood surface before wrapping with the Epoxy FRP reinforcement. It is concluded that the HMR significantly improved the bond strength and durability of the Epoxy FRP-wood interface.

CHAPTER 3

SHEAR STRENGTH OF INTERFACE BOND

3.1 Introduction

In this chapter, tests to establish shear strengths and percent material failures for adhesively bonded wood-wood and FRP-wood interfaces were performed using a modified ASTM D 905 test method. Based on the best parameter combinations identified from the modified ASTM D 2559 test (Phenolic FRP-wood: RF adhesive with pressure: p = 210 psi and open/closed assembly time: t = 5/30 min; Epoxy FRP-wood: HMR and RF Coupling agents), see Chapter 2, both wood-wood and FRP-wood block-shear samples were manufactured and tested under dry and wet conditions (see Figure 3.1 and Figure 3.2). The average shear strengths and percent material (cohesive) failures for both wood-wood and FRP-wood interfaces under dry and wet conditions are given, and the results are discussed.

A modified ASTM D 905 test method for strength properties of adhesive bonds in shear by compression loading was used to determine the shear strength and percent material failure for dry and wet samples. In the following section, the materials, test methods, test specimen preparation and specimen manufacturing for the modified ASTM D 905 tests are described first and the testing results are then presented.

3.2 Materials

The wood material used was Red Maple, and the reinforcing material consisted of either E-glass fiber rovings embedded in a Phenolic resin matrix (Figure 2.3, Chapter 2), or

E-glass fiber rovings filament wound in an Epoxy matrix (Figure 2.5, Chapter 2). The Phenolic fiber reinforced plastic (Phenolic FRP) composite material was produced by the pultrusion process; whereas the Epoxy fiber reinforced plastic (Epoxy FRP) composite material was produced by the filament winding process. Pultrusion and filament winding are both well controlled and relatively low cost manufacturing processes that are used in the production of FRP composites.

The Phenolic FRP composite contains Continuous Strand Mat (CSM) layers on both outside surfaces which provides a desirable surface texture for obtaining a good adhesive bond interface. The lay-up of the Phenolic FRP laminate is shown in Figure 2.4. The Phenolic FRP surfaces were sanded and cleaned as explained in Section 2.2.2. A commercial Resorcinol Formaldehyde wood adhesive (RF, Penacolite® G-1131, Indspec Chemical Corporation, Pittsburgh, PA) was used to bond the wood-wood and Phenolic FRP-wood samples. As concluded from the modified ASTM D 2559 test (Chapter 2), there is no need to prime the wood surface for improved bond strength; therefore, the coupling agent hydroxymethylated resorcinol (HMR, Vick 1996) was not used in the shear strength study for the Phenolic FRP-wood samples.

The Epoxy FRP composite was filament wound around primed Red Maple beams (Section 2.2.3). The beams were primed with either hydroxymethylated resorcinol (HMR) or Resorcinol Formaldehyde (RF), and the effects of the coupling agents on the shear strength and percent material failure of the Epoxy FRP-wood interface under dry and wet conditions were investigated.

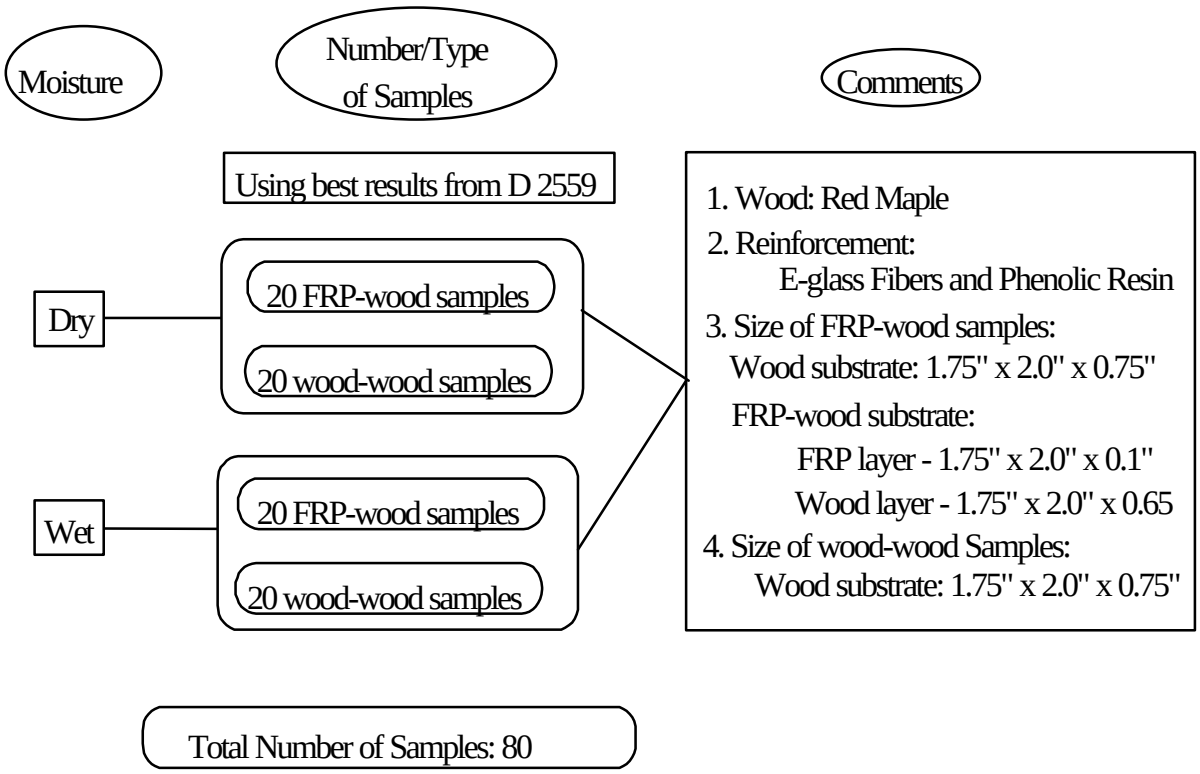

Figure 3.1. Experimental program for Phenolic FRP-wood ASTM D905 standard test

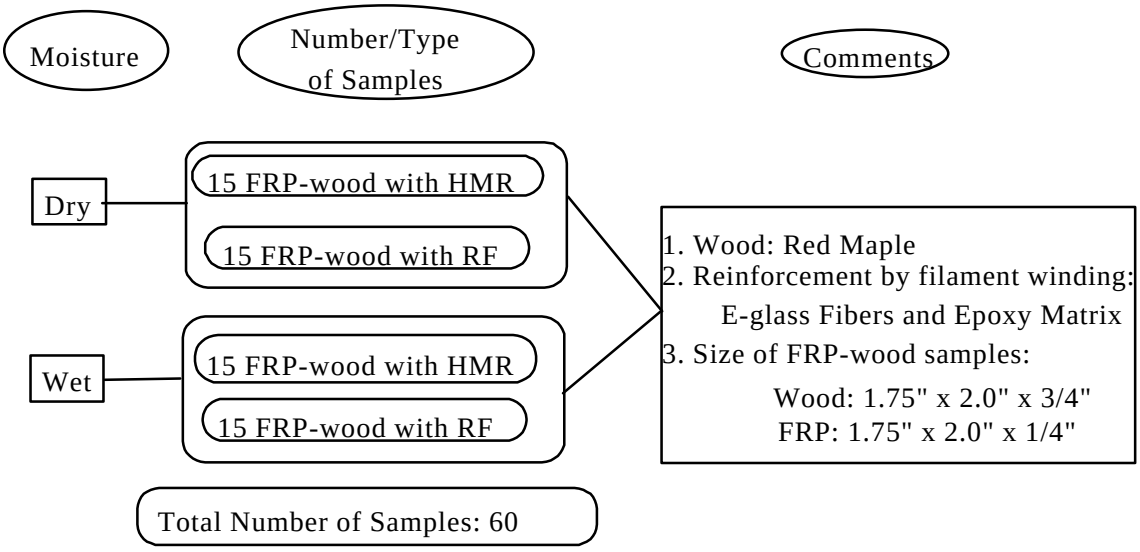

Figure 3.2. Experimental program for Epoxy FRP-wood ASTM D 905 standard test

3.3 Manufacturing of Block-Shear Test Samples

3.3.1 Phenolic FRP-Wood

According to the ASTM D 905 standards, the bonded interfaces for wood substrates should be made from boards of approximately ¾" x 2-½" x 12". The wood substrates can be obtained in these dimensions, but the Phenolic FRP substrates provided by industry are of a reduced thickness (0.1" x 2-½" x 12"). Therefore, an extra Red Maple substrate of 0.65" x 2-½" x 12" was bonded to the exterior surface of the composite substrate to form a constant thickness of ¾" as specified in ASTM D 905 (see Figure 3.3). All Red Maple boards were conditioned to equilibrium moisture content (MC) of about 12% before bonding. Prior to bonding, the Phenolic FRP composite was lightly sanded with a belt-sander and 100 grit sandpaper to remove the top glossy resin surface and provide a smooth surface for bonding. After sanding, all surfaces of the Phenolic FRP were blown clean with compressed air and then cleaned with a solvent. The Red Maple was knife-planed prior to bonding and cleaned with compressed air.

The RF adhesive was applied on one surface only, either wood or FRP, with a mechanical spreading roller to maintain a constant spread rate of 0.006 to 0.008 lb/ft^2 as recommended by industry. As established from the modified ASTM D 2559 test (Chapter 2), a pressure of 210 psi and open/closed assembly time of 5/30 min were used to bond the Phenolic FRP composite and wood substrates. Each 12-inch long bonded laminate was then cut into five block-shear specimens. A total of 40 wood-wood and 40 Phenolic FRP-wood samples were obtained for a total sample number of 80. Specimens were randomly assigned to be tested either dry or wet: 20 wood-wood and 20 Phenolic FRP-wood dry and the other 20 wood-wood and 20 Phenolic FRP-wood wet (see Figure 3.1).

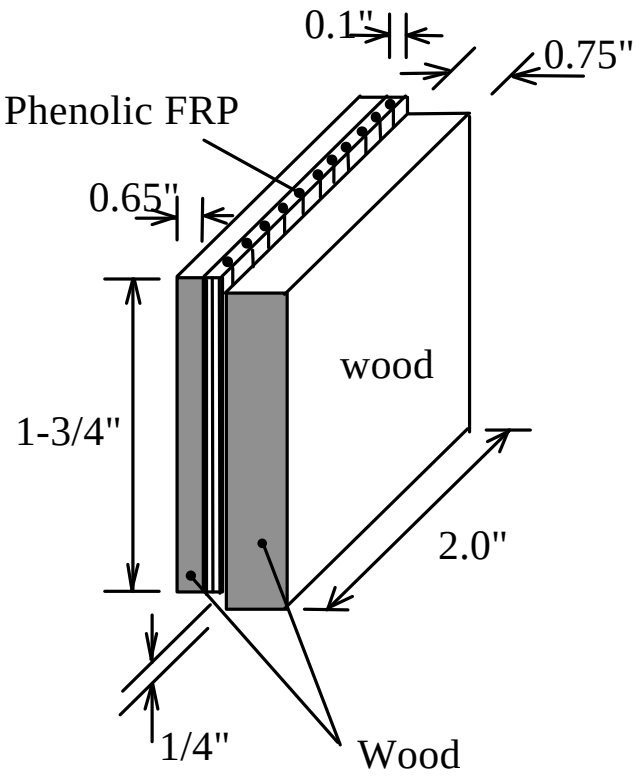

Figure 3.3. Modified ASTM D 905 Phenolic FRP-wood specimen for block-shear test

3.3.2 Epoxy FRP-Wood

Block-shear test specimens were manufactured from the Epoxy FRP-wood laminates, which were cut from the beams (Figure 2.5), as described in Section 2.2.3. According to the ASTM D 905 standards, the interface bonds for wood substrates should be made from strips of approximately ¾" x 2-½" x 12". The wood substrates can be obtained in these dimensions, but the Epoxy FRP composite substrates manufactured by filament winding are relatively thin (about ¼"). This relatively thin layer of composite can provide enough bearing area to sustain the shear loading; hence, the dimensions of composite substrates used in this study were about ¼" x 2-½" x 12". Each Epoxy FRP-

wood laminate, which consisted of wood and Epoxy FRP substrates, was cut into five block-shear specimens as shown in Figure 3.4. The specified ASTM D 905 block-shear samples were slightly modified, because of the limitation in thickness of the Epoxy FRP layer. A set of 15 samples for each combined coupling-agent and moisture-condition combination were manufactured, which resulted in a total number of 60 samples, as shown in Figure 3.2.

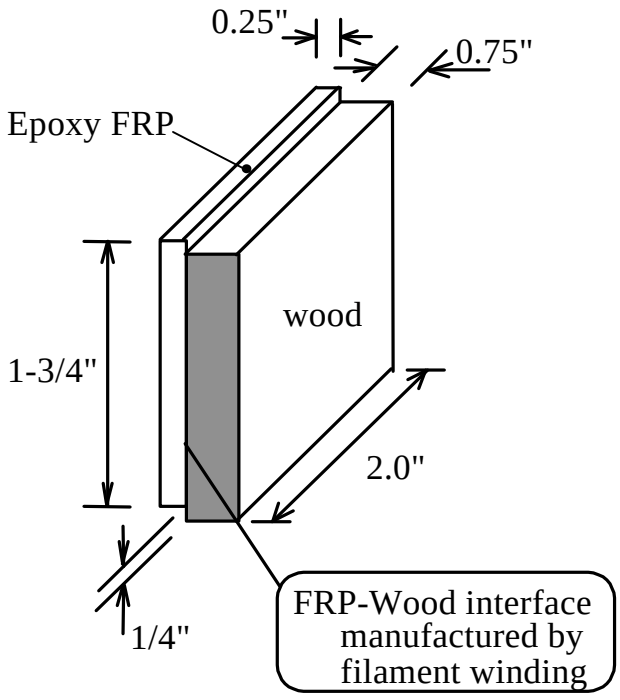

Figure 3.4. Modified ASTM D 905 Epoxy FRP-wood specimen for block-shear test

3.4 Experimental Design and Testing

To examine the bond strength due to moisture effects, both dry (at 12% moisture content) and wet (more than 100% moisture content) samples were tested following the ASTM D 905 standard. Initially, all the block-shear samples were conditioned to a wood equilibrium moisture content (MC) of 12% in an environmentally controlled chamber. To obtain the wet condition, half of the block-shear wood-wood and FRP-wood samples,

initially at 12% MC, were subjected to a vacuum-pressure-soak cycle. The samples were first placed in a container and submerged in water, and the container was then placed in a cylinder that was equipped to apply vacuum and pressure. A vacuum of 25 inches Hg was applied for 40 minutes, and then, a pressure of 100 psi was applied for another 40 minutes. This vacuum-pressure soak cycle was found satisfactory for impregnating the wood layers with water (Gardner et al. 1994). The increase in moisture content by weight of the wood substrates was more than 100% at the end of this cycle. The vacuum-pressure soaked wood-wood and FRP-wood block-shear specimens were immediately tested wet for shear strength according to the ASTM D 905 standard. All the block-shear specimens were tested in an MTS machine, and a loading rate (displacement controlled mode) of 0.015 in/min specified by the test standard was used.

3.5 Test Results

3.5.1 Phenolic FRP-Wood

The shear strength and percent material failure values for samples of wood-wood and Phenolic FRP-wood bonded interfaces under both dry and wet conditions are shown in Tables 3.1 through 3.4, and a summary of the test results is given in Table 3.5. A graphical representation of the shear strength values is given in Figure 3.5. As indicated in Table 3.6, the moisture content in wood had a major effect on the shear strength of wood-wood specimens (about 55% decrease for wet samples). Where as for Phenolic FRP-wood specimens, there was a lesser influence of moisture content on the shear strength (about 6% decrease for wet samples).

Table 3.1. Shear strengths and percent material failures for wood-wood samples at 12% MC

Specimen No	Load (lbs)	Area (in^2)	Shear Strength (psi)	Material Failure (%)
1	6698	3.1412	2132.3	87.42
2	6768	3.1053	2179.5	89.42
3	6804	3.1466	2162.3	92.85
4	4762	3.1110	1530.7	86.92
5	6632	3.0722	2158.7	89.58
6	6362	3.0922	2057.4	100.00
7	5676	3.0523	1859.6	100.00
8	6130	3.0677	1998.2	41.61
9	5666	3.0759	1842.0	100.00
10	6634	3.0340	2186.6	100.00
11	5524	2.9243	1889.0	25.08
12	4390	3.0674	1431.2	100.00
13	6398	3.0823	2075.7	100.00
14	5860	2.9197	2007.1	85.17
15	6046	2.9668	2037.9	86.66
16	5752	3.0941	1859.0	64.75
17	6114	3.0372	2013.0	90.75
18	7048	3.1496	2237.7	84.50
19	4986	3.0820	1617.8	65.00
20	5444	2.9487	1846.2	31.92

Table 3.2. Shear strengths and percent material failures for Phenolic FRP-wood samples at 12% MC

Specimen No	Load (lbs)	Area (in^2)	Shear Strength (psi)	Material Failure (%)
1	3458	3.0646	1128.4	100.00
2	2412	3.0705	785.5	50.81
3	4018	3.0350	1323.9	91.00
4	3264	2.9968	1089.2	49.75
5	4038	3.0605	1319.4	48.67
6	2460	3.0080	817.8	100.00
7	4334	3.0326	1429.1	85.72
8	3000	3.0775	974.8	60.89
9	3330	2.9183	1141.1	100.00
10	3136	3.0700	1021.5	95.83
11	3748	3.0411	1232.4	82.33
12	2424	2.9715	815.7	46.50
13	2722	2.9772	914.3	68.08
14	3644	3.0428	1197.6	100.00
15	2420	3.0363	797.0	97.58
16	3394	2.9827	1137.9	74.00
17	2074	2.9468	703.8	83.83
18	2598	3.0128	862.3	100.00
19	2866	3.0163	950.2	82.50
20	3028	2.9692	1019.8	98.08

Note: Material failure in CSM layer of Phenolic FRP

Table 3.3. Shear strengths and percent material failures for wood-wood samples at saturation MC (more than 100% MC)

Specimen No	Load (lbs)	Area (in^2)	Shear Strength (psi)	Material Failure (%)
1	2738	3.0654	893.2	91.25
2	2902	2.9641	979.0	100.00
3	2722	3.0796	883.9	0.00
4	2074	3.0272	685.1	29.27
5	2056	2.9539	696.0	59.42
6	3000	3.0045	998.5	100.00
7	2780	3.0639	907.3	27.18
8	2560	3.0563	837.6	22.34
9	2784	3.0665	907.9	27.58
10	2324	3.1012	749.4	33.39
11	3028	3.0987	977.2	88.75
12	2740	2.9897	916.5	50.75
13	2750	3.0042	915.4	75.00
14	3136	3.0834	1017.1	89.50
15	3016	3.0469	989.9	76.75
16	2914	3.1157	935.3	80.33
17	2694	3.0480	883.8	89.60
18	2378	2.9862	796.3	8.50
19	2714	3.0797	881.3	100.00
20	2588	2.9306	883.1	0.00

Table 3.4. Shear strengths and percent material failures for Phenolic FRP-wood samples at saturation MC (more than 100% MC)

Specimen No	Load (lbs)	Area (in^2)	Shear Strength (psi)	Wood Failure (%)	CSM Failure (%)	Total Material Failure (%)
1	3264	2.9929	1090.6	28.58	56.00	84.58
2	2423	2.9656	817.0	0.00	100.00	100.00
3	2590	3.0280	855.3	22.75	62.08	84.83
4	2558	2.9926	854.8	0.00	87.92	87.92
5	3328	3.0867	1078.2	0.00	84.00	84.00
6	2948	3.0172	977.1	15.50	72.83	88.33
7	2204	2.9582	745.1	0.00	86.50	86.50
8	3114	3.0453	1022.6	42.67	38.97	81.58
9	3124	3.1007	1007.5	5.40	57.18	62.58
10	3208	3.0627	1047.4	16.08	2.00	18.08
11	2516	3.0093	836.1	0.00	100.00	95.92
12	3408	3.1093	1096.1	0.00	100.00	99.08
13	2226	2.9447	755.9	0.00	100.00	94.92
14	2368	2.9885	792.4	0.00	100.00	100.00
15	4112	3.0627	1342.6	0.00	100.00	98.67
16	3152	3.0173	1044.7	20.83	72.58	93.42
17	3110	2.9206	1064.8	0.00	100.00	100.00
18	4042	3.0672	1317.8	-	-	100.00
19	2326	2.9318	793.4	64.42	10.75	75.67
20	2920	2.9514	989.4	0.00	100.00	100.00

Table 3.5. Shear strength and percent material failure of wood-wood and Phenolic FRP-wood interface block-shear specimen

Bonded Interface (condition)	No. of Samples	Mean Shear Strength (psi)	Min. Shear Strength (psi)	Max. Shear Strength (psi)	Std. Dev. (psi)	COV (%)	Material Failure (%)
Wood-Wood (dry)	20	1956	1431	2238	224	11.5	81.1
FRP-Wood (dry)	20	1033	704	1429	205	19.8	80.8[(a)]
Wood-Wood (wet)	20	887	685	1017	94	10.6	57.5
FRP-Wood (wet)	20	976	745	1342	171	17.5	86.8[(b)]

[(a)] Material failure in FRP-wood bonded interface occurred in the CSM layer of the FRP substrate.

[(b)] Material failure: 76% in CSM and 10.8% in wood.

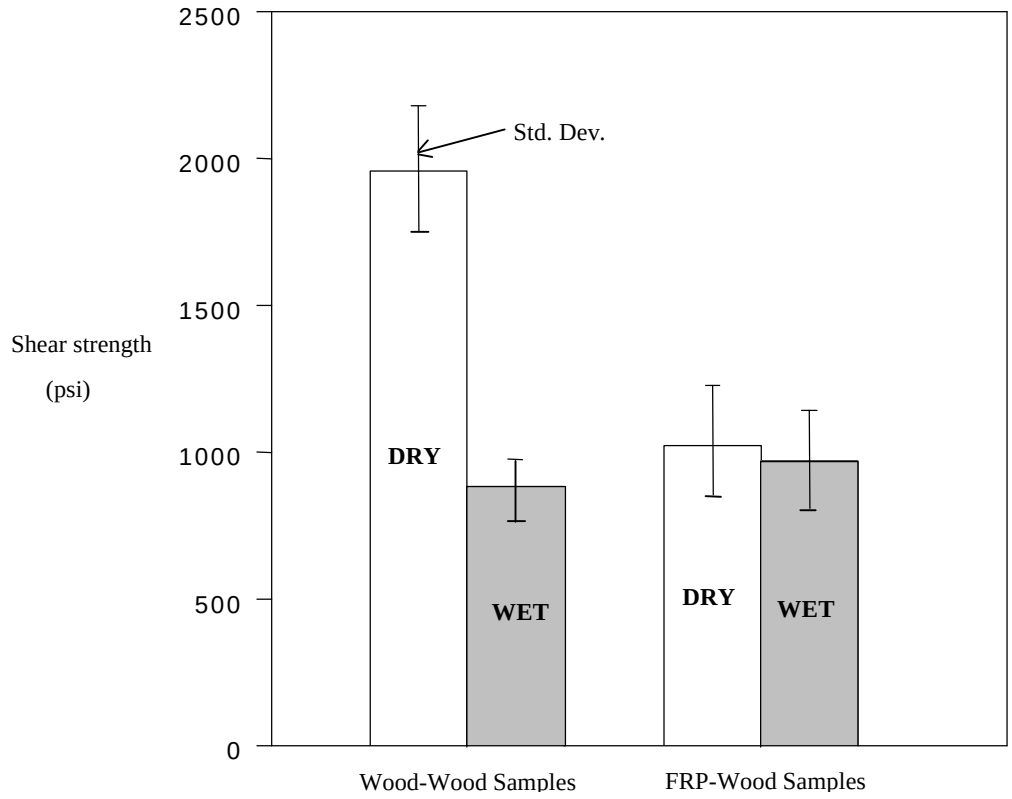

Figure 3.5. Shear strength for wood-wood and Phenolic FRP-wood specimens

Table 3.6. Moisture effects on mean shear strength for wood-wood and Phenolic FRP-wood specimens

Wood-Wood (dry)	Wood-Wood (wet)	Difference
1956 psi	887 psi	54.7%
FRP-Wood (dry)	FRP-Wood (wet)	Difference
1033 psi	976 psi	5.5%

The percent material failure (wood or composite failure) for the wood-wood and Phenolic FRP-wood bonded shear specimens are shown graphically in Figure 3.6, and the results are summarized in Table 3.7. The average percent material (cohesive) failure for the wood-wood samples decreased by 29%, from about 81% for dry to 58% for wet. In contrast, the average percent material failure for the Phenolic FRP-wood samples was about 81% for dry and 87% for wet, with a small increase of 7%.

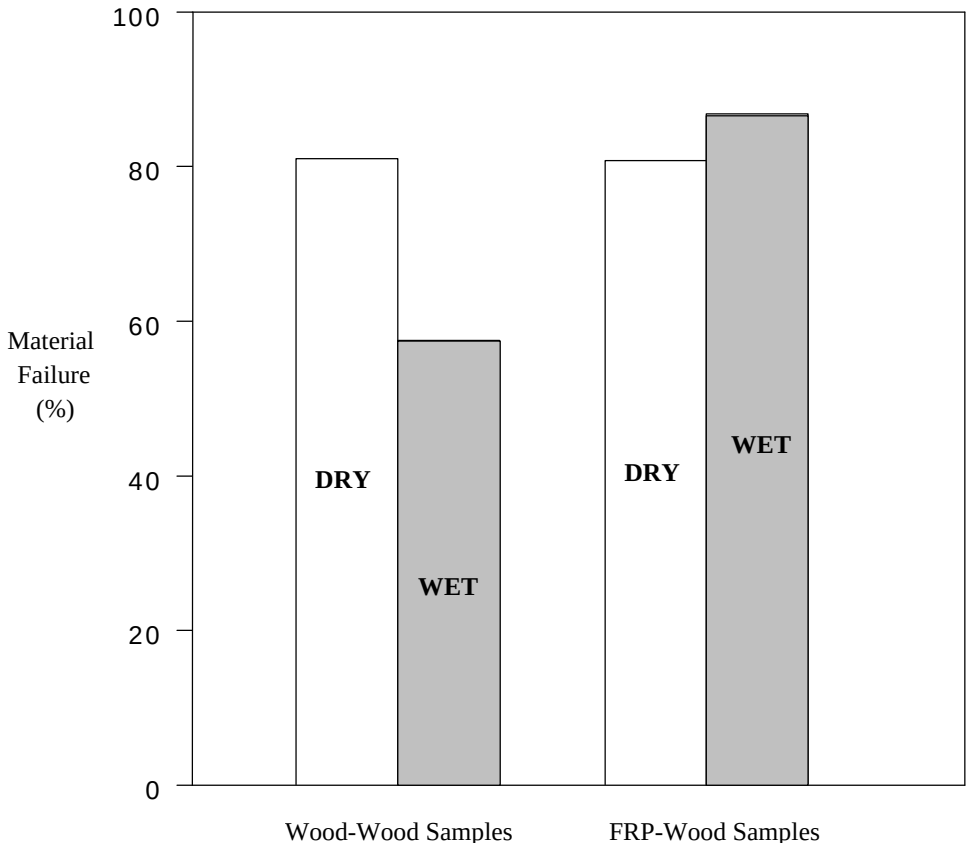

Figure 3.6. Material failure for wood-wood and Phenolic FRP-wood specimens

Table 3.7. Moisture effects on percent material failure for wood-wood and Phenolic FRP-wood specimens

Wood-Wood (dry)	Wood-Wood (wet)	Difference
81.1%	57.5%	29.1%
FRP-Wood (dry)[(a)]	FRP-Wood (wet)[(b)]	Difference
80.8%	86.8%	-7.4%

[(a)]Material failure entirely in CSM layer;

[(b)]Material failure: 76% in CSM and 10.8% in wood.

3.5.2 Epoxy FRP-Wood

The shear strength and percent material failure values for samples of wood-wood and Phenolic FRP-wood bonded interfaces under both dry and wet conditions are shown in Tables 3.8 through 3.11, and a summary of the test results is given in Table 3.12. A graphical representation of the shear strength values is given in Figure 3.7. As indicated in Table 3.13, the moisture content in wood had a significant effect on the shear strength of Epoxy FRP-wood specimens with RF coupling agent (about 42.8% decrease for wet samples). Where as for Epoxy FRP-wood specimens with HMR, there was a less significant influence (about 26.2% decrease for wet samples) of moisture content on the shear strength. The Epoxy FRP-wood specimens with HMR showed higher shear strengths than the Epoxy FRP-wood with RF for both dry and wet condition (about 8.4% for dry and 28.9% for wet, see Table 3.14). The results in Table 3.14 indicate that the HMR coupling agent enhances the strength of interface bond.

Table 3.8. Shear strengths and percent material failures for Epoxy FRP-wood/HMR samples at 12% MC

Specimen No	Load (lbs)	Area (in^2)	Shear Strength (psi)	Material Failure (%)
1	4740	2.9529	1605.2	83.05
2	3268	2.7234	1200.0	66.57
3	3892	2.8195	1380.4	100.00
4	4410	2.9146	1513.1	33.71
5	4062	3.0058	1351.4	22.33
6	3940	2.8649	1375.2	96.55
7	3588	2.9853	1201.9	83.00
8	3828	2.8897	1324.7	100.00
9	4062	2.9222	1390.1	97.18
10	4234	2.9517	1434.4	61.83
11	4004	2.9204	1371.0	97.41
12	4228	3.0206	1399.7	100.00
13	3634	2.8658	1268.1	88.02
14	4142	2.6705	1551.0	89.25
15	4626	2.9506	1567.8	45.17

Note: Material Failure all in wood substrate

Table 3.9. Shear strengths and percent material failures for Epoxy FRP-wood/RF samples at 12% MC

Specimen No	Load (lbs)	Area (in^2)	Shear Strength (psi)	Material Failure (%)
1	4362	3.0601	1425.5	11.13
2	2718	2.8314	959.9	95.92
3	4430	2.8607	1548.6	0.00
4	3130	3.0338	1031.7	14.67
5	3078	2.9223	1053.3	0.00
6	4856	2.8281	1717.0	57.58
7	3884	2.9806	1303.1	27.25
8	3848	2.8284	1360.5	48.97
9	3702	2.9029	1275.3	8.28
10	3924	3.0982	1266.6	30.56
11	3882	3.0709	1264.1	35.08
12	3720	2.6575	1399.8	19.50
13	2616	2.8783	908.9	13.28
14	4672	2.8317	1649.9	24.00
15	3018	2.9565	1020.8	13.17

Note: Material Failure all in wood substrate

Table 3.10. Shear strengths and percent material failures for Epoxy FRP-wood/HMR samples at saturation MC (more than 100% MC)

Specimen No	Load (lbs)	Area (in^2)	Shear Strength (psi)	Material Failure (%)
1	3034	2.9719	1020.9	100.00
2	2864	2.9796	961.2	100.00
3	3036	2.9004	1046.8	55.83
4	3068	2.8669	1070.1	80.17
5	3194	2.9490	1083.1	100.00
6	3082	2.9024	1061.9	98.08
7	3146	2.9024	1083.9	83.75
8	2682	2.7340	981.0	92.33
9	2924	2.9404	994.4	100.00
10	2994	2.9728	1007.1	91.27
11	3164	2.9138	1085.9	50.00
12	2598	2.7171	956.2	100.00
13	3566	3.4038	1047.6	94.58
14	2908	2.9755	977.3	100.00
15	3078	2.8674	1073.5	99.00

Note: Material Failure all in wood substrate

Table 3.11. Shear strengths and percent material failures for Epoxy FRP-wood/RF samples at saturation MC (more than 100% MC)

Specimen No	Load (lbs)	Area (in^2)	Shear Strength (psi)	Material Failure (%)
1	1190	2.7609	431.0	0.00
2	2128	2.8192	754.8	100.00
3	2048	2.9325	698.4	0.00
4	2506	2.9704	843.6	0.00
5	2464	2.9692	829.9	25.17
6	2134	2.9276	728.9	0.00
7	3000	2.9855	1004.9	25.75
8	1822	2.8717	634.5	0.00
9	1800	2.9946	601.1	2.00
10	2334	2.9272	797.4	6.08
11	1838	2.9324	626.8	0.00
12	2374	2.9099	815.8	96.00
13	1786	2.9364	608.2	0.00
14	2142	2.9513	725.8	29.08
15	2572	2.9265	878.9	31.67

Note: Material Failure all in wood substrate

Table 3.12. Shear strength and percent material failure of Epoxy FRP-wood interface block-shear specimens

FRP-wood Bonded Interface (condition)	No. of Samples	Mean Shear Strength (psi)	Min. Shear Strength (psi)	Max. Shear Strength (psi)	Std. Dev. (psi)	COV (%)	Material Failure (%)
with HMR (dry)	15	1396	1200	1605	123	8.8	77.6
with HMR (wet)	15	1030	956	1086	47	4.6	89.7
with RF (dry)	15	1279	909	1717	248	19.4	26.6
with RF (wet)	15	732	431	1005	140	19.1	21.1

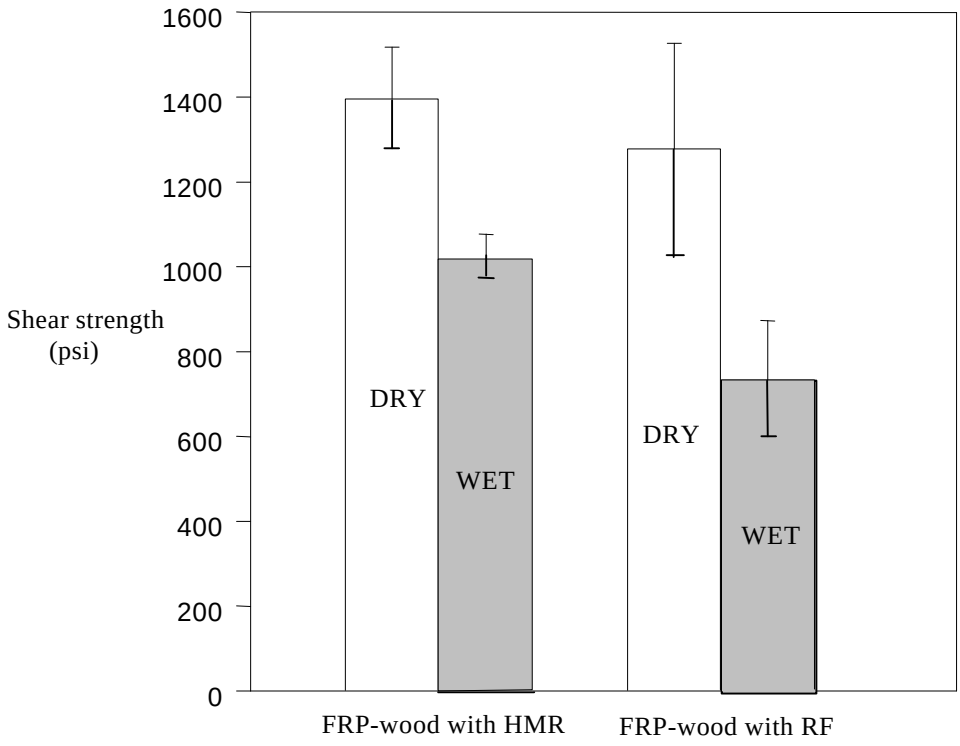

Figure 3.7 Shear strength comparison for Epoxy FRP-wood specimens

Table 3.13. Moisture effects on shear strength for Epoxy FRP-wood specimens

FRP-wood (HMR: dry)	FRP-wood (HMR: wet)	Difference
1396 psi	1030 psi	26.2%
FRP-wood (RF: dry)	FRP-wood (RF: wet)	Difference
1279 psi	732 psi	42.8%

Table 3.14 Coupling agents (primer) effects on shear strength for Epoxy FRP-wood specimens

FRP-wood (HMR: dry)	FRP-wood (RF: dry)	Difference
1396 psi	1279 psi	8.38%
FRP-wood (HMR: wet)	FRP-wood (RF: wet)	Difference
1030 psi	732 psi	28.93%

The percent material, cohesive, failure for the Epoxy FRP-wood interface shear specimens occurred entirely in wood and is shown graphically in Figure 3.8; the results are summarized in Table 3.15. The average percent material (cohesive) failure for the Epoxy FRP-wood samples with HMR coupling agent increased by 15.6%, from about 77.6% for dry to 89.7% for wet. In contrast, the average percent material failure for the Epoxy FRP-wood samples with RF coupling agent had a small percentage of cohesive failure and was about 26.6% for dry and 21.1% for wet, with a decease of 20.7%. The effects of coupling agents on the percent material failure are also shown in Table 3.16; the Epoxy FRP-wood interfaces with HMR showed a large percent of material failure which indicates an improved interface bond.

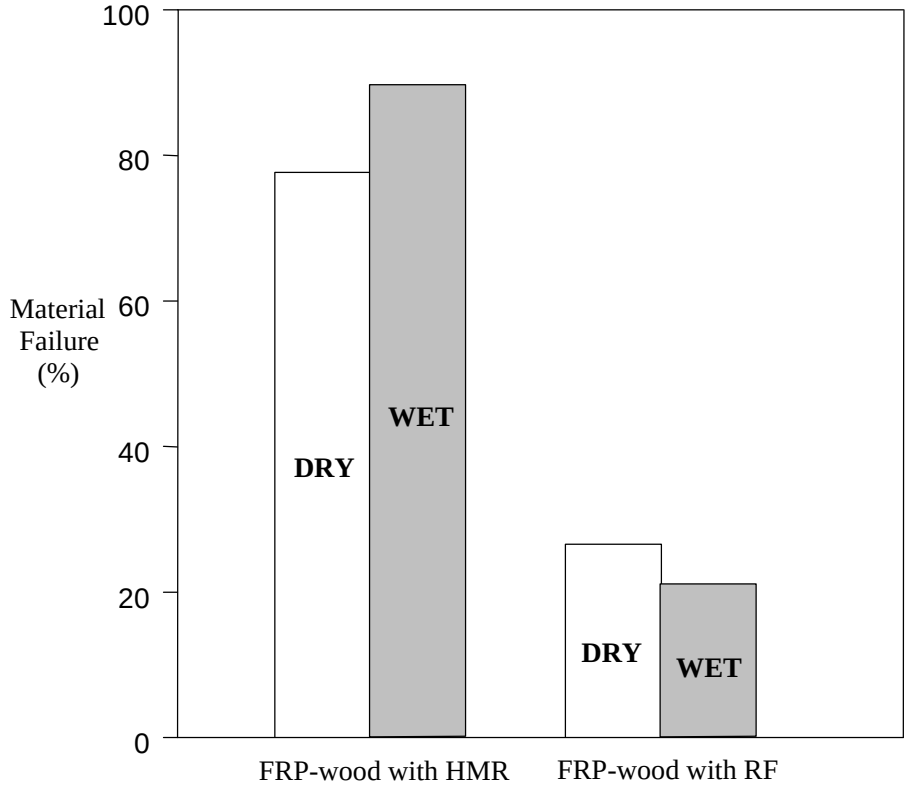

Figure 3.8 Material failure comparison for Epoxy FRP-wood specimens

Table 3.15. Moisture effects on percent material failure for Epoxy FRP-wood specimens

FRP-wood (HMR: dry)	FRP-wood (HMR: wet)	Difference(*)
77.6%	89.7%	-15.59%
FRP-wood (RF: dry)	FRP-wood (RF: wet)	Difference
26.6%	21.1%	20.68%

(*)based on dry condition

Table 3.16. Coupling agents (primer) effects on percent material failure for Epoxy FRP-wood specimens

FRP-wood (HMR: dry)	FRP-wood (RF: dry)	Difference(*)
77.6%	26.6%	65.72%
FRP-wood (HMR: wet)	FRP-wood (RF: wet)	Difference
89.7%	21.1%	76.48%

(*)based on HMR condition

3.6 Discussion of Test Results

3.6.1 Phenolic FRP-Wood

A discussion of the test results is presented, based on the following two observations:

(1) For the dry samples, the shear strength for wood-wood is 90% higher than for Phenolic FRP-wood (Table 3.6), while the percent material or cohesive failures are nearly identical for both types of samples (about 81% in Table 3.7).
(2) For the wet samples, the shear strength for wood-wood is 10% lower than for Phenolic FRP-wood (Table 3.6), but the percent material failure for wood-wood is 50% lower than for Phenolic FRP-wood (Table 3.7).

The results obtained for both dry and wet Phenolic FRP-wood samples in relation to wood-wood samples are due mainly to the nature of the failure modes observed. The failure for the Phenolic FRP-wood samples occurred primarily in the CSM layer of the FRP composite, and therefore, the response of these samples was governed by the CSM in-plane or interlaminar shear strength, which is typically a relatively low value. Not only are the dry and wet shear strengths nearly identical for dry and wet Phenolic FRP-wood samples, but the average value is coincidentally close to the shear strength for wet wood-wood samples.

This indicates that the interlaminar shear strength of the CSM, which was about the same for wet or dry samples, is nearly identical to the wet wood-wood bond interface strength; the failure of Phenolic FRP-wood samples was characterized by mixed-mode failure of about 13.2% adhesive-failure and 86.8% cohesive-failure (76% in CSM and 10.8% in wood; Table 3.7).

This distinct failure mode for the Phenolic FRP-wood samples resulted in a consistent percent material or cohesive failure for dry and wet conditions (81% and 87%, respectively). However, for the Phenolic FRP-wood samples both the dry and wet shear strengths, which are about equal, are about one half of the strength of wood-wood dry specimens. The extent of the influence of moisture on the Phenolic FRP-wood interface could not be determined because of the preferential failure of the CSM layer before reaching either the wet wood strength or adhesive strength.

3.6.2 Epoxy FRP-wood

A discussion of the test results is presented, based on the following two observations:

(1) For the dry samples, the shear strength for Epoxy FRP-wood with HMR is 8.4% higher than for Epoxy FRP-wood with RF (Table 3.14), while the percent material or cohesive failure for Epoxy FRP-wood with HMR is about three times larger than for Epoxy FRP-wood with RF (Table 3.16).
(2) For the wet samples, the shear strength for Epoxy FRP-wood with HMR is 28.9% higher than for Epoxy FRP-wood with RF (Table 3.14), also the percent material failure for Epoxy FRP-wood with HMR is 76.5% larger than for Epoxy FRP-wood with RF (Table 3.16).

The favorable results obtained for both dry and wet Epoxy FRP-wood samples with HMR in relation to Epoxy FRP-wood samples with RF is due mainly to the coupling agent

effects on the bond strength. The failure for the Epoxy FRP-wood samples with HMR occurred primarily in the wood layer, and therefore, the response of these samples was governed by the shear strength of wood. The failure for the Epoxy FRP-wood samples with RF mainly happened within the bond interface between the Epoxy FRP and wood, which resulted in lower shear strength and percent material failure, especially for wet samples. This distinct failure mode for the Epoxy FRP-wood samples with HMR resulted in a consistent percent material or cohesive failure for dry and wet conditions (77.8% and 89.7%, respectively). For the Epoxy FRP-wood samples with HMR, it is noted that the percent material failure (about 78% for dry and 90% for wet) is close to the AITC-specified allowable value of 80% wood failure.

3.7 Conclusions

3.7.1 Phenolic FRP-Wood

The shear strength and percent material failure for adhesively bonded wood-wood and Phenolic FRP-wood interfaces were evaluated using a modified ASTM D 905 test method. The shear strength of wood-wood samples was 1956 psi for dry (12% MC) and 887 psi for wet (moisture saturated), while the percent wood or cohesive failure was 81% and 58%, respectively. Due to the lower in-plane (interlaminar) shear strength of the CSM layer on the bonding surface of the Phenolic FRP composite, the Phenolic FRP-wood samples mainly failed in the CSM layer and produced similar results under both dry (1033 psi and 81% CSM failure) and wet (976 psi and 76% CSM failure and 10.8 wood failure) conditions. Coincidentally, the dry and wet strength of the interface, which occurred mainly in the CSM layers, for Phenolic FRP-wood samples was nearly equal to the wet wood-wood strength, and due to the CSM-dominated failure of Phenolic FRP-wood samples, the effect of moisture on the interface was not fully evaluated. The performance tests conducted by the modified ASTM D 2559 (Chapter 2) and D 905 can be used to study the effects of bonding parameters (pressure, primer type, assembly conditions) on bond strength, and

obtain apparent interface shear strength under dry and wet conditions for Phenolic FRP-wood joints provided by secondary bonding.

3.7.2 Epoxy FRP-Wood

The shear strength and percent material failure for Epoxy FRP-wood interfaces were evaluated using a modified ASTM D 905 test method. The Epoxy FRP-wood interface was manufactured by the filament winding process, and two distinct primers (HMR and RF) were applied on the wood surface before wrapping the Epoxy FRP around the wood core. The dry Epoxy FRP-wood samples with HMR primer exhibited high shear strength and higher percent material failure. Due to the HMR enhancement of bond strength at the interface, the Epoxy FRP-wood samples with HMR failed mainly in the wood layer and produced similar results under both dry and wet conditions. However, the shear strength results obtained for Epoxy FRP-wood samples with RF showed a larger variation (see Table 3.12), and the percent material failures were relatively lower compared to those for Epoxy FRP-wood samples with HMR. As indicated in Tables 3.14 and 3.16, the Epoxy FRP-wood interface with HMR coupling agent performed well, as determined by the block-shear dry and wet tests, and the results were consistent with those obtained by the modified ASTM D 2559 tests (see Section 2.6.2.1). The performance tests conducted by the modified ASTM D 2559 and D 905 can be used to study the coupling agent effects on bond strength and obtain apparent interface shear strength under dry and wet conditions for Epoxy FRP-wood assemblies produced by filament winding.

CHAPTER 4

DESIGN APPROACH FOR CDCB SPECIMENS

4.1 Introduction

The conventional method for determining the strength of an adhesive interface under Mode-I fracture is by testing Double Cantilever Beam (DCB) specimens under cleavage loading (Carlsson and Pipe 1987). The critical strain energy release rate, G_{Ic}, which is a measure of the fracture toughness of an interface bond under Mode-I loading, is given by

$$G_{Ic} = \frac{P_c^{\,2}}{2b}\frac{dC}{da} \qquad (4.1)$$

where, P_c = critical load, b = width of the specimen, and dC/da = rate of change of compliance C with respect to crack length a. The testing for fracture toughness of interface bonds obtained with conventional DCB specimens requires simultaneous measurements of critical load and crack length for each load step. The value of dC/da in Equation 4.1 depends on the accuracy of the crack length measurement, which is generally a difficult task. The measurement of crack length can be avoided by contouring the DCB specimen, such that dC/da is a constant, and in this case, the specimen is known as the Contoured Double Cantilever Beam (CDCB). To use the CDCB specimen for interface bonds of dissimilar adherends, it is convenient to use constant-thickness adherends bonded to contoured portions made of a material that is easy to shape, such as wood-based materials. Due to the relative complexity of defining the shape of a CDCB specimen, a numerical method based on the Rayleigh-Ritz solution was recently developed (Davalos, Raman and Qiao 1997) to design the shape of the test specimens. For a given crack length,

the CDCB specimen is modeled as a cantilever beam to obtain its compliance; the expression for compliance of the specimen is derived using a Rayleigh-Ritz solution and defined as a function of the crack length and the slope of the contour. A first-order shear deformation theory (Davalos and Raman 1996) is used to account for shear deformation, which is important for materials such as FRP and wood.

Based on the compliance derived from the Rayleigh-Ritz solution, a methodology for the design of the contour of a CDCB specimen was proposed by Davalos, Raman and Qiao (1997). A graphical representation of the geometric parameters used in defining the CDCB specimen is shown in Figure 4.1, where the constant height of the base adherend is h_b, and the bonded contoured portion of the CDCB specimen is assumed to have an initial constant height h_1 for an initial crack length a_1. This initial constant height should provide sufficient material to accommodate loading fixtures, such as an attached hinge or a pin through the specimen. The expression for *dC/da* is obtained by differentiating the expression for the compliance with respect to the crack length. For each discrete crack length ($a \geq a_1$), a linear shape of the contour is assumed. The following step-by-step procedure summarizes the methodology for the design of the contoured specimen:

1) Compute the compliance of the CDCB specimen by the Rayleigh Ritz method (Davalos, Raman and Qiao 1997) as a function of crack-length and slope: $C = C(a, p)$.
2) Differentiate the compliance function to obtain *dC/da*.
3) Evaluate *dC/da* for a discrete value of *a*, say $a = a_2$ for $a_2 > a_1$ (Figure 4.1).
4) Equate *dC/da*, evaluated at a discrete crack-length, to a predefined constant value *K* to solve for the slope, say $p = p_2$. That is, let $\frac{dC}{da}(a_2, p_2) = K$ and solve for p_2.
5) Then, $h(a) = h_1 + p_2(a-a_1)$ for $a > a_1$, say $h_2 = h_1 + p_2 (a_2 - a_1)$.
6) Repeat steps 1 through 5 to solve for p_3.

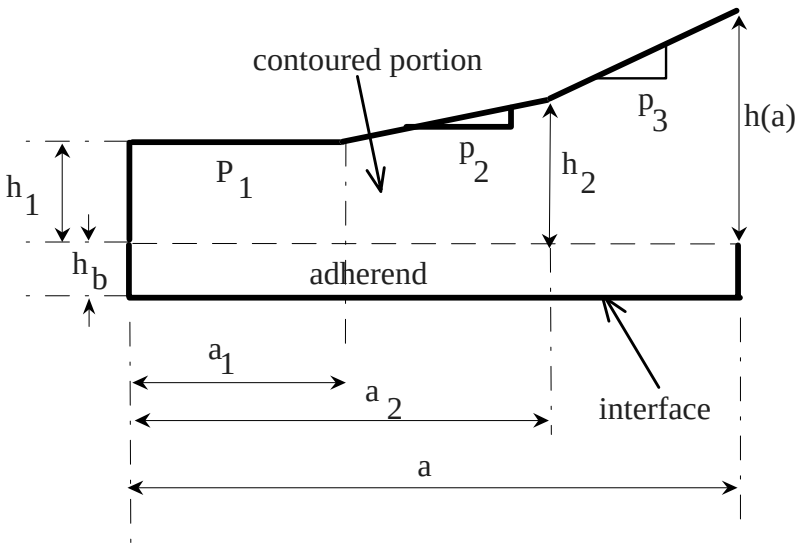

Figure 4.1. Geometric parameters of the contour of the CDCB specimen

This procedure is repeated for each incremental crack-length until the contour for the entire length of the CDCB specimen is obtained. When the interface of dissimilar materials is considered, the contour has to be developed for each adherend. This is since the stiffness of the adherends would be different, and the shape of the contour would be different on either side of the interface bond in order to achieve the same rate of compliance change for each half of the specimen.

The exact contour obtained from the above procedure has a convex shape (Davalos, Raman and Qiao 1997), obtained by fitting a polynomial function through the discritized heights. However, the effort and cost involved in accurately manufacturing such a complex geometry can be significant, particularly since it is often necessary to test several specimens to obtain a good estimate of the fracture toughness of the interface. The exact contour can be simplified by a linear approximation function obtained through regression of the discrete heights (Davalos, Raman and Qiao 1997). Then, through experimental and analytical investigations of the compliance rate change of the simplified linear-slope CDCB specimens (Davalos et al. 1998), the linearity of the compliance crack-length relationship of linear-slope CDCB specimens can be verified for specific ranges of crack lengths.

The design of an exact contoured specimen is a time-consuming process and involves several design steps (stated earlier in Section 4.1). To simplify the above design approach, a modified method is introduced next.

4.2 Design of CDCB specimens by the Rayleigh-Ritz Method

A numerical approach for the design of complex shapes of CDCB specimen by the Rayleigh-Ritz method has been developed by Raman (1995). In this method, the CDCB specimen is modeled as a cantilevered beam to obtain its compliance for a given cracked length, and First-Order Shear Deformation Theory (FSDT) is used to account for shear deformation, which is important for anisotropic materials such as wood and composites. To design a specimen with a constant compliance rate change, the exact contour shape of the specimen should be a relatively linear function with respect to crack length as evidenced by Davalos, Raman and Qiao (1997). Also, a constant compliance rate change can be obtained for a linear-tapered specimen only over a certain crack length range based on experimental and numerical studies (Finite element and Rayleigh-Ritz methods) (Davalos, et al. 1998).

The formulation presented in this section is nearly identical to that given by Raman (1995) and Davalos, Raman and Qiao(1997), and it is reproduced in this thesis for completeness and future use by other investigators.

The total strain energy of a beam element is given by

$$U = \frac{1}{2}\int_V \sigma_{ij}\,\varepsilon_{ij}\,dV \qquad (4.2)$$

where, σ_{ij}, ε_{ij} are the stresses and strains, respectively, and V is the volume of the element. The kinematics of the beam consistent with FSDT is given by

$$u = -y\ \phi_x(x)$$
$$v = v(x) \tag{4.3}$$

where, ϕ_x is the rotation of the normal to the midplane about the *z* axis, and *v* is the displacement in the *y* coordinate. The strain-displacement relations resulting from the kinematics assumed above are

$$\varepsilon_x = -y\ \phi_{x,x}$$
$$\gamma_{xy} = v_{,x} - \phi_x \tag{4.4}$$

where, a comma denotes differentiation with respect to the variable following it. The stress-strain relations are defined by

$$\sigma_x = E\ \varepsilon_x$$
$$\sigma_{xy} = G\ \gamma_{xy} \tag{4.5}$$

Substituting equations (4.4) and (4.5) into equation (4.2), the following expression is obtained:

$$\begin{aligned} U &= \frac{1}{2}\int_0^a \int_A E\, y^2 \phi_{x,x}^{\ 2} + G(v_{,x} - \phi_x)^2\ dx\, dA \\ &= \frac{1}{2}\int_0^a \left[\left(\int_A Ey^2 dA\right)\phi_{x,x}^{\ 2} + \left(\int_A GdA\right)(v_{,x} - \phi_x)^2 \right] dx \\ &= \frac{1}{2}\int_0^a \left[EI\,\phi_{x,x}^{\ 2} + \kappa GA(v_{,x} - \phi_x)^2 \right] dx \\ &= \frac{1}{2}\int_0^a \left[D(x)\phi_{x,x}^{\ 2} + F(x)(v_{,x} - \phi_x)^2 \right] dx \end{aligned} \tag{4.6}$$

where, *I* is the moment of inertia of the cross section, *A* is the area of the cross section, κ is the transverse shear correction factor, and *a* represents the total cracked length of the

CDCB specimen (length of the cantilever portion). $D(x) = EI$ and $F(x) = \kappa GA$, are the bending and shear stiffnesses of the CDCB specimen, respectively.

To use the CDCB specimen for interface bonds of dissimilar adherends, it is convenient to maintain a constant thickness of the adherends and to attach them to contoured portions made of a material that is easy to shape, such as wood. This approach can simplify the fabrication of the CDCB specimen. The following describes the procedure to determine the effective beam bending (*D*) and shear stiffness (*F*) for one-half of the CDCB specimen, where an adherend of constant cross section is attached to a contoured portion made of a different material. The concept of a transformed cross section is used to obtain the effective bending and shear stiffness of the CDCB specimen consisting of a two-layer laminate (Figure 4.2a), where the adherend is converted to an equivalent contour material (Figure 4.2b). The terms $D(x) = EI$ and $F(x) = \kappa GA$ that respectively represent the beam bending and shear stiffness in equation (4.6) are expressed as

$$D(x) = b\sum E_i\left(t_i \bar{y}_i^{\,2} + \frac{t_i^{\,3}}{12}\right) \quad ; \quad F(x) = b\kappa\sum G_i t_i \;\; i = 1,2 \tag{4.7}$$

where, E_i and G_i are the elastic and shear moduli of the *i*th layer, t_i is the thickness of the *i*th layer of the cross section ($t_1 = h_c$ and $t_2 = h_b$, Figure 4.2), and $\bar{y}_i$ is the distance of the centroidal axis of the *i*th layer from the neutral axis of the cross section ($\bar{y}_1 = \bar{y}_c$ and $\bar{y}_2 = \bar{y}_b$, Figure 4.2). The neutral axis of bending is defined by eliminating the bending-extension coupling coefficient ($B = 0$). For convenience in this study, the neutral axis is defined in terms of the transformed section (Fig. 4.2b) as

$$y_{na} = \frac{m h_b^{\,2} + h_c^{\,2} + 2 h_b h_c}{2(h_c + m h_b)} \tag{4.8}$$

where, $m=E_b / E_c$, and the subscripts *c* and *b* refer respectively to the contour and base adherend of the CDCB specimen.

The expressions for $\bar{y}_i$ of the layers are given by

$$\bar{y}_1 = \bar{y}_c = \frac{m(h_b^{\,2} + h_b h_c)}{2(h_c + m h_b)} \quad ; \quad \bar{y}_2 = \bar{y}_b = \frac{h_c^{\,2} + h_b h_c}{2(h_c + m h_b)} \tag{4.9}$$

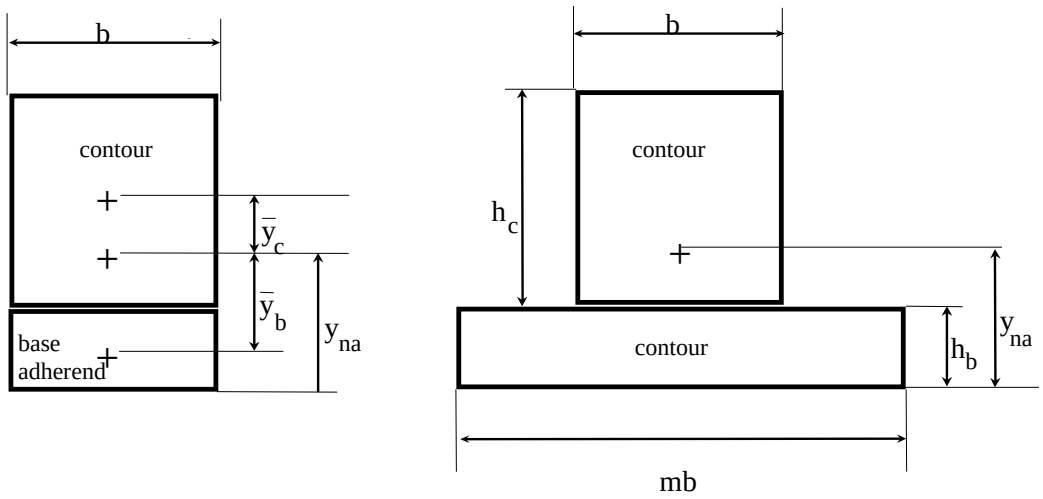

Fig. 4.2a Actual cross section **Fig. 4.2b Transformed cross section**

Substituting equation (4.9) into equation (4.7) and simplifying, the stiffnesses are defined as

$$D(x) = EI = \frac{bE_c}{12}\left[\frac{3mh_c h_b(h_c + h_b)^2}{h_c + mh_b} + h_c^{\,3} + m h_b^{\,3}\right]$$
$$F(x) = \kappa GA = b\kappa(G_b h_b + G_c h_c) \tag{4.10}$$

Assuming a linearlized contour shape,

$$\begin{aligned} h_c &= (h_o + kx) = h_c(x) \\ h_b &= constant \end{aligned} \tag{4.11}$$

where k is the slope of the linear tapered specimen. From equation (4.10), the beam bending and shear stiffnesses are expressed as functions of x and k:

$$\begin{aligned} D(x,k) &= \frac{bEc}{12}\left[\frac{3m(h_o+kx)h_b(h_o+kx+h_b)^2}{h_o+kx+mh_b} + (h_o+kx)^3 + mh_b{}^3\right] \\ F(x,k) &= bK\left[G_b h_b + G_c(h_o+kx)\right] \end{aligned} \tag{4.12}$$

The Rayleigh Ritz solution requires a representation of the variation of the displacement and rotational degrees of freedom by interpolation functions over the entire domain of the system. Hence, the displacement and rotational degrees of freedom are approximated as

$$\begin{aligned} v(x) &= v_i \; N_i(x) \\ \phi_x(x) &= \phi_i \; M_i(x) \qquad i = 1,2,..n \end{aligned} \tag{4.13}$$

where, n is chosen to achieve a desired degree of accuracy, v_i and ϕ_i are the unknown coefficients of the variables, and $N_i(x)$ and $M_i(x)$ are the interpolation functions satisfying the essential boundary conditions, namely $v(a) = \phi_x(a) = 0$.
Algebraic functions satisfying these boundary conditions are given by

$$N_i(x) = M_i(x) = (a - x)^i \tag{4.14}$$

Substituting equations (4.12) and (4.13) in equation (4.6), the strain energy can be written as

$$U = \frac{1}{2}\int_0^a D(x,k)(\phi_i M_{i,x} \phi_j M_{j,x})\,dx$$

$$+\frac{1}{2}\int_0^a F(x,k)(v_i N_{i,x} - \phi_i M_{i,x})(v_j N_{j,x} - \phi_j M_{j,x})\,dx \qquad (4.15)$$

$$i, j = 1,2,..n$$

Equation (4.15) is rearranged in matrix form and is expressed as

$$U = \frac{1}{2}\int_0^a D(x,k)[\phi_i][M_{i,x} M_{j,x}]\{\phi_j\}\,dx$$

$$+\frac{1}{2}\int_0^a F(x,k)[v_i][N_{i,x} N_{j,x}]\{v_j\}\,dx$$

$$-\int_0^a F(x,k)[v_i][N_{i,x} M_j]\{\phi_j\}\,dx \qquad (4.16$$

$$+\frac{1}{2}\int_0^a F(x,k)[\phi_i][M_i M_j]\{\phi_j\}\,dx$$

$$i, j = 1,2,..n$$

After grouping similar terms, equation (4.16) is written in a concise form as

$$U = \frac{1}{2}[\phi_i][[A_1] + [A_3]]\{\phi_j\} + \frac{1}{2}[v_i][A_4]\{v_j\} - [v_i][A_2]\{\phi_j\} \qquad (4.17)$$
$$i, j = 1,2,..n$$

where,

$$A_{1ij} = \int_0^a D(x,k) M_{i,x} M_{j,x}\, dx$$

$$A_{2ij} = \int_0^a F(x,k) N_{i,x} M_j\, dx$$

$$A_{3ij} = \int_0^a F(x,k) M_i M_j\, dx$$

$$A_{4ij} = \int_0^a F(x,k) N_{i,x} N_{j,x}\, dx$$

$$i, j = 1,2,..n$$

The work done by the applied concentrated tip-load at $x = 0$ is given by

$$W = P\, v(0)$$
$$= [v_i]\{R\},\ where \{R\} = P\{N_i(0)\} \quad i = 1,2,..n \qquad (4.18)$$

The total potential energy can be expressed using equations (4.17) and (4.18) as

$$\Pi = \frac{1}{2}[\phi_i][[A_1] + [A_3]]\{\phi_j\} + \frac{1}{2}[v_i][A_4]\{v_j\} - [v_i][A_2]\{\phi_j\} - [v_i]\{R\} \qquad (4.19)$$
$$i, j = 1,2,..n$$

The minimization of the total potential energy with respect to the unknown displacement vectors, yields the expressions

$$\begin{aligned} \frac{\partial \prod}{\partial [v_i]} &= [A_4]\{v_j\} - [A_2]\{\phi_j\} - \{R\} = 0 \\ \frac{\partial \prod}{\partial [\phi_i]} &= -[A_2]^T\{v_j\} - [[A_1] + [A_3]]\{\phi_j\} = 0 \end{aligned} \tag{4.20}$$

From equation (4.20), the variables $\{v_i\}$ and $\{\phi_i\}$ are determined by solving the following simultaneous equations:

$$\begin{Bmatrix} \{v_i\} \\ \{\phi_i\} \end{Bmatrix} = \begin{bmatrix} [A_4] & -[A_2] \\ -[A_2]^T & [[A_1] + [A_3]] \end{bmatrix}^{-1} \begin{Bmatrix} \{R\} \\ \{0\} \end{Bmatrix} \tag{4.21}$$

The solution of equation (4.20) yields the displacement parameter $\{v_i\}$, which is substituted in equation (4.13) to evaluate the displacement function $v(x)$. Finally, the compliance is obtained by computing $v(x)$ at $x = 0$, for a unit tip-load.

For a linear tapered specimen loaded with a unit tip-load, the compliance is expressed as

$$C = v(0) = f_C(a,k) \tag{4.22}$$

where, k is the linear slope of specimen, and a is the length of cantilever beam. Further, the compliance rate change can be derived as

$$\frac{dC}{da} = \frac{df_c(a,k)}{da} \tag{4.23}$$

Equations (4.22) and (4.23) are the expressions for compliance and compliance rate change, and they are functions of the length and slope of cantilever beam.

The above computational procedure involves symbolic mathematical operations, such as matrix inversion and differentiation, and therefore, the solution is obtained using the mathematics symbolic manipulator MAPLE (Char B.W. et al. 1991). The MAPLE programs used are included in Appendix A and Appendix B.

4.3 Simplified Design Procedure and Parametric Study

In this section, a simplified numerical approach for the design and analysis of a linearlized CDCB specimen is developed. The basic idea is to simplify the procedures presented above and to express the compliance rate change in terms of the slope of the linearlized contour and cantilever beam length (or crack length) using the Rayleigh-Ritz method. The steps involved in the modified Rayleigh Ritz solution to derive the expression for the compliance of the CDCB specimen in terms of the tapered specimen slope (k) and the crack length (a) are described in this section.

For a given constant $\frac{dC}{da}$, the slopes (k) for various cantilever (crack) lengths (a) can be determined; these slopes can be linearlized through linear regression, and this "global and approximate" linear slope can be used as the design slope for the specimen. Based on this simplified design, which expresses the compliance rate change in terms of crack length and specimen slope, a two-step design approach is provided. Further, a parametric study based on the simplified Rayleigh-Ritz method is conducted; the variation of slopes with respect to compliance rate changes and variation of compliance rate change for various slopes are investigated.

4.3.1 Two-step design procedure

The relatively complicated design procedure of (Section 4.1) is simplified and reduced to a two-step procedure:

1) From Equation 4.23, for a given constant dC/da, compute the slopes k for various crack lengths.

2) Linearize the set of slopes obtained in (1), and define it as the specimen global slope; further, the *dC/da* used in (1) becomes the specimen compliance rate change.

4.3.2 Parametric study

Following the above two-step design procedure, a parametric study is conducted to study the degree of accuracy of the design.

First, contours were designed with constant *dC/da* values, and the slopes (*k)* at each crack length were obtained. The thickness of the contours included 0.750 in, 1.000 in, and 1.250 in (see Figure 4.3 through Figure 4.5). Second, the linearlized slope (*k)* from each specimen thickness was used to solve for the dC/da at each crack length of the specimen (see Figure 4.6 through Figure 4.8). The linearlized slope, *k,* and compliance rate change, *dC/da*, data are respectivelyshown in Table 4.1 and Table 4.2.

The first step of the parametric study is to design a contour with constant *dC/da* value and then plot the corresponding slopes vs. crack length. This is shown in Figure 4.3 through Figure 4.5 (Contour thickness equals 0.750 in, 1.000 in, and 1.250 in). Next, the slope functions are linearlized, and the best fit line over a crack length range is chosen to be the design slope of the contour. The linearlized global slope for each contour is given in Table 4.1, with the optimum value shown in bold type.

Following the two-step design procedure, the parametric study is continued by calculating the dC/da at each crack length using the global linear slope from the first step. This is shown in Figure 4.6 through Figure 4.8 (Contour thickness equals 0.750 in, 1.000 in, and 1.250 in). Next, the *dC/da* curve is linearlized and the best fit over a crack length range is the designed dC/da of the contour. The linearlized *dC/da* value for each contour is given in Table 4.2, with the optimum value shown in bold type.

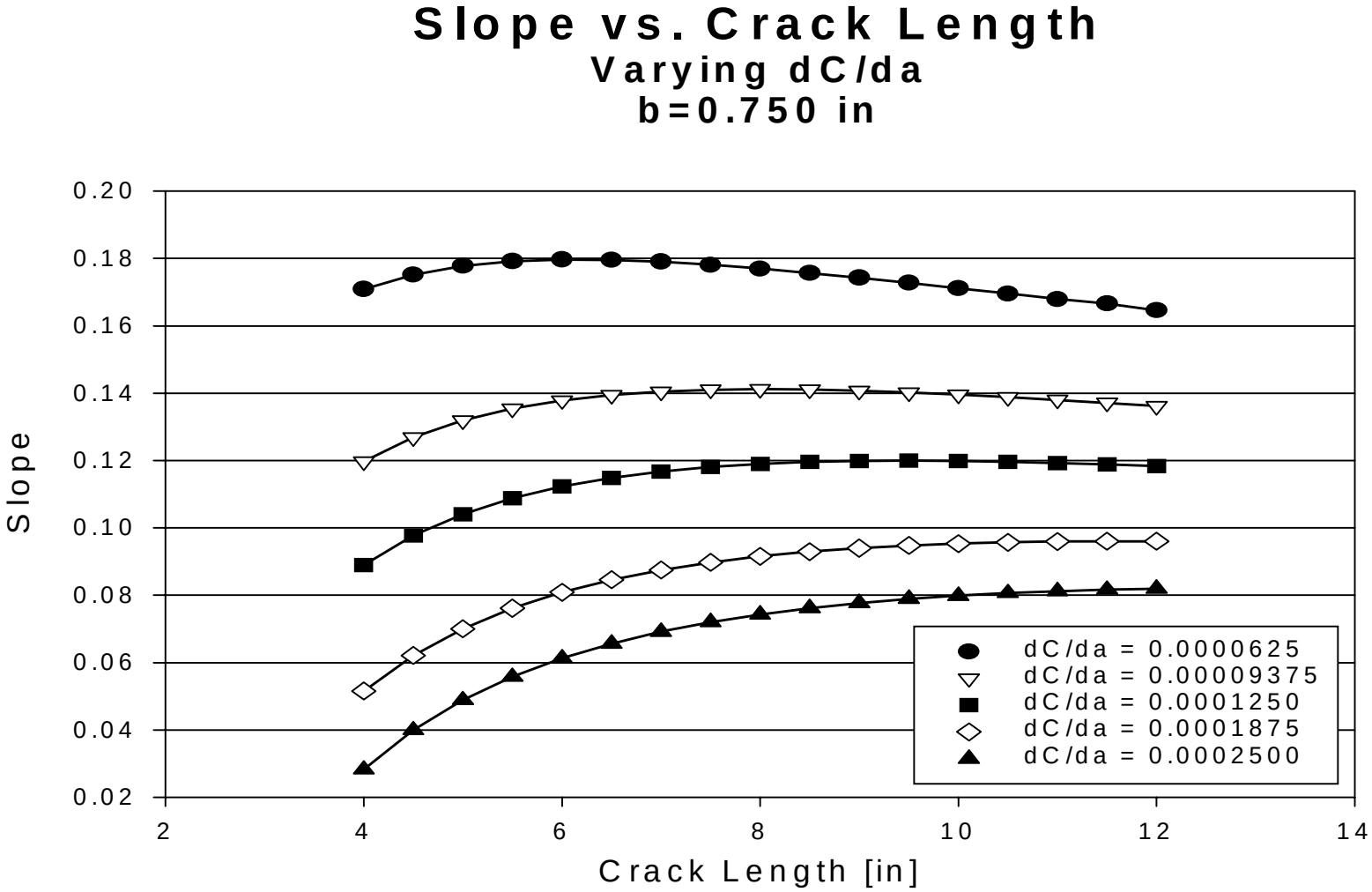

Figure 4.3. Slope vs Crack length (b = 0.750 in)

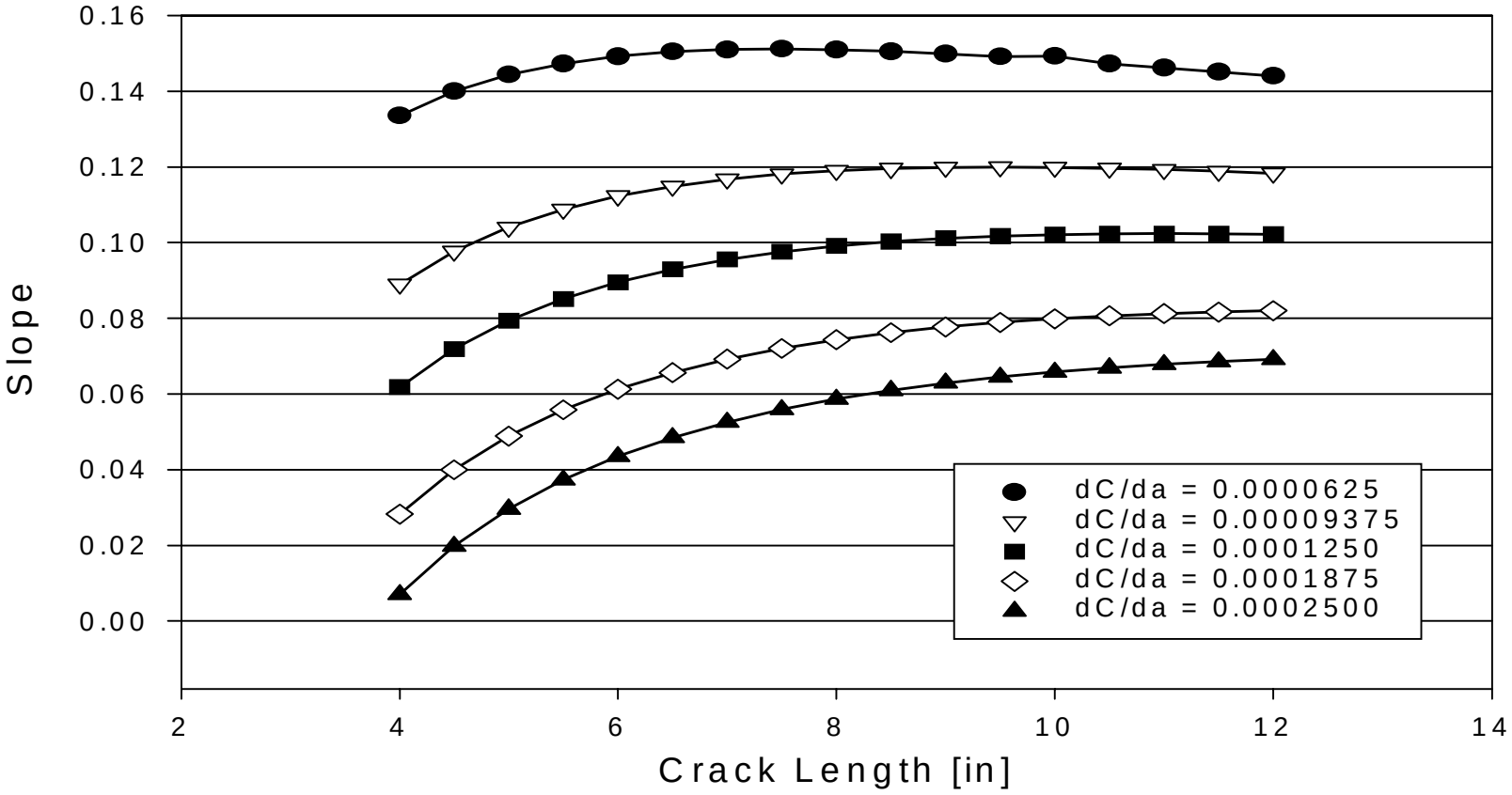

Figure 4.4. Slope vs Crack length (b = 1.000 in)

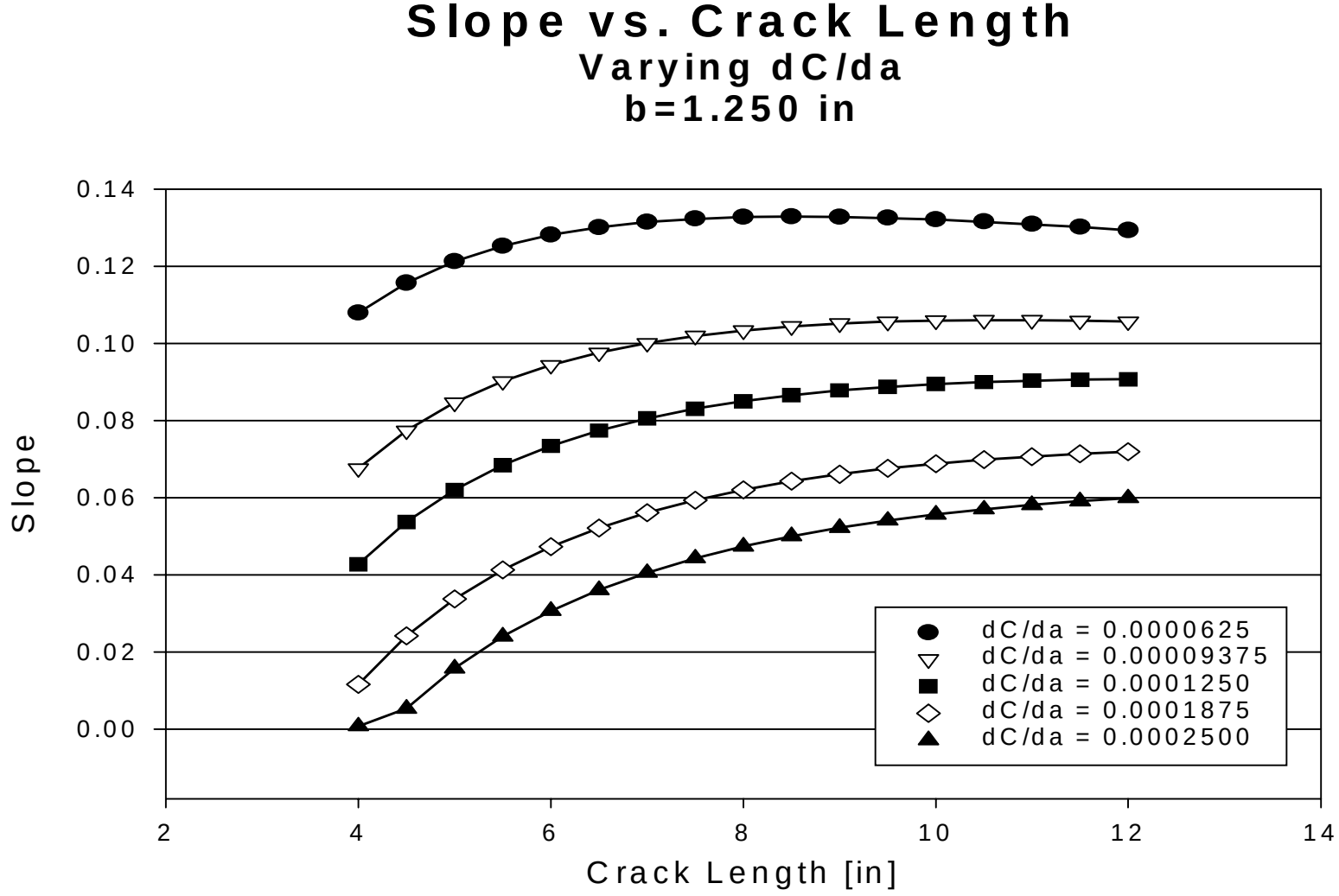

Figure 4.5. Slope vs Crack length (b = 1.250 in)

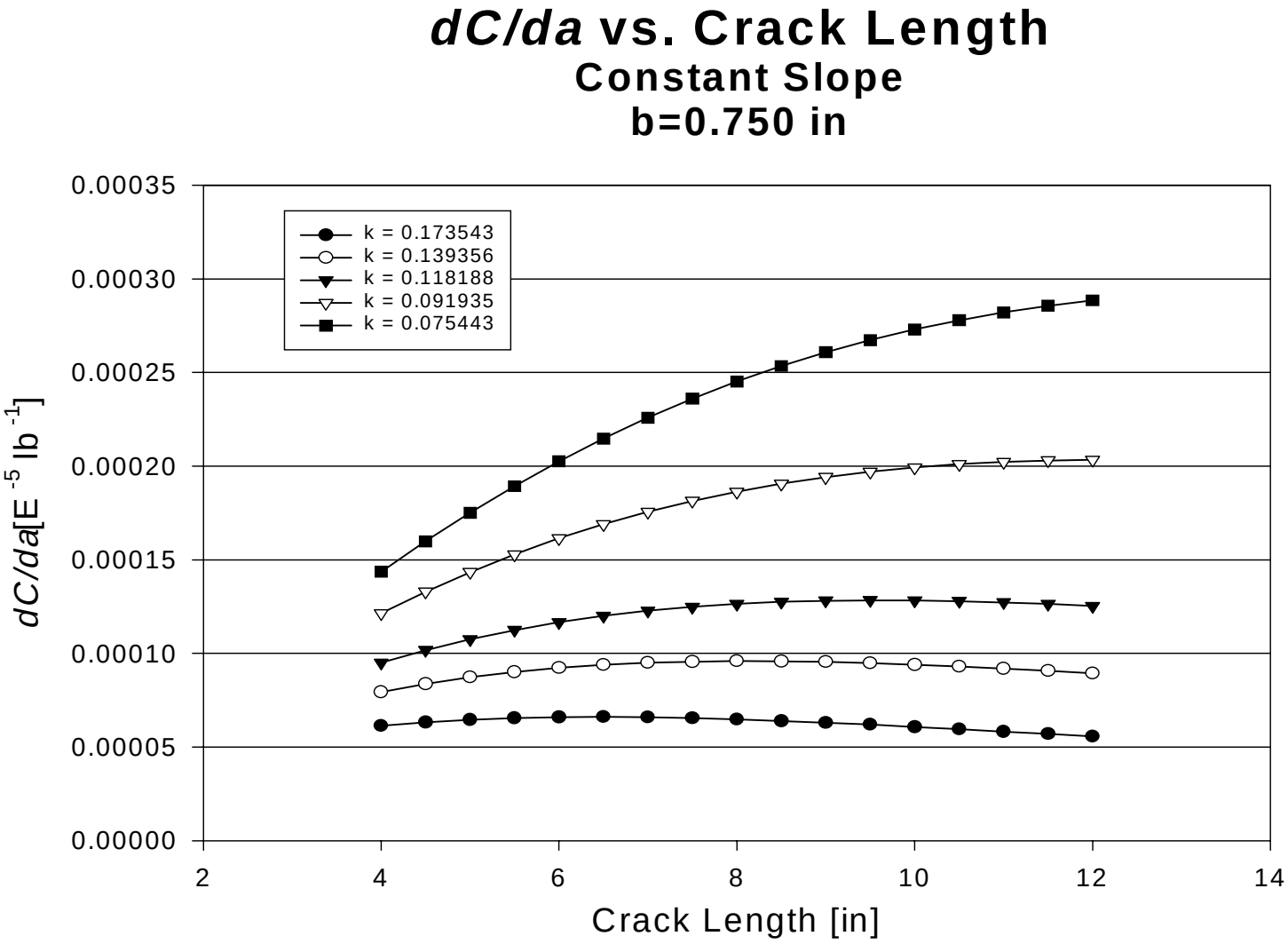

Figure 4.6. *dC/da* vs Crack Length (b = 0.750 in)

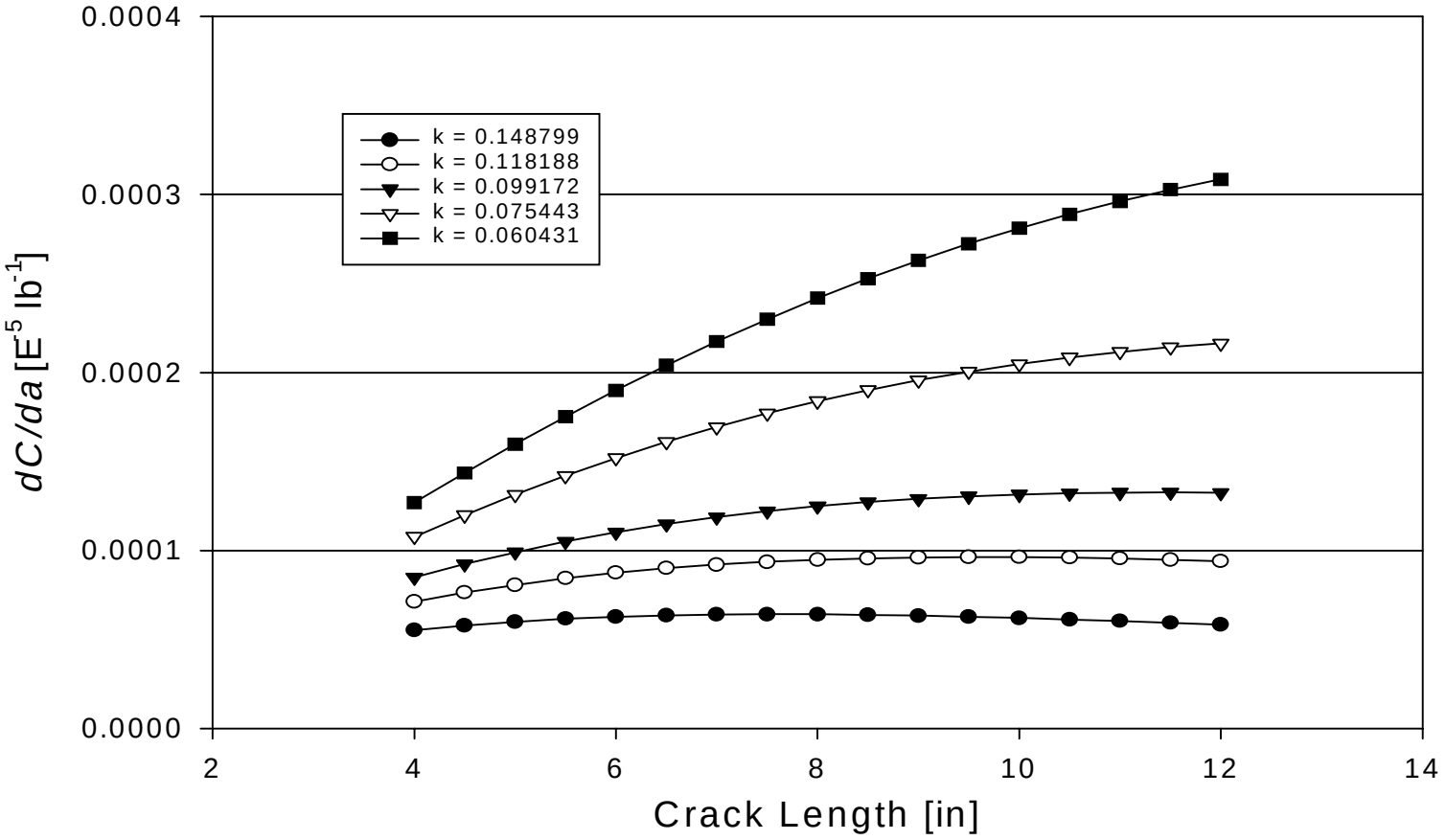

Figure 4.7. *dC/da* vs Crack Length (b = 1.000 in)

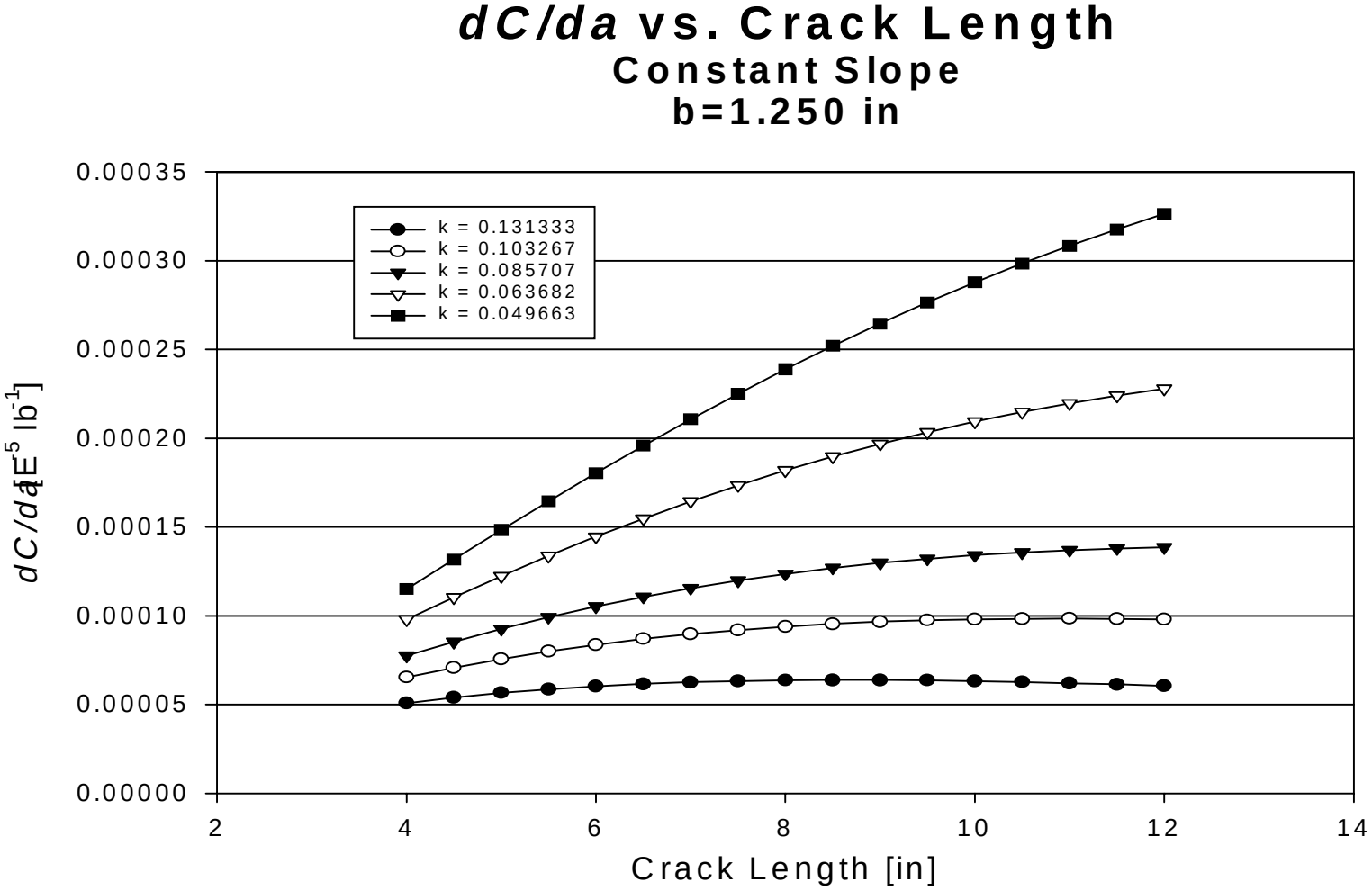

Figure 4.8. ***dC/da*** **vs Crack Length (b = 1.250 in)**

Table 4.1 Linearlized slopes with constant *dC/da*

CDCB Thickness [in]	*DC/da* [E $^{-5}$ lb $^{-1}$]	Slope, k* [in/in] (COV %)
0.750	6.25	0.17354 (COV = 2.98%)
	9.375	**0.13936 (COV = 1.18%)**
	12.50	0.11818 (COV = 1.94%)
	18.75	0.09193 (COV = 5.34%)
	25.00	0.07544 (COV = 8.78%)
1.000	**6.25**	**0.14880 (COV = 1.59%)**
	9.375	0.11819 (COV = 1.94%)
	12.50	0.09917 (COV = 4.19%)
	18.75	0.07544 (COV = 8.78%)
	25.00	0.06043 (COV = 13.56%)
1.250	**6.25**	**0.13133 (COV = 1.13%)**
	9.375	0.10327 (COV = 3.62%)
	12.50	0.08571 (COV = 6.49%)
	18.75	0.06368 (COV = 12.34%)
	25.00	0.04966 (COV = 18.78%)

* Crack lengths from 6 in to 12 are considered

Table 4.2 Linearlized *dC/da* for constant slope, *k*

CDCB Thickness [in]	Slope, k* [in/in]	*dC/da* [E^{-5} lb^{-1}] (COV %)
0.750	0.173543	6.22 (COV = 5.85%)
	0.139356	**9.36 (COV = 2.24%)**
	0.118188	12.54 (COV = 2.86%)
	0.091935	18.95 (COV = 7.34%)
	0.075443	25.48 (COV = 11.05%)
1.000	0.148798	6.23 (COV = 3.13%)
	0.118188	**9.40 (COV = 2.86%)**
	0.099172	12.60 (COV = 5.92%)
	0.075442	19.11 (COV = 11.05%)
	0.060431	25.75 (COV = 15.03%)
1.250	**0.131333**	**6.25 (COV = 1.92%)**
	0.103267	9.44 (COV = 5.17%)
	0.085707	12.67 (COV = 8.67%)
	0.063682	19.26 (COV = 14.11%)
	0.049663	26.02 (COV = 18.30%)

* Crack lengths from 6 in to 12 are considered

As seen from Table 4.1 and Table 4.2 of this parametric study, the optimum thickness and *dC/da* values for the design of CDCB specimens are 1.250 inch and 6.25 E^{-5} lb^{-1}, respectively.

CHAPTER 5

FRACTURE TOUGHNESS OF DRY/WET FRP-WOOD BONDED INTERFACE

5.1 Introduction

Once the performance of the bonded interface is established by the ASTM D 2559 and ASTM D 905 standard tests (see Chapters 2 and 3), Contoured Double Cantilever Beam (CDCB) specimens are designed to conduct mode-I fracture tests and obtain fracture toughness data of the interface bonds. In this chapter, bi-layer CDCB specimen are designed by the Rayleigh-Ritz method and used for fracture toughness tests of bonded wood-wood and FRP-wood interfaces. Using linear-slope CDCB specimens, fracture tests are performed for dry and wet specimens to determine critical loads for crack initiation and crack arrest, from which the critical strain energy release rates (G_{Ic}) are evaluated by making use of experimentally-verified constant compliance rate changes over defined crack lengths.

In this chapter, the following five tasks are performed: (1) Material characterization (2) Design of CDCB specimens, (3) Experimental compliance calibration tests, (4) Finite element modeling of specimens and verification of compliance rate change, and (5) Experimental evaluation of fracture toughness of bonded interfaces.

5.2. Materials

5.2.1 Wood materials

The wood materials used for the manufacturing of the Mode-I fracture samples were Red Maple (see Chapter 2, section 2.2.1) and Yellow Poplar Laminated Veneer Lumber (LVL). The Yellow Poplar LVL was produced by Truss Joist MacMillen (TJM), Buckhannon, WV. The LVL was produced to a nominal size of 2" x 10" of which the needed materials were cut. The LVL lay-up consists of 15 layers of Yellow Poplar, each 1/8 inch thick (see Figure 5.1).

Figure 5.1 Lay-up of Linear Veneered Lumber (LVL)

5.2.2 FRP materials

The FRP materials consisted of either E-glass fiber rovings embedded in a Phenolic resin matrix (Figure 2.3, Chapter 2), or E-glass fiber rovings filament wound in an Epoxy matrix (Figure 2.5, Chapter 2). The Phenolic fiber reinforced plastic (Phenolic FRP) composite material was produced by the pultrusion process; whereas the Epoxy fiber reinforced plastic (Epoxy FRP) composite material was produced by the filament winding process. Pultrusion and filament winding are both well controlled and relatively low cost manufacturing processes that are used in the production of FRP composites.

The Phenolic FRP composite contains Continuous Strand Mat (CSM) layers on both outside surfaces which provides a desirable surface texture for obtaining a good adhesive bond interface. The lay-up of the Phenolic FRP laminate is shown in Figure 2.4. The Phenolic FRP surfaces were sanded and cleaned, before bonding, as explained in Section 2.2.2.

The Epoxy FRP composite was filament wound around primed Red Maple beams (Section 2.2.3). The beams were primed with either hydroxymethylated resorcinol (HMR) or Resorcinol Formaldehyde (RF), and the effect of these primers on the Mode-I fracture toughness of the Epoxy FRP-wood interface were investigated under dry and wet conditions.

5.2.3 Material characterization

To design the CDCB specimens for dry and wet conditions, the material properties of the wood and FRP material under the required moisture conditions must be obtained. For instance, the contoured shapes of the moisture saturated samples should be defined accounting for the degraded stiffness properties of the materials due to moisture effects. The change in stiffness properties of the FRP laminates due to moisture ingress can be neglected, and the properties of the dry FRP samples are used for design of both dry and

wet conditions. The stiffness properties of the wood and FRP materials are given in (Table 5.1 through Table 5.4).

Table 5.1 Material properties of Red Maple under dry and wet conditions

	E (10^6 psi)	G (10^6 psi)
Dry Samples	1.989 (COV = 4.57%)	0.181 (COV = 5.40%)
Wet Samples	1.311 (COV = 12.24%)	0.085 (COV = 3.72%)

Table 5.2 Material properties of LVL under dry and wet conditions

	E (10^6 psi)	G (10^6 psi)
Dry Samples	1.958 (COV = 5.96%)	0.063 (COV = 3.81%)
Wet Samples	1.221 (COV = 9.85%)	0.029 (COV = 3.77%)

Table 5.3 Material properties of Phenolic FRP

	E (10^6 psi)	G (10^6 psi)
Experiment	4.410 (COV = 0.55%)	--
Micro/Macromechanics	4.378	0.650

Table 5.4 Material properties of Epoxy FRP

	E (10^6 psi)	G (10^6 psi)
Experiment	0.932 (COV = 5.29%)	--
Micro/Macromechanics	0.947	1.110

The longitudinal-tensile and shear moduli of the Red Maple and LVL were obtained from tension and torsion coupon tests, respectively. For dry tension tests, 12 specimens (Red Maple: 1" x 1/2" x 20"; LVL: 1” x 3/8” x 20”) were conditioned to 12% moisture content (MC) in an environmental chamber; for wet tension tests, another 12 specimens of the same dimensions were immersed in a water bath and subjected to one

cycle of 40-minute vacuum and 40-minute pressure soak in a closed cylinder to saturate the wood samples with more than 100% MC; then, the samples were immediately tested. Similarly, eight dry and eight wet samples (Red Maple: 1-1/2" x 1-1/2" x 17"; LVL: 1-1/2" x 1" x 17") were also prepared for the torsion tests.

Six Phenolic FRP and six Epoxy FRP strips (see Figure 2.4 and Figure 2.5, respectively) were also tested under tension. The tensile modulus was compared with the Micro/macromechanics model prediction (Davalos et al. 1996). The FRP strips were too flexible to be tested in torsion; therefore, the shear modulus predictions by the micro/macromechanics model were used in design. The material properties in Tables 5.1 to 5.4 are used to design the contour shapes of wood-wood, FRP-FRP and FRP-wood CDCB specimens.

5.3 Contour Shapes of the Designed CDCB Specimens

Based on the design procedure given in section 4.3 and the material properties described in section 5.2.3, the contour shapes of the CDCB specimens were designed using the Rayleigh-Ritz method. The compliance rate change (*dC/da*) for the linear-slope CDCB specimens were predicted by the Rayleigh-Ritz (RR) method (Davalos, Raman and Qiao 1997). Also a modified Rayleigh-Ritz (MRR) method was further developed, in which higher-order shape functions for the deflection and rotation were used to replace the quadratic shape functions used in the original Rayleigh-Ritz method. The linear contour shape of the CDCB specimens and values of *dC/da* are given in the following sections.

5.3.1 Wood-Wood

The wood-wood CDCB specimens were designed as described in section 5.3. The lay-ups of the CDCB specimens are given in Figure 5.2.

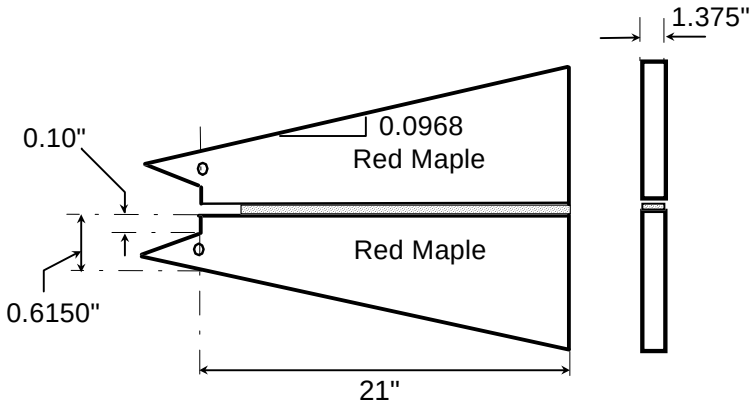

(a) Geometry of wood-wood/Dry Specimen

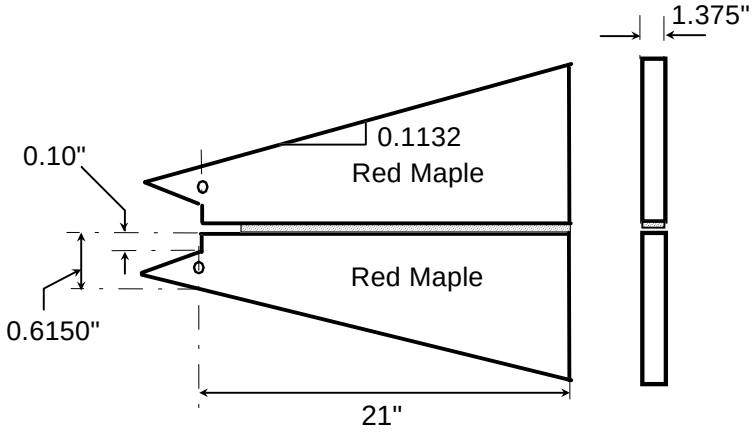

(b) Geometry of wood-wood/Wet Specimen

Figure 5.2. Contour shapes for CDCB wood-wood specimens

5.3.2 Phenolic FRP-Phenolic FRP

The Phenolic FRP-Phenolic FRP CDCB specimens were designed according to the procedures described in Chapter 4. The lay-ups of the CDCB specimens are given in Figure 5.3.

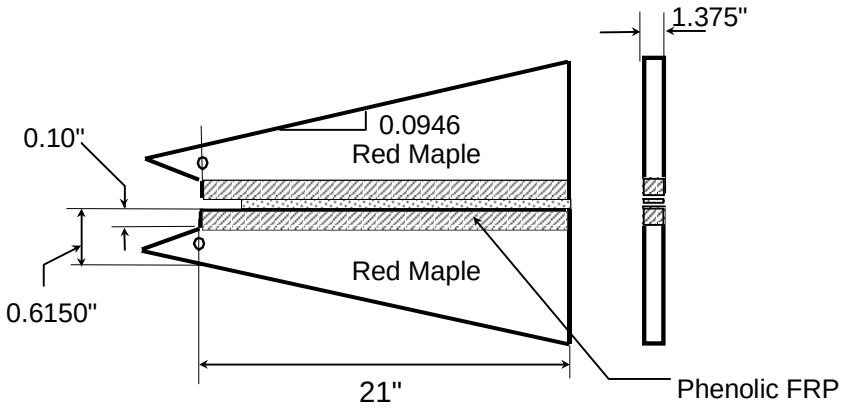

(a) Geometry of Phenolic FRP-Phenolic FRP/Dry Specimen

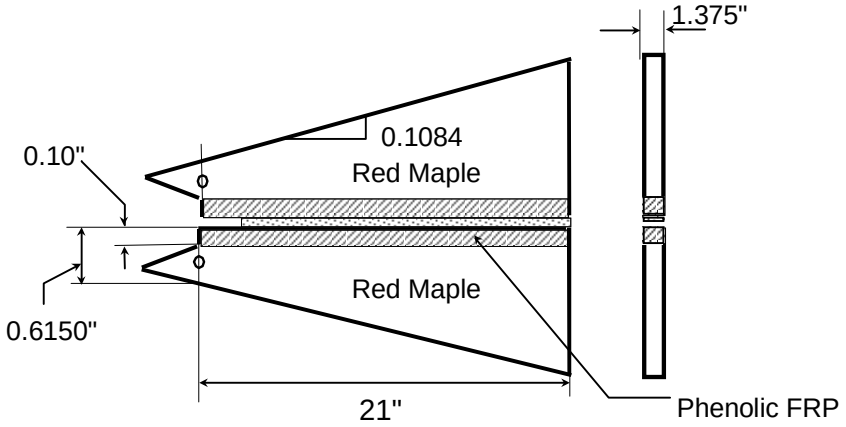

(b) Geometry of Phenolic FRP-Phenolic FRP/Wet Specimen

Figure 5.3. Contour shapes for CDCB Phenolic FRP-Phenolic FRP specimens

5.3.3 Epoxy FRP-Wood

The Epoxy FRP-wood CDCB specimens were designed based on the simplified design described in Chapter 4. The lay-ups of the CDCB specimens are given in Figure 5.4. The CDCB specimens were produced with both HMR and RF coupling agents at the Epoxy FRP and Red Maple interface during Filament Winding.

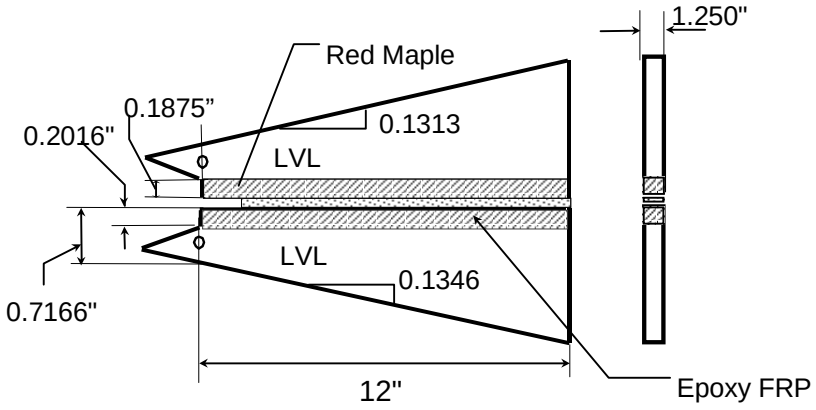

(a) Geometry of Epoxy FRP-wood/Dry

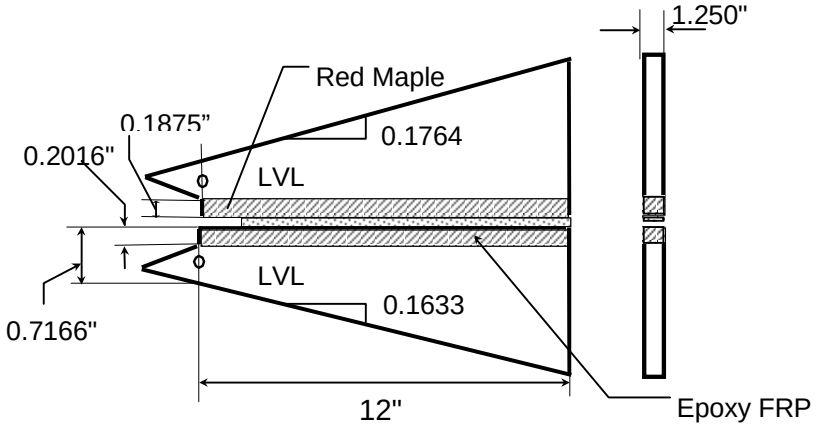

(b) Geometry of Epoxy FRP-wood/Wet

Figure 5.4. Contour shapes for CDCB Epoxy FRP-wood specimens

5.3.4 Compliance rate change of CDCB specimens

The compliance rate change *dC/da* of the designed CDCB specimens are given in Table 5.5.

Table 5.5 Compliance rate change of linear tapered specimens*

Specimen types	Slope	*dC/da* (x 10^{-5} lb^{-1})				% Diff.
		RR	MRR	Exp.	FE	Exp. Vs. FE
Wood-Wood/Dry	0.0968	23.83	26.35	29.85	27.43	8.11
Wood-Wood/Wet	0.1132	24.92	27.03	25.25	27.10	7.30
Phenolic FRP-Phenolic FRP/Dry	0.0946	24.04	26.79	29.33	27.10	7.60
Phenolic FRP-Phenolic FRP/Wet	0.1084	24.03	26.73	28.43	27.12	4.61
Epoxy FRP-wood/dry	0.1346	12.2	--	--	--	--
Epoxy FRP-wood/Wet	0.1633	12.5	--	--	--	--

**dC/da* obtained for crack lengths from 4 in to 14 in., for wood-wood, Phenolic FRP-Phenolic FRP specimens; From 4 in to 11 in for Epoxy FRP-wood Specimens.
Note: Due to material availability and time constraints, experimental and FE dC/da values were not calculated for Epoxy FRP specimens.

5.4 Experimental Compliance Calibration of the CDCB Specimens

Once the geometries of linear-slope test specimens were defined by the Rayleigh Ritz method, the specimens were calibrated experimentally to verify the linearity of compliance rate-change with respect to crack length. Considering wood-wood and Phenolic FRP-Phenolic FRP interfaces, CDCB specimens for four material/moisture conditions were manufactured (Figures 5.2 and 5.3). The adhesive used to bond wood to

wood, wood to Phenolic FRP, and Phenolic FRP to Phenolic FRP was the Resorcinol-Formaldehyde (RF, G-1131) resin as described in section 2.2.5. The best combination of pressure and assembly time obtained from the modified ASTM D 2559 was used to bond the specimens (pressure p = 210 psi and open/closed assembly times t = 5/30 min).

During the compliance calibration of the specimens, various crack lengths were simulated to experimentally determine the compliance crack-length relationship. For both wood-wood and Phenolic FRP-Phenolic FRP bonded interfaces, these cracks were produced by sawing the interfaces to the required lengths, starting from the smallest crack length of 2.0 in. The compliance calibration experiments were performed on an MTS servo hydraulic testing machine. The load was applied using a loading fixture made of aluminum (Figure 5.5). For testing, the tip of the specimen was connected to the loading fixture, while the specimen was supported vertically by a plastic thread attached to the upper frame of the testing machine (Figure 5.5). The experiment was conducted under displacement-controlled mode with a displacement rate of 0.002 in/s. By monitoring the control console, a maximum load of approximately 100 lbs was applied, and for every crack length, the load and displacement data were continuously recorded. An MTS crack-opening gage was clipped to the specimen tip, and it measured the transverse displacement of the specimen at the point of load application. The compliance values with respect to crack length obtained experimentally are plotted in Figures 5.6 through 5.9, and the compliance rate change values (dC/da) obtained experimentally and analytically for crack lengths from 4 to 14 in are shown in Table 5.5.

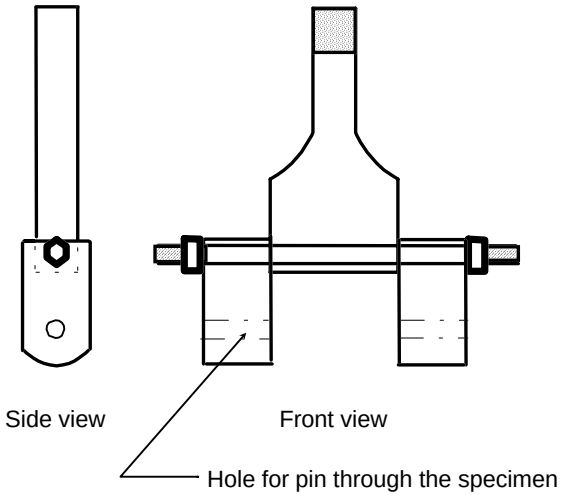

(a) Loading fixture for the CDCB specimen

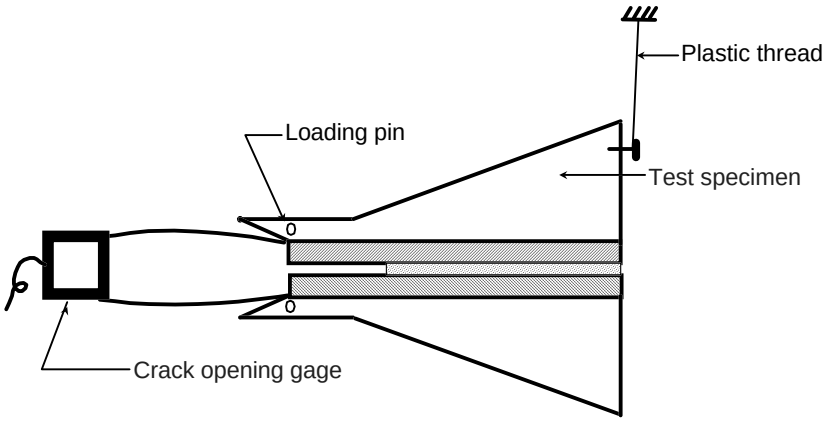

(b) CDCB specimen and crack opening gage

Figure 5.5. Experimental set-up for calibration and mode-I fracture tests

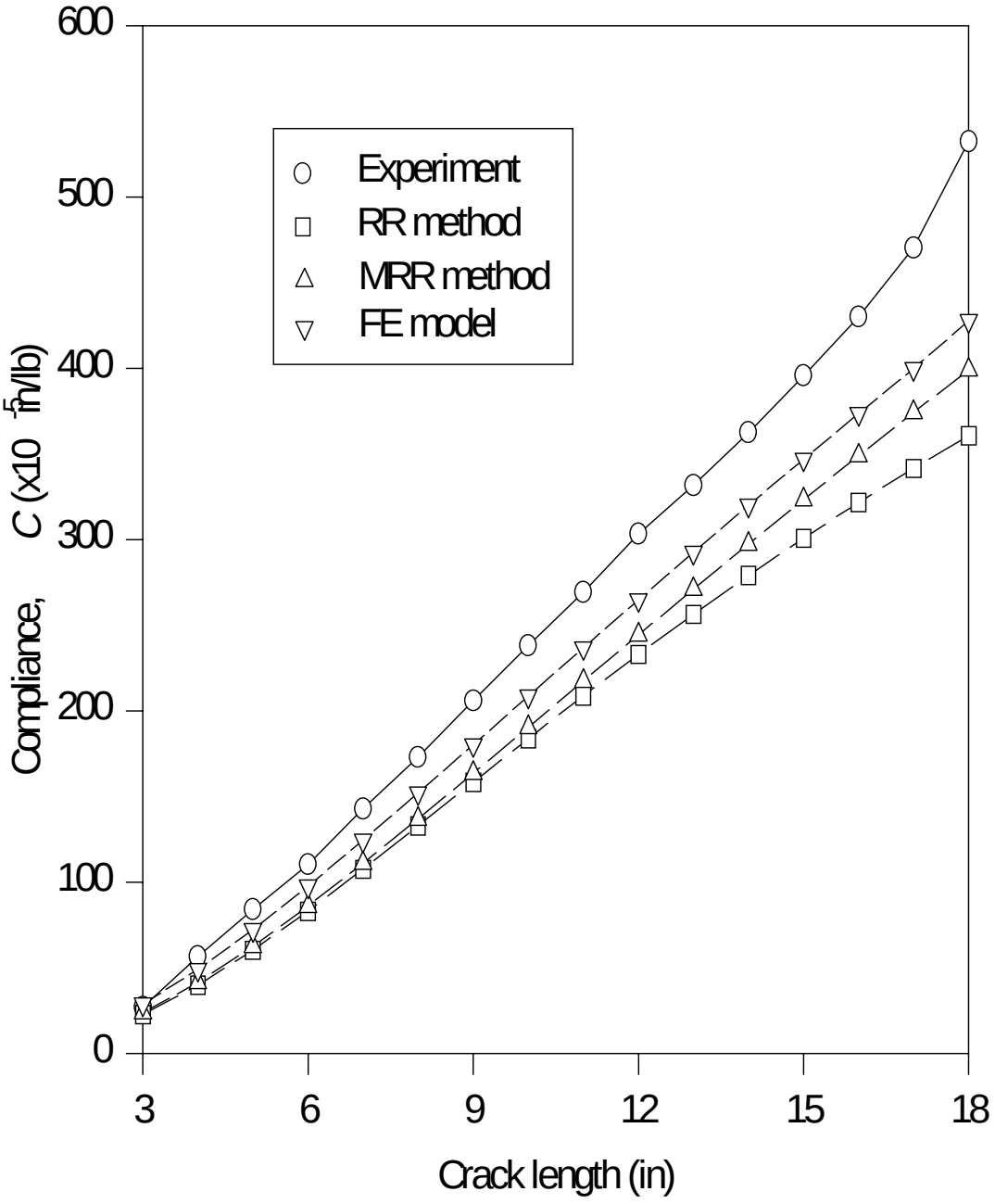

Figure 5.6. Compliance vs. crack length for wood-wood/dry specimen

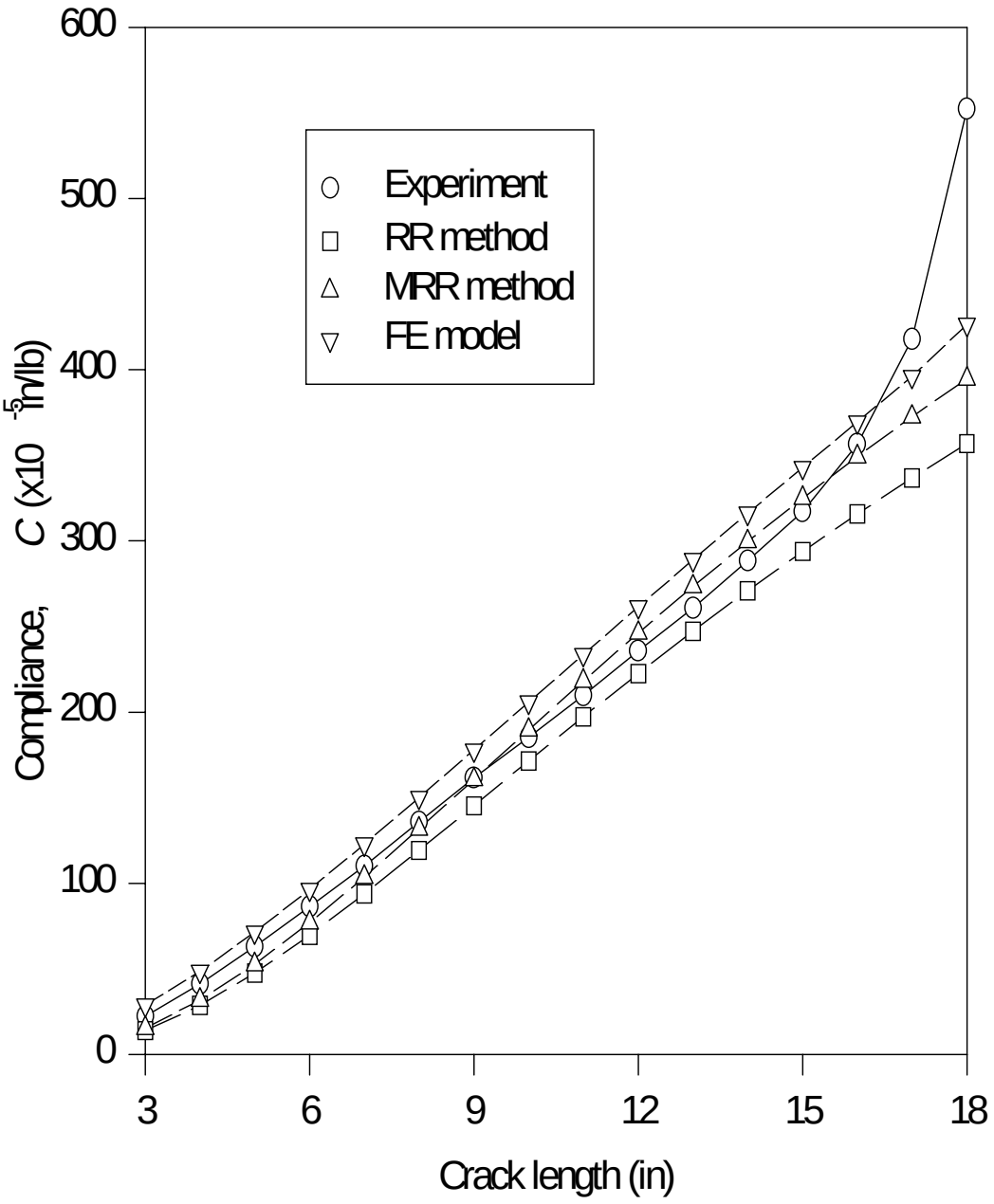

Figure 5.7. Compliance vs. crack length for wood-wood/wet specimen

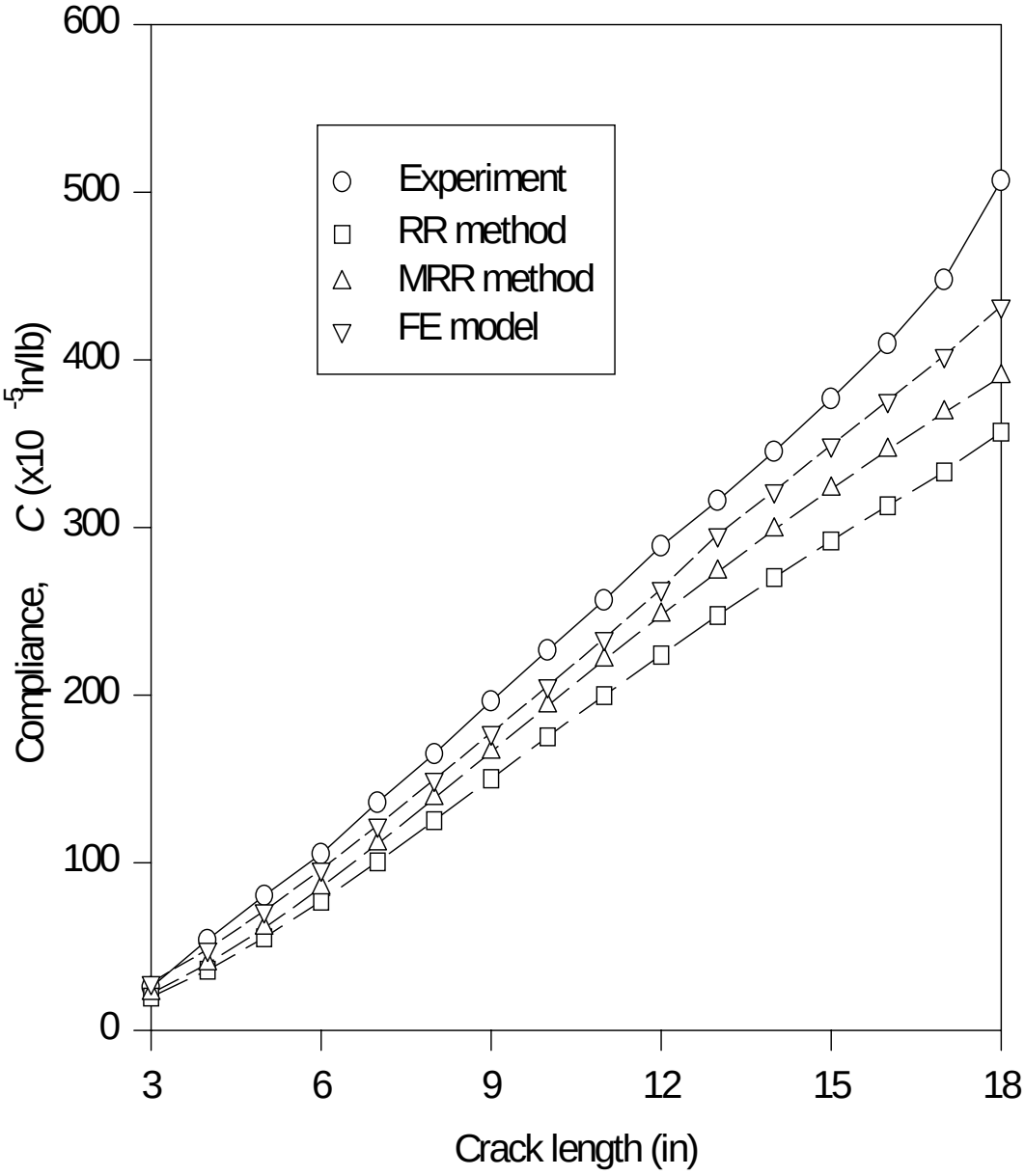

Figure 5.8. Compliance vs. crack length for Phenolic FRP-Phenolic FRP/dry specimen

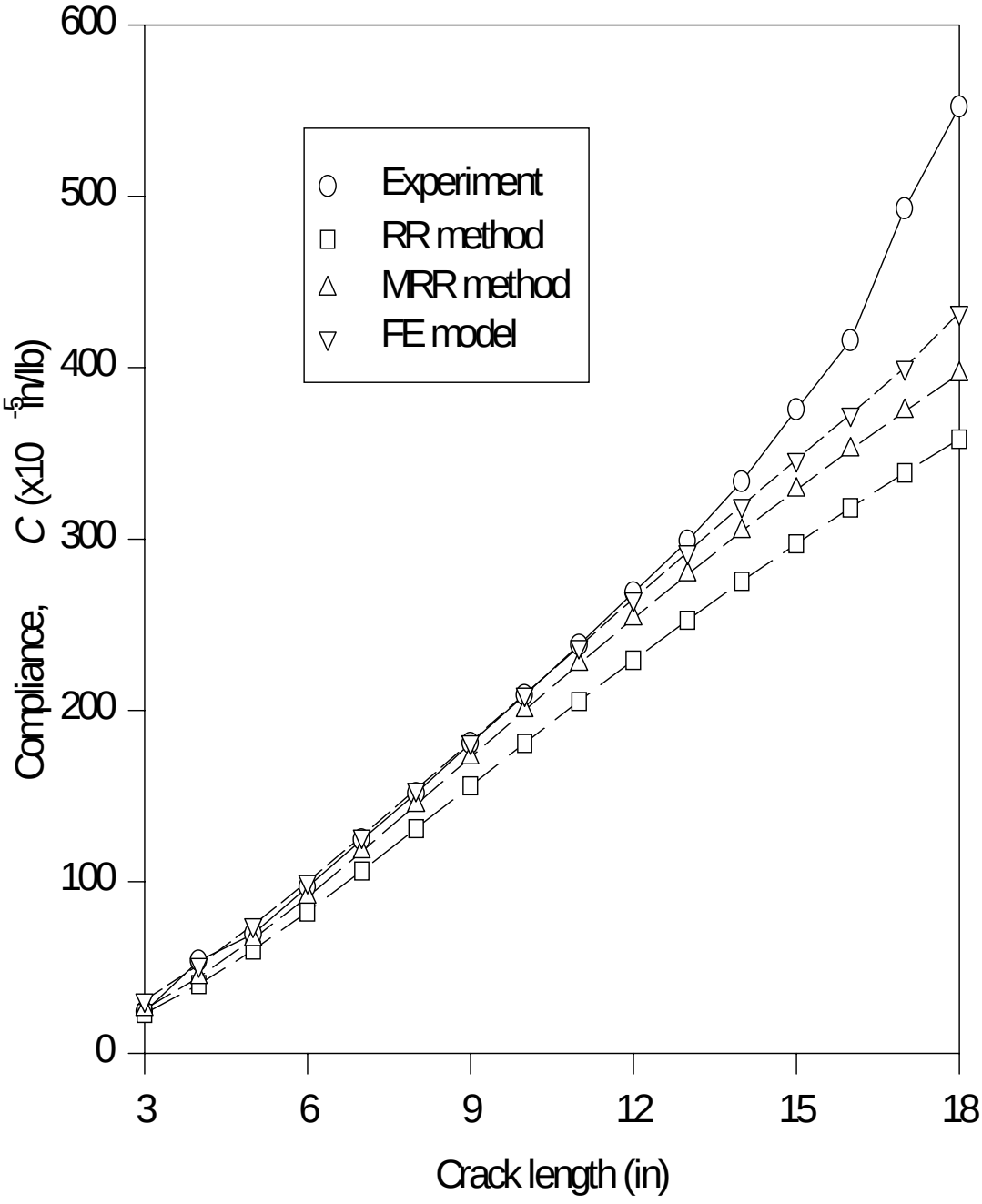

Figure 5.9. Compliance vs. crack length for Phenolic FRP-Phenolic FRP/wet specimen

5.5 Finite Element Modeling of the CDCB Specimens

One of the major concerns with tests using the contoured DCB specimen is the linearity of the compliance versus crack length, which must be achieved over a significant length of the specimen. To validate the linearity of the compliance, specimens can be tested to define the crack length region over which the response is linear; however, the experimental effort can be minimized by predicting the response of the specimen by the finite element (FE) method or the modified Rayleigh-Ritz method. The finite element model represents, as accurately as possible, the actual behavior of the specimen. The CDCB specimens were modeled using plane-stress isoparametric eight-node quadrilateral elements in NISA (1994) - a commercial finite element software. A representative element mesh and displacement contour of half of a symmetric CDCB specimen is shown in Figure 5.10. Similar to the experimental calibration of compliance change, the FE model was used to obtain compliance values with respect to crack lengths, as shown in Figures 5.6 through 5.9, and the compliance rate changes by FE predictions are also listed in Table 5.5.

As indicated in Table 5.5, the compliance rate changes by the modified Rayleigh-Ritz (MRR) method are within 4% of the predictions by the FE model. Figures 5.6 through 5.9 also show that the compliance crack-length relationship remains linear for crack lengths ranging from 4 in. to 14 in. The maximum difference of compliance rate change (dC/da) between experiment and FE model is about 12.7% for wood-wood/dry specimens.

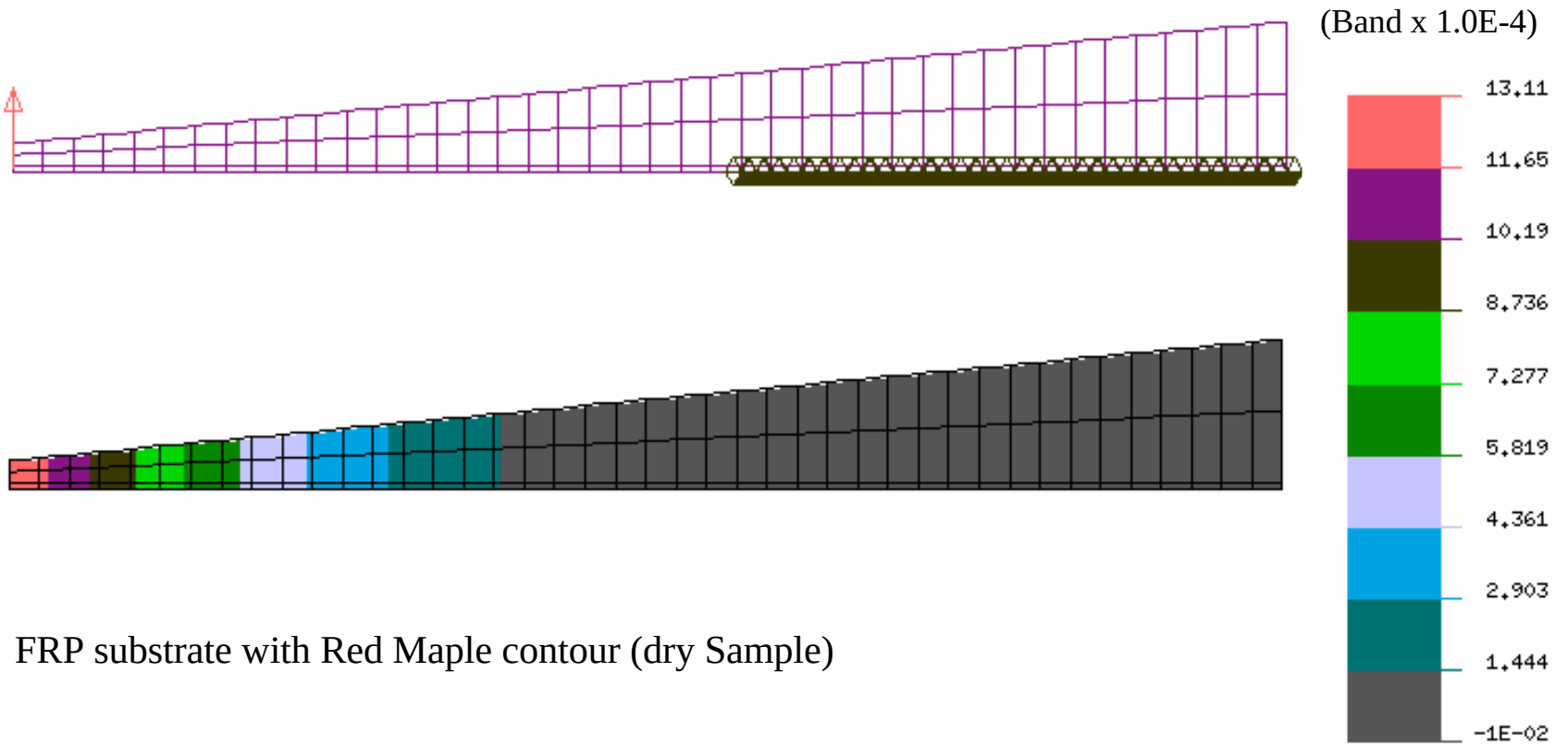

Figure 5.10. Finite element modeling and displacement contour of half of CDCB specimen

5.6 Experimental Evaluation of Fracture Toughness

Based on the most favorable assembly conditions evaluated from the modified ASTM D 2559 and the calibration studies of Section 5.4, wood-wood, Phenolic FRP-wood, Epoxy FRP-wood/HMR and Epoxy FRP-wood/RF samples were manufactured and tested under dry and wet conditions. Following testing, the mode-I fracture toughness of the interface was evaluated. A set of 8 samples for each material/moisture condition was manufactured and tested (except Epoxy FRP-wood: 7 samples each), which resulted in a total number of 60 samples.

5.6.1 Material and specimen preparation

The CDCB specimens were manufactured based on the design of the contoured shapes given in Section 5.3. The interface material/moisture condition combinations include: (1) wood-wood/dry (Figure 5.11(a)), (2) wood-wood/wet (Figure 5.11(b)), (3) Phenolic FRP-wood/dry (Figure 5.12(a)), (4) Phenolic FRP-wood/wet (Figure 5.12(b)), (5) Epoxy FRP-wood/HMR/dry (Figure 5.13(a)), (6) Epoxy FRP-wood/HMR/wet (Figure 5.13(b)), (7) Epoxy FRP-wood/RF/dry (Figure 5.13(a)), and (8) Epoxy FRP-wood/RF/wet (Figure 5.13(b)).

Since the compliance rate change is approximately constant for crack lengths beyond an initial length of 4 in., the CDCB specimens were manufactured with an initial crack length of 4 in. For the dry samples, the specimens were conditioned to 12% MC in an environmental chamber; whereas, the wet specimens were obtained by submerging the samples in a water bath under 40-minute vacuum (25 psi) and 40-minute pressure (100 psi) soaking cycle, and the specimens were tested immediately after the end of the cycle. The vacuum/pressure soaking cycle was used to saturate the specimens with moisture contents beyond fiber saturation point (Gardner et al. 1994), and the wet samples obtained by this process exhibited more than 100% moisture contents by weight.

5.6.1.1 wood-wood specimens

Both the adherends and contour portions for each side of the wood-wood specimens consisted of an integral Red Maple piece (Figure 5.11). The adhesive used for all the bonded interfaces was Resorcinol Formaldehyde (RF, G-1131), and the optimum pressure and assembly time used in the bonding process were those identified from the modified ASTM D 2559 tests (pressure p=210 psi and open/closed assembly time t=5/30 min).

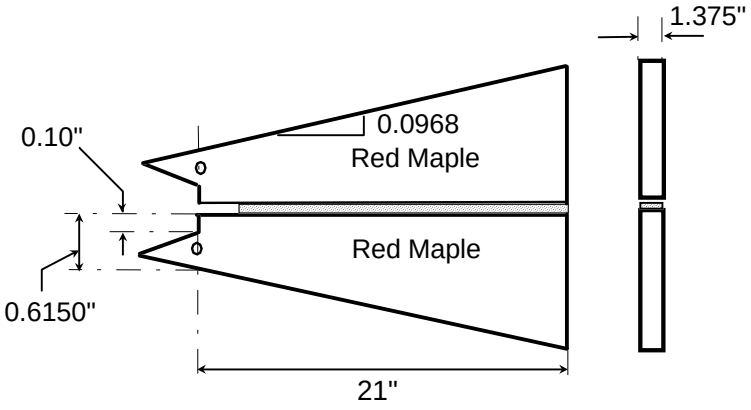

(a) Geometry of wood-wood/Dry Specimen

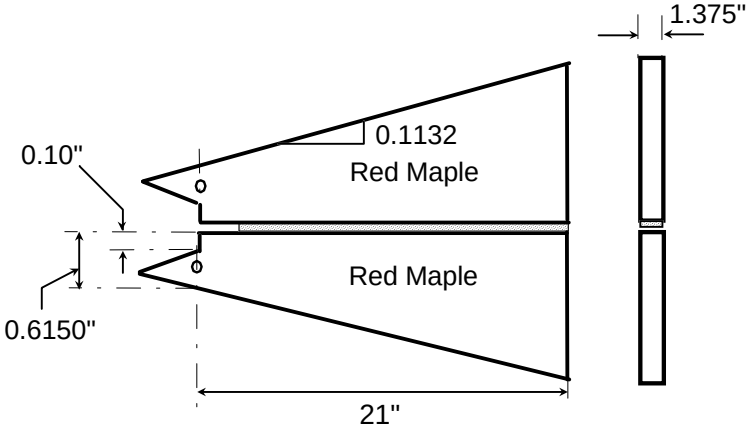

(b) Geometry of wood-wood/Wet Specimen

Figure 5.11. Contour shapes for CDCB wood-wood specimens for Mode-I fracture tests

5.6.1.2 Phenolic FRP-wood specimens

The Phenolic FRP-wood bonded interface consisted of E-glass/Phenolic putruded FRP and an integral Red Maple adherend-contour combination (Figure 5.12). The adhesive used for all the bonded interfaces was Resorcinol Formaldehyde (RF, G-1131), and the optimum pressure and assembly time used in the bonding process were those identified from the modified ASTM D 2559 tests (pressure p=210 psi and open/closed assembly time t=5/30 min).

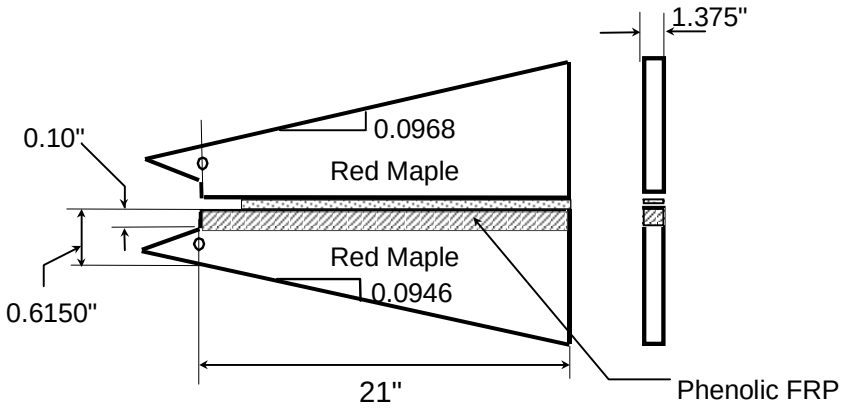

(a) Geometry of Phenolic FRP-wood/Dry Specimen

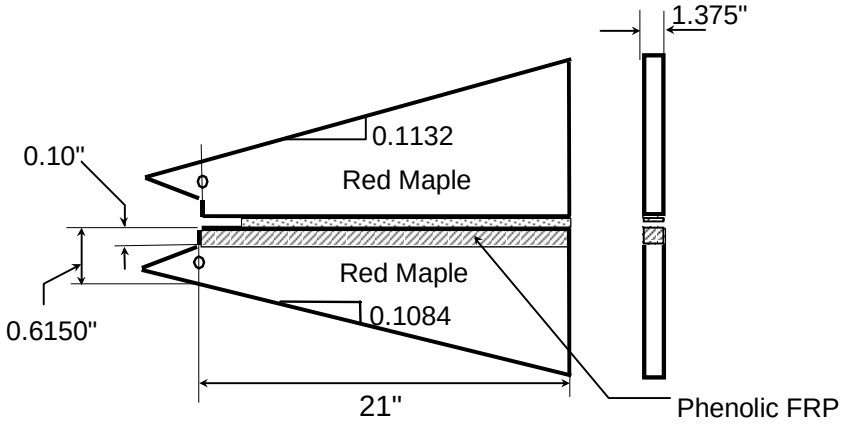

(b) Geometry of Phenolic FRP-wood/Wet Specimen

Figure 5.12. Contour shapes of CDCB Phenolic FRP-wood specimens for Mode-I fracture tests

5.6.1.3 Epoxy FRP-wood specimens

The Epoxy FRP-wood bonded interface consisted of E-glass/Epoxy filament wound FRP and an integral Red Maple adherend. The material used for the contour was Yellow Poplar LVL (Figure 5.13). The adhesive used for bonding the LVL-Red Maple interface was Resorcinol Formaldehyde (RF, G-1131), and the optimum pressure and assembly time used in the bonding process were those identified from the modified ASTM D 2559 tests (pressure p=210 psi and open/closed assembly time t=5/30 min). The Epoxy FRP-LVL interface was bonded using Magnobond 56 (a two part epoxy resin system, Magnolia Plastics, Inc., Chamblee, GA).

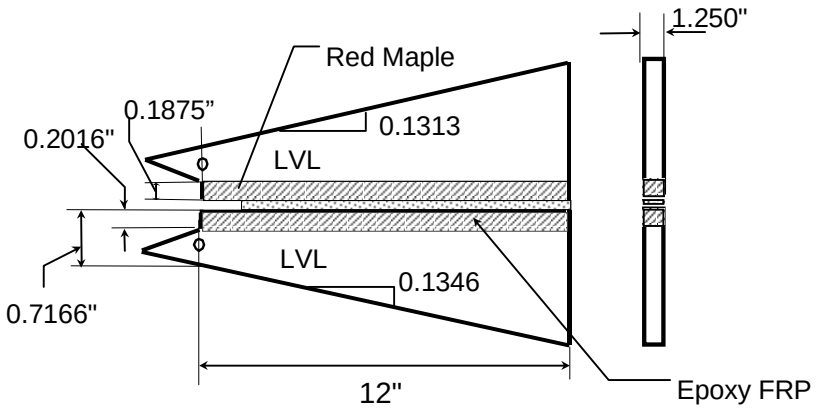

(a) Geometry of Epoxy FRP-wood/Dry Specimen

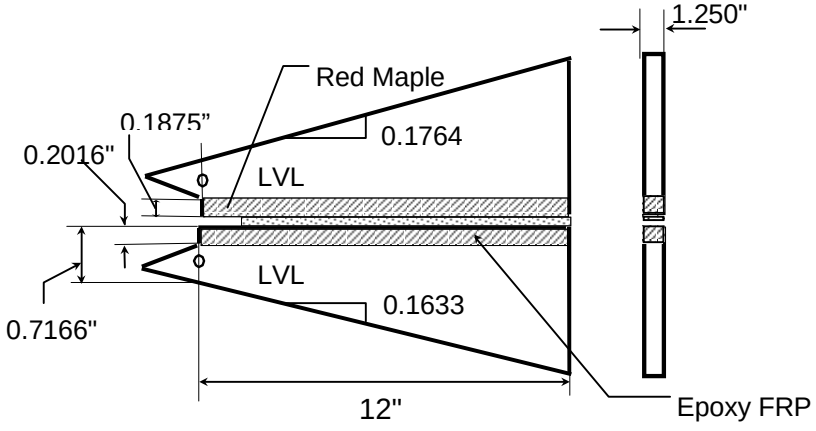

(b) Geometry of Epoxy FRP-wood/Wet Specimen

Figure 5.13. Contour shapes of CDCB Epoxy FRP-wood specimens for Mode-I fracture tests

5.6.2 Testing procedure

Similar to the compliance calibration tests, the fracture tests were also conducted using the MTS servo hydraulic testing machine. The specimens were loaded using the same loading fixture shown in Figure 5.5. The experiment was performed under displacement control mode with a loading rate of 0.002 in/s. Under displacement control, the crack propagation is stable, since the energy required for crack extension is obtained from the release of elastic strain energy (Anderson 1995). The load was applied continuously to initiate and sustain the crack propagation in the specimen. Since the compliance rate change (*dC/da*) was already established for the test specimens (see Equation 4.1), it was required to measure only the critical loads from which the fracture toughness could be evaluated. To monitor the crack propagation, the critical loads versus crack opening displacements were plotted. An accurate measurement of the crack opening displacements is not essential, and therefore, the load grip displacements were recorded and used to interpret the test results.

5.6.3 Fracture Failure Mode: Pattern of crack initiation and arrest

In general, for CDCB specimens with constant compliance rate change, the load versus crack length, or load vs. crack opening displacement, during fracture tests can be characterized by a curve shown in Figure 5.14. Initially, as the applied load increases, the elastic strain energy stored in the specimen increases until the internal elastic energy is equal to the energy required to initiate the crack. The crack initiation is characterized by a drop in the applied load as seen in Figure 5.14. Each peak load value corresponds to the critical load of crack initiation (Points A, B, C, D, and E in Figure 5.14). As the crack extends, the applied load is relaxed, and the stored elastic strain energy decreases, resulting in a crack arrest without complete fracture of the specimen. When the crack is arrested, the applied load increases once again. The critical load value at which the load-crack opening curve shows a "valley" is the critical load of crack arrest (Points a, b, c, d, and e in Figure 5.14). This sequence of crack initiation and arrest continues as the crack extends, and finally, a catastrophic failure of the interface bond is observed (at Point F in Figure 5.14).

Based on the design of a constant compliance rate change specimen, the assumed theoretical critical load values for crack initiation or arrest should remain constant along the bond interface.

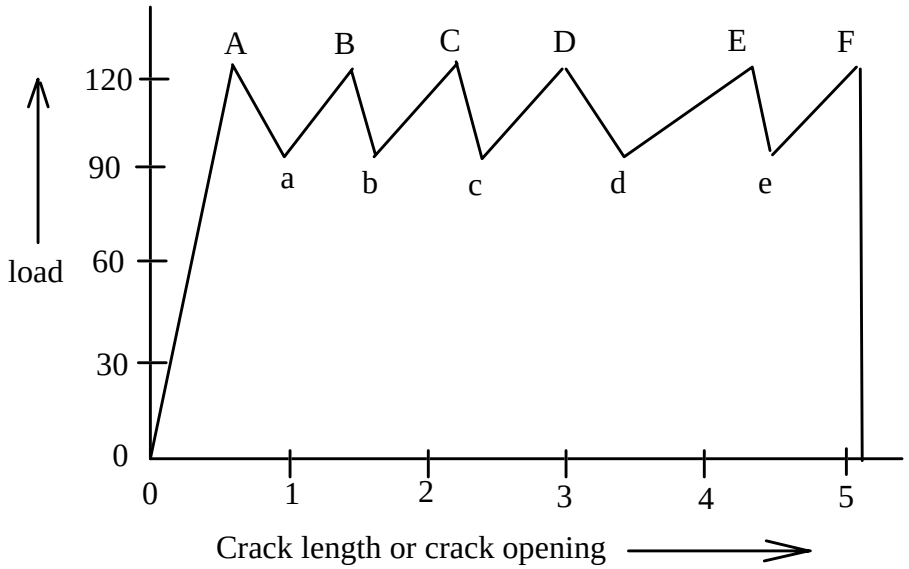

Figure 5.14. Typical crack pattern for contoured double-cantilever beam test

In the following sections, the fracture patterns of specimens under different types of material/moisture conditions are described based on experimental observations, and their corresponding fracture toughness values are reported. Since the experimental values of *dC/da* (Table 5.5) are assumed to be accurate, these are used to evaluate the Mode-I fracture toughness from Equation 4.1. For the dry and wet Phenolic FRP-wood specimens, the average experimental values of *dC/da* for wood-wood and Phenolic FRP-Phenolic FRP specimens were used to evaluate the fracture toughness.

5.6.4 Mode-I fracture toughness for wood-wood bonded interface

5.6.4.1 Wood-Wood dry condition

The linear-slope CDCB specimen shown in Figure 5.11(a) was used for Mode-I fracture test of wood-wood bonded interface under dry condition. The specimen was designed by the method described in Section 4.2. Eight specimens numbered WWD1 through WWD8 were fabricated and then tested to obtain the critical loads for crack initiation and arrest. The experimental setup and a specimen under fracture are shown in Figure 5.15. A representative test result is shown in Figure 5.16 for specimen WWD1. As indicated in Figure 5.16, several distinct crack initiations and arrests occurred during crack propagation. The fracture failure modes showed a combined wood cohesive failure and adhesive failure along the bond lines, with an average cohesive failure of about 60% of the fracture surfaces. The data for two specimens (WWD2 and WWD6) were disregarded because the fracture occurred completely in the wood substrate. The critical loads for crack initiation and crack arrest were obtained for the remaining six specimens, and the results are given in Table 5.6. An analysis of the critical loads yields a mean crack-initiation load value of 175.70 lb. with a COV of 14.13%, and a mean crack-arrest load value of 131.72 lb. with a COV of 20.29%. The critical strain energy release rates (fracture toughness) given by Equation 4.1 are computed using the mean value of the critical loads and the compliance rate change, *dC/da*, obtained experimentally (see Table 5.5). Using Equation 4.1, the fracture toughness under mode-I fracture for crack initiation (G_{Ic}^{i}) and crack arrest (G_{Ic}^{a}) are 3.53 lb/in and 1.98 lb/in, respectively.

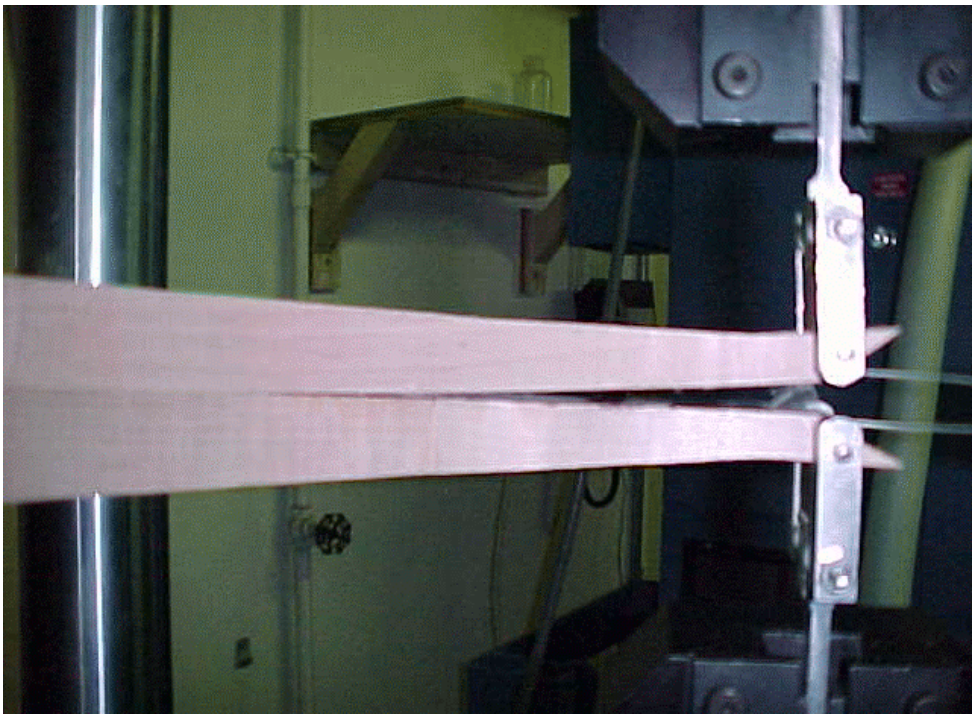

Figure 5.15. Fracture of wood-wood/dry interface for CDCB specimens

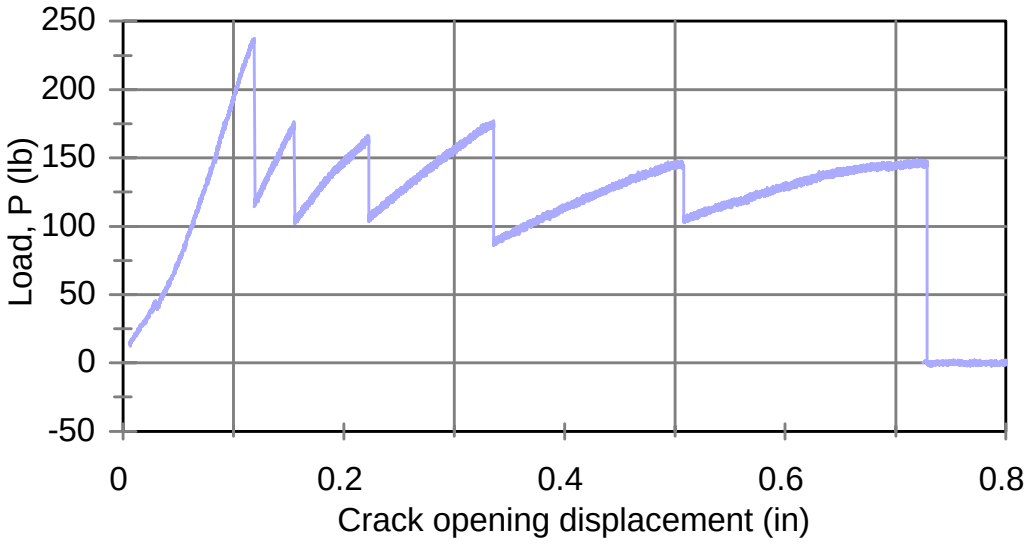

Figure 5.16 Load vs. crack-opening displacement for specimen WWD1

Table 5.6. Crack loads of CDCB specimens with wood-wood/dry interface

Specimen No.	Critical loads (lb)	
	Crack initiation (P_{Ic}^{i})	Crack arrest (P_{Ic}^{a})
WWD1	174.7	104.5
	163.7	103.4
	174.7	85.8
	145.0	108.7
WWD3	173.9	114.8
	170.3	133.5
	170.1	96.9
WWD4	156.5	140.1
	195.3	180.0
	197.1	188.9
	197.5	164.3
WWD5	155.7	142.2
	153.9	139.0
	148.6	143.0
	153.0	141.8
WWD7	229.1	143.9
	209.3	127.5
	185.9	126.2
	195.1	160.7
WWD9	216.7	125.7
	165.3	128.6
	133.9	98.4
Average values	175.7 (COV = 14.1%)	131.7 (COV = 20.3%)

5.6.4.2 Wood-Wood wet condition

The linear-slope CDCB specimen for wood-wood bonded interface under wet condition is based on the design given in Figure 5.11(b). Eight specimens numbered WWW1 through WWW8 were fabricated and subjected to one cycle of water vacuum/pressure soaking that achieved a moisture content of over 100% by weight. The specimens were tested immediately after water-saturation, and the critical loads for crack initiation and arrest were obtained. A photograph of a wood-wood/wet interface specimen (WWW4) under fracture is shown in Figure 5.17. Figure 5.18 shows the fractured interface of specimen WWW4. Observations of the fracture surface showed predominantly adhesive failure of nearly 60%. Representative test results of load vs. crack opening are shown in Figure 5.19 for specimen WWW7. Specimen WWW2 failed around the loading pin and was discarded. Similarly, the contour portion of specimen WWW3 failed after some initial crack propagation, and this specimen was also disregarded. The critical loads for crack initiation and crack arrest were obtained for six specimens, and the results are given in Table 5.7. An analysis of the critical loads yields a mean crack-initiation load value of 198.91 lb. with a COV of 12.89%, and a mean crack-arrest load value of 183.15 lb. with a COV of 14.79%. The critical strain energy release rates (fracture toughness) given by Equation 4.1 are computed using the mean value of the critical loads and the compliance rate change, *dC/da*, obtained experimentally (see Table 5.5). Using Equation 4.1, the fracture toughness under mode-I fracture for crack initiation (G_{Ic}^{i}) and crack arrest (G_{Ic}^{a}) are 3.63 lb/in and 3.08 lb/in, respectively.

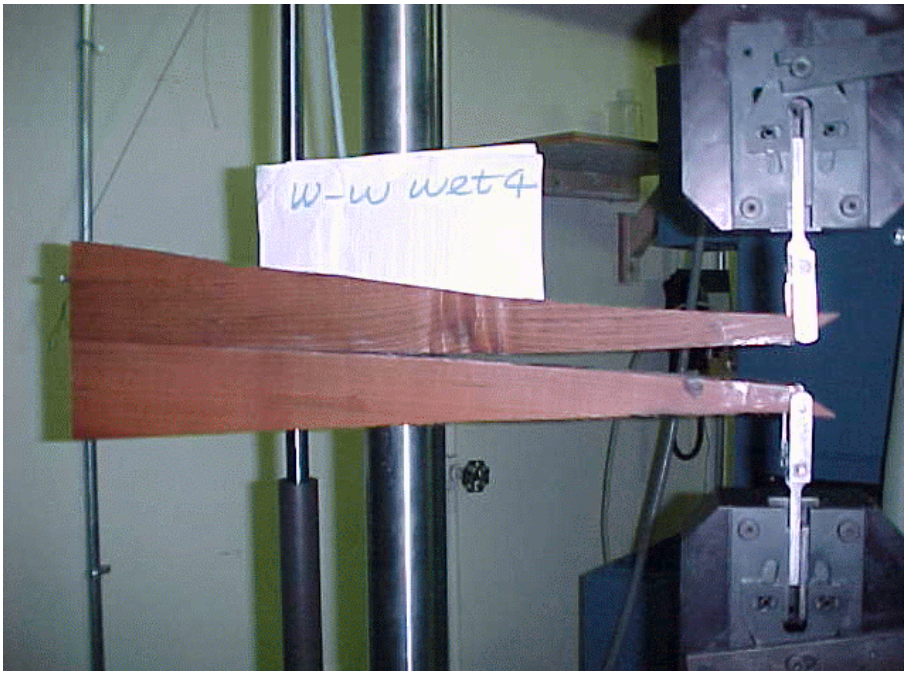

Figure 5.17. Fracture of wood-wood/wet CDCB specimen

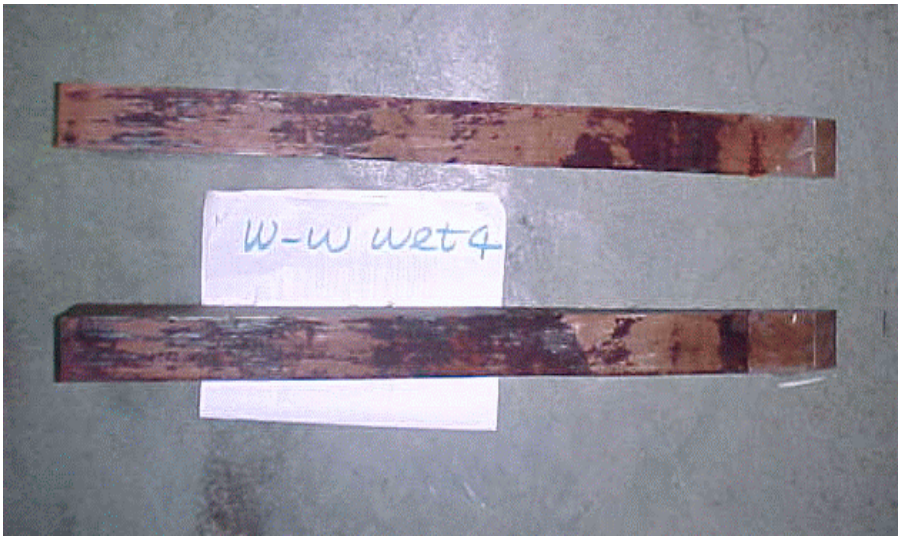

Figure 5.18. Fractured surface of wood-wood/wet specimen

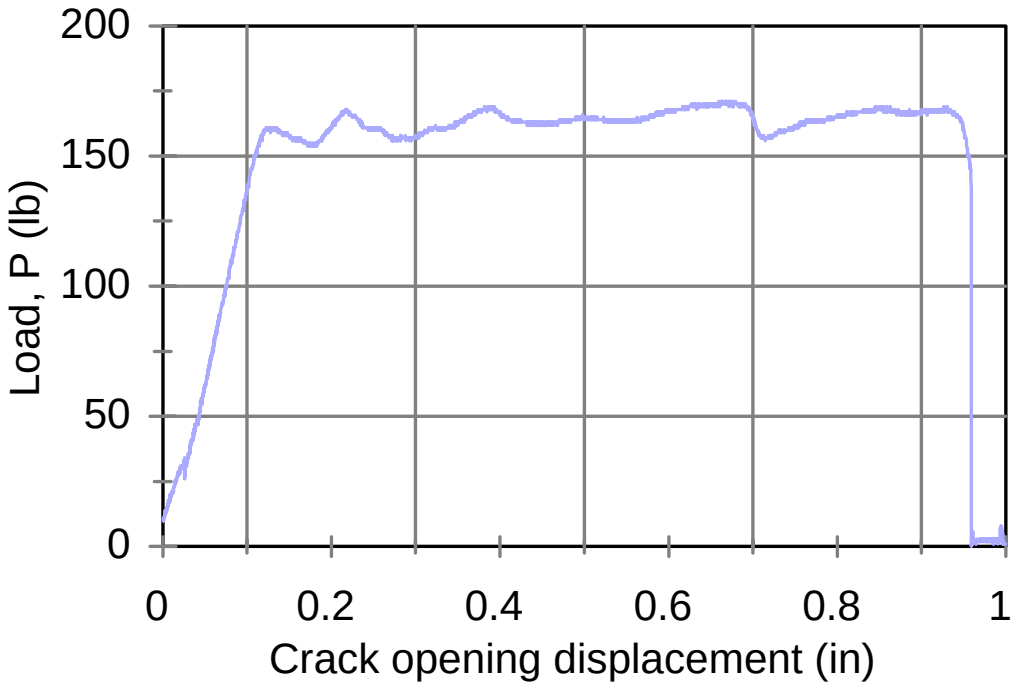

Figure 5.19. Load vs. crack-opening displacement for specimen WWW7

Table 5.7. Crack loads of CDCB specimens with wood-wood/wet interface

Specimen No.	Critical loads (lb)	
	Crack initiation (P_{Ic}^{i})	Crack arrest (P_{Ic}^{a})
WWW1	206.3	177.2
	215.9	211.0
	239.2	228.1
WWW4	142.3	126.2
WWW5	196.0	186.9
	211.2	189.6
	194.0	181.5
WWW6	205.9	202.1
	214.9	211.0
	221.5	193.9
WWW7	168.5	156.0
	169.1	162.2
	171.0	157.5
WWW8	212.7	159.0
	215.2	205.1
Average (COV)	198.9 (COV = 12.9%)	183.2 (COV = 14.8%)

5.6.4.3 Discussion for Wood-Wood samples

Critical loads and Fracture Toughness:

The experimental results of the critical strain energy release rates (fracture toughness) for the wood-wood/dry and wood-wood/wet samples are summarized and discussed in this section. As indicated in Table 5.8, the mean critical load values for wood-wood/wet interface bonds are higher than the corresponding values for wood-wood/dry interface bonds. The fracture toughness values for the wood-wood interface bonds are given in Table 5.9. The saturated (wet) samples show an increase in the fracture toughness, which indicates that the absorption of water in the CDCB specimens had a tendency to toughen the interface bonds. This increase at first may appear to be strange, but it is a phenomenon that has been observed also for interlaminar delamination of graphite/epoxy composites (Hooper and Subramanian, 1993). Due to the moisture-induced plastification of both the adherends and adhesive, the failure mode was much more plastic, resulting in higher critical loads and a much more “smooth” crack propogation response; this phenomenon can be seen by the smaller variations in the peaks and valleys of critical loads, as shown in Figure 5.19 (wood-wood/wet) compared to those of Figure 5.16 (wood-wood/dry).

Brittleness Index:

In addition to fracture toughness data, a "brittleness index, *I*" (River and Okkonen 1993) which is the ratio of energy lost during crack growth to the energy required to initiate crack growth, can also be used to indicate stability of crack growth:

$$I = \frac{G_{Ic}{}^{i} - G_{Ic}{}^{a}}{G_{Ic}{}^{i}} \tag{5.1}$$

A large *I* value corresponds to a catastrophic and unstable crack growth that is independent of the rate of loading, and a small *I* value indicates a slow tearing or growth in small increments. In the study conducted by River and Okkonen (1993), a value of $I = 0.43$ was considered to represent a strong and moderately unstable crack growth, and a value of *I* =

0.06 showed a moderately strong and stable crack growth. Based on the fracture toughness data obtained, the corresponding *I* values for both dry and wet samples were computed and given in Table 5.9. The wood-wood/dry interfaces exhibited moderately unstable crack growth and a relatively stable crack propagation was observed for the wood-wood/wet specimens. The crack growth in the wet samples, for each CDCB specimen type, is more stable than the corresponding crack growth of the dry samples.

Table 5.8. Critical initiation and arrest loads for wood-wood interface bonds

	P_c^i (lb)	P_c^a (lb)
Wood-Wood/Dry	175.7 (COV = 14.1%)	131.7 (COV = 20.3%)
Wood-Wood/Wet	198.9 (COV = 12.9%)	183.2 (COV = 14.8%)

Table 5.9. Fracture toughness of wood-wood interface bonds

	G_{Ic}^i (lb/in)	G_{Ic}^a (lb/in)	*Brittleness Index*
Wood-Wood/Dry	3.35	1.88	0.44
Wood-Wood/Wet	3.63	3.08	0.14

5.6.5 Mode-I fracture toughness for Phenolic FRP-wood bonded interface

5.6.5.1 Phenolic FRP-wood dry condition

The linear-slope CDCB specimen shown in Figure 5.12(a) was used for the Mode-I fracture test of Phenolic FRP-wood bonded interface under dry conditions. The specimen was designed by combining the contour shapes of wood-wood/dry (Figure 5.2(a)) and Phenolic FRP-Phenolic FRP/dry (Figure 5.3(a)) presented in Section 5.3. Eight specimens numbered WFD1 through WFD8 were fabricated and then tested to obtain the critical loads for crack initiation and arrest. A typical specimen (WFD3) under mode-I fracture load is shown in Figure 5.20, and the corresponding fractured surfaces are displayed in Figure 5.21. As observed in the tests, most of the interface fracture happened within the Continuos Strand Mat (CSM) layer of the FRP substrate in combination with interface adhesive failure; for several specimens, substantial fiber-bridging was evident during the fracture process, as a close-up photograph shows in Figure 5.22 for specimen WFD6. A representative test result is given in Figure 5.23 for specimen WFD4. The critical loads for crack initiation and crack arrest were obtained for all eight specimens, and the results are given in Table 5.10. An analysis of the critical loads yields a mean crack-initiation load value of 109.50 lb. with a COV of 15.38%, and a mean crack-arrest load value of 100.02 lb. with a COV of 17.01%. The critical strain energy release rates (fracture toughness) given by Equation 4.1 are computed using the mean value of the critical loads and the compliance rate change, *dC/da*, obtained experimentally (see Table 5.5). Using Equation 4.1, the fracture toughness under mode-I fracture for crack initiation (G_{Ic}^{i}) and crack arrest (G_{Ic}^{a}) are 1.35 lb/in and 1.12 lb/in, respectively.

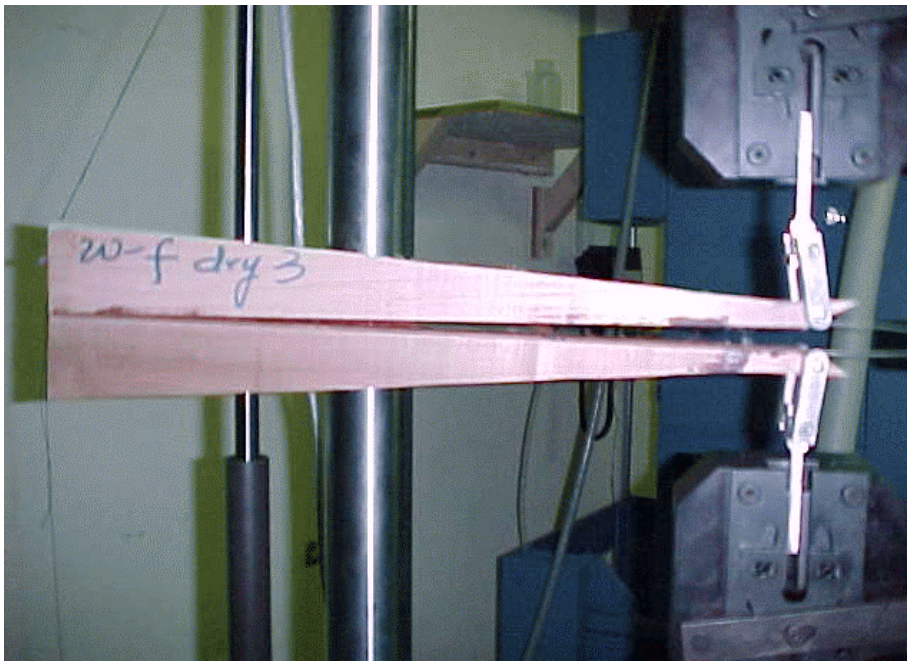

Figure 5.20. Fracture test of Phenolic FRP-wood/dry interface (Specimen WFD3)

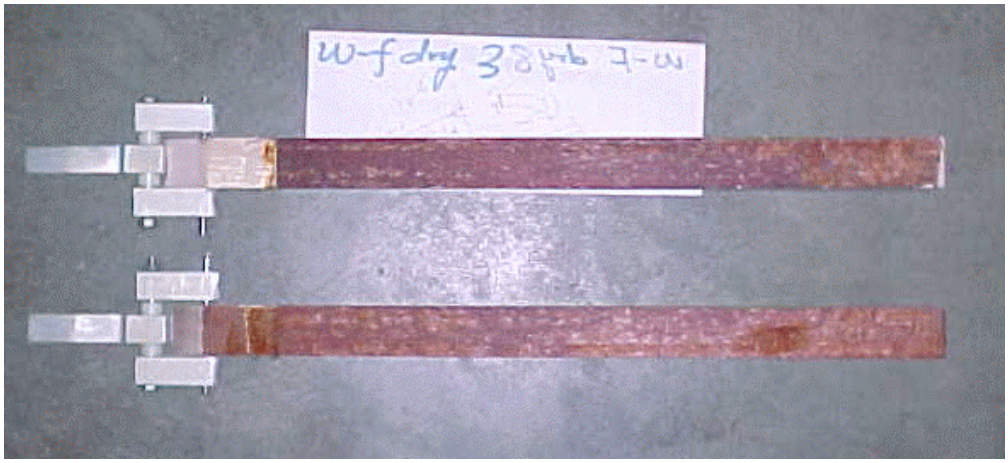

Figure 5.21. Fracture surfaces of Phenolic FRP-wood/dry specimen (WFD3)

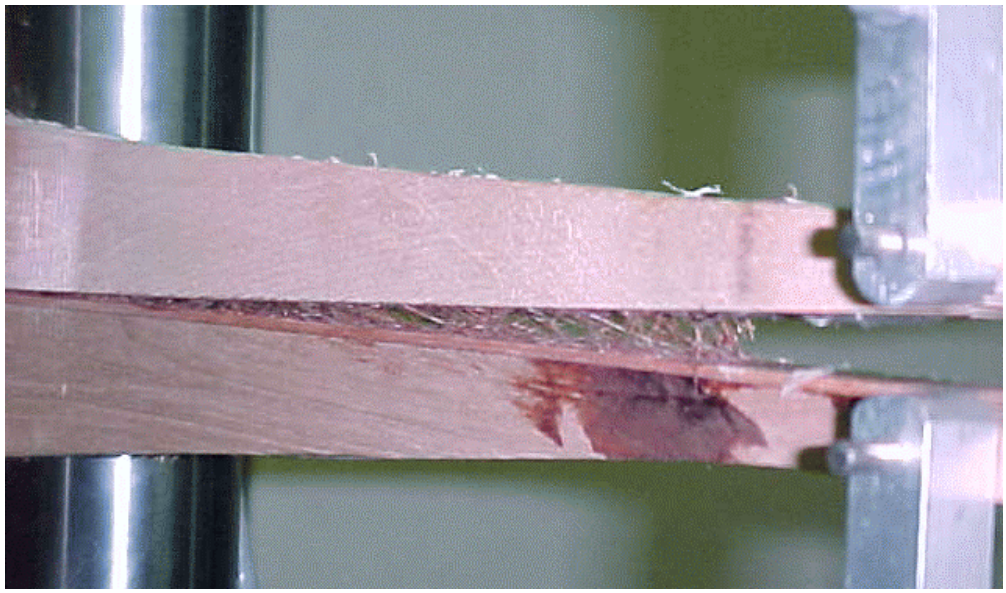

Figure 5.22. A close-up observation of fiber bridging along the interface (WFD6)

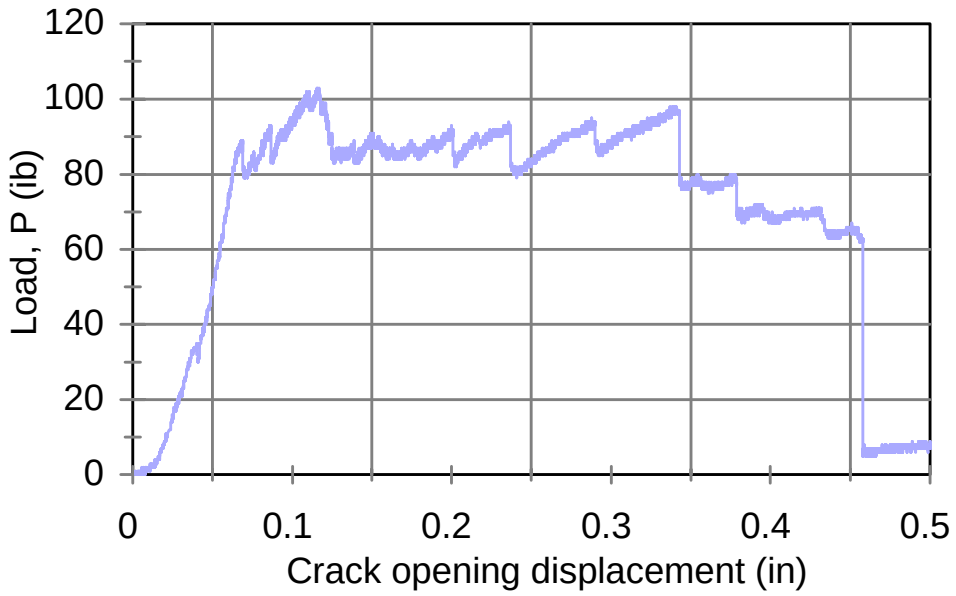

Figure 5.23. Load vs. crack-opening displacement for specimen WFD4

Table 5.10. Crack loads of CDCB specimens with Phenolic FRP-wood/dry interface

Specimen No.	Critical loads (lb)	
	Crack initiation (P_{Ic}^{i})	Crack arrest (P_{Ic}^{a})
WFD1	131.9	123.5
	131.8	125.6
	131.0	119.2
	134.5	127.1
	134.0	130.0
	133.6	125.4
	134.2	125.2
	134.9	129.0
	134.8	121.8
	129.9	122.5
	134.8	127.1
	133.7	125.1
WFD2	88.6	83.2
	91.4	79.9
	83.5	76.8
	80.7	74.9
	84.3	77.1
	85.7	81.0
	96.5	90.1
WFD3	112.3	104.8
	110.0	104.3
	113.2	107.6
	106.1	110.0
	114.3	112.5
	125.1	103.7
	124.5	114.2
	117.3	110.6
	117.0	105.1

WFD3 (continue)	126.1	112.3
	117.0	105.9
	114.9	100.9
	106.8	101.0
	107.5	102.3
	119.9	108.4
	125.9	115.0
WFD4	86.1	80.8
	93.9	82.8
	102.4	97.0
	103.7	82.9
	90.9	84.6
	89.3	84.5
	93.5	82.3
	94.8	79.5
	95.0	85.0
	97.8	75.7
WFD5	104.5	95.0
	114.8	97.5
	111.9	102.3
	110.0	102.7
	108.0	98.8
	106.3	100.0
	107.2	101.5
	117.1	109.0
	123.9	105.5
	123.1	112.3
	125.5	115.0
WFD6	128.1	117.5
	124.6	116.8
	122.3	116.4

WFD (continue)	125.7	117.4
	122.5	112.7
	117.0	112.1
	117.8	107.8
	114.8	105.6
	112.4	103.9
WFD7	124.0	94.1
	105.1	97.6
	110.0	90.0
	95.4	82.3
	89.1	83.7
	93.5	85.6
	96.4	86.9
	99.9	90.0
WFD8	93.1	83.9
	89.2	81.3
	92.4	77.7
	85.0	68.2
	75.0	62.7
	72.3	68.6
	87.3	80.9
Average (COV)	109.5 (COV = 15.4%)	100.0 (COV = 17.0%).

5.6.5.2 Phenolic FRP-wood wet condition

The linear-slope CDCB specimen shown in Figure 5.12(b) was used for Mode-I fracture test of Phenolic FRP-wood bonded interface under wet condition. The specimen was designed by the method described in Section 4.2. Eight specimens numbered WFW1 through WFW8 were fabricated and then tested to obtain the critical loads for crack initiation and arrest. Figure 5.24 shows a Phenolic FRP-wood/wet specimen (WFW2) under fracture, and the fractured surfaces of the specimen are illustrated in Figure 5.25. For most of the specimens, the interface fracture failures happened mainly within the CSM layer in the Phenolic FRP substrate. Similar to the Phenolic FRP-wood/dry samples, significant fiber-bridging was observed at the interface during fracture propagation. A close-up photograph in Figure 5.26 shows this bridging effect. A representative test result is shown in Figure 5.27 for specimen WFW2. The critical loads for crack initiation and crack arrest were obtained for all the specimens, and the results are given in Table 5.11. An analysis of the critical loads yields a mean crack-initiation load value of 157.50 lb. with a COV of 13.13%, and a mean crack-arrest load value of 146.87 lb. with a COV of 15.07%. The critical strain energy release rates (fracture toughness) given by Equation 4.1 are computed using the mean value of the critical loads and the compliance rate change, *dC/da*, obtained experimentally (see Table 5.5). Using Equation 4.1 the fracture toughness under mode-I fracture for crack initiation (G_{Ic}^{i}) and crack arrest (G_{Ic}^{a}) are 2.70 lb/in and 2.35 lb/in, respectively.

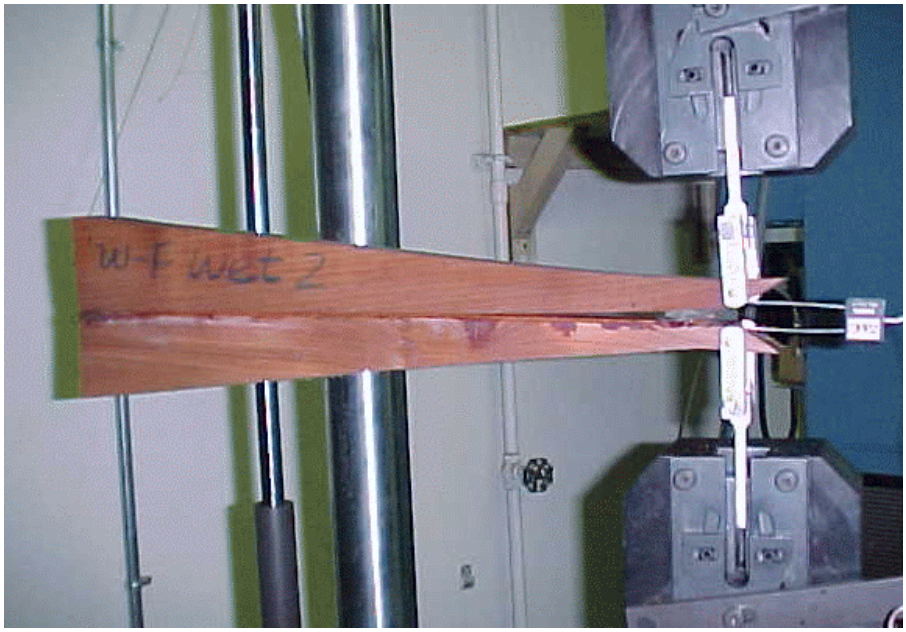

Figure 5.24. Fracture test of Phenolic FRP-wood/wet (Specimen WFW2)

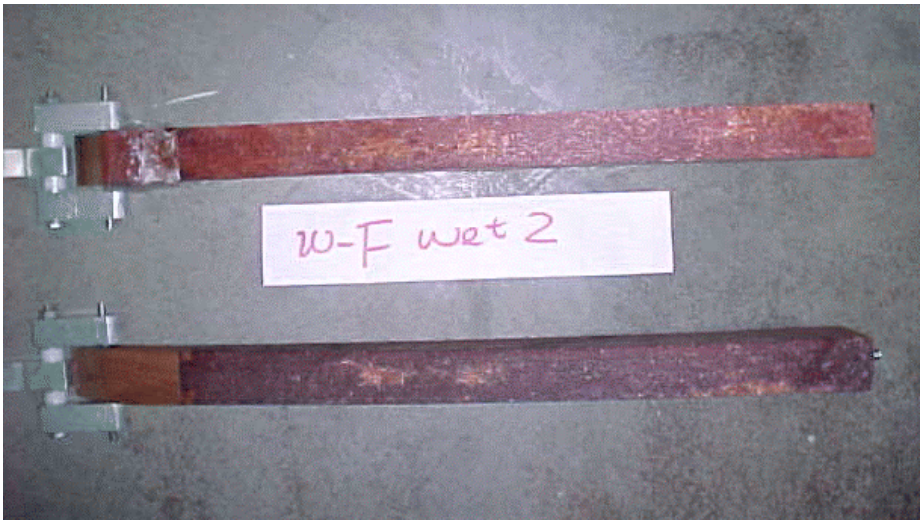

Figure 5.25. Fractured faces of Phenolic FRP-wood/wet specimen (WFW2)

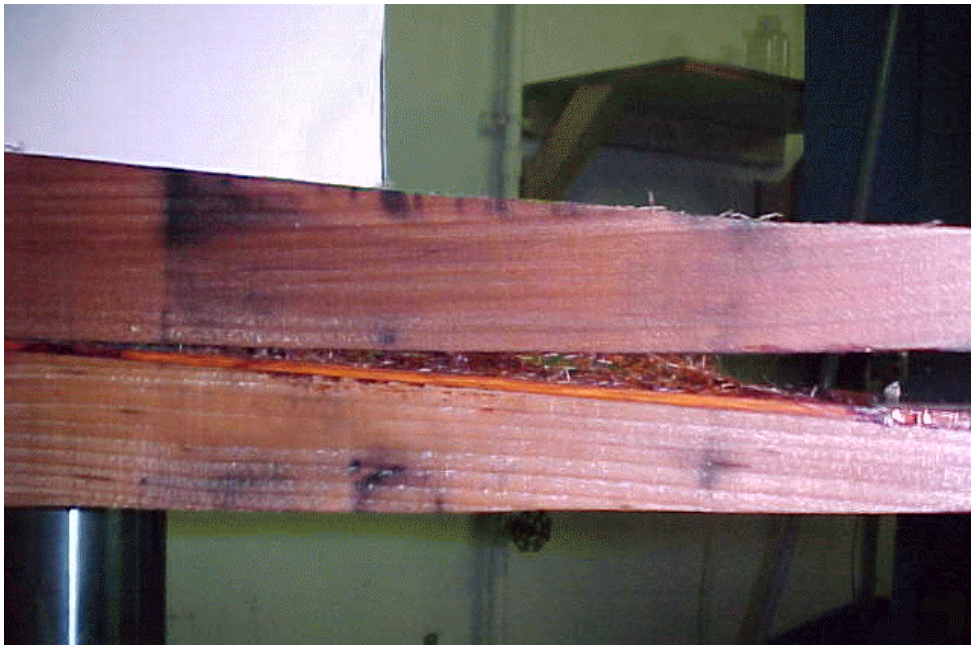

Figure 5.26. A close-up look of fiber bridging in Phenolic FRP-wood/wet specimen (WFW2)

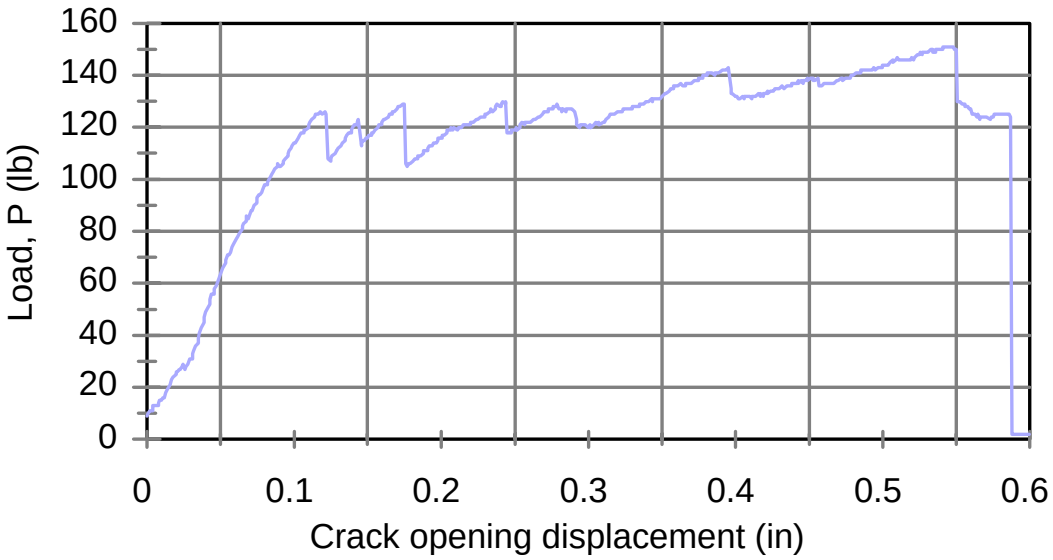

Figure 5.27. Load vs. crack-opening displacement for specimen WFW2

Table 5.11. Crack loads of CDCB specimens with Phenolic FRP-wood/wet interface

Specimen No.	Critical loads (lb)	
	Crack initiation (P_{Ic}^{i})	Crack arrest (P_{Ic}^{a})
WFW1	180.7	177.1
	188.8	172.9
	182.3	149.6
WFW2	124.3	112.5
	130.0	104.9
	130.1	117.2
	129.8	120.0
	143.3	130.8
	139.8	135.3
WFW3	134.3	126.1
	131.2	120.9
	134.8	132.4
	148.1	119.2
	145.1	136.3
	156.4	145.9
	155.0	150.0
WFW4	132.0	118.6
	153.6	147.8
	159.3	150.5
	157.9	149.7
	166.7	142.9
WFW5	145.2	137.3
	153.1	146.5
	165.1	151.0
	169.0	148.1
	158.4	146.3
WFW6	142.8	139.2
	142.9	132.4

WFW6 (continue)	141.8	132.0
	146.1	142.3
	156.8	136.4
	150.0	147.1
WFW7	187.5	182.4
	182.3	169.7
	170.0	161.6
WFW8	194.3	187.8
	193.2	183.5
	186.0	179.7
	180.8	174.3
	181.0	184.6
	187.6	178.7
Average (COV)	157.50 lb (COV = 3.1%)	146.87 lb (COV = 15.1%)

5.6.5.3 Discussion for Phenolic FRP-wood samples

The experimental results of the critical strain energy release rates (fracture toughness) for the Phenolic FRP-wood/dry and Phenolic FRP-wood/wet samples are summarized and discussed in this section. As indicated in Table 5.12, the mean critical load values for Phenolic FRP-wood/wet interface bonds are much higher than the corresponding values for Phenolic FRP-wood/dry interface bonds. The fracture toughness values for the Phenolic FRP-wood interface bonds are given in Table 5.13. The saturated (wet) samples show an increase in the fracture toughness of over 100%, which indicates that the absorption of water in the CDCB specimens had a tendency to toughen the interface bonds. Due to the moisture-induced plastification of both the polymeric adherends and adhesive, the failure mode was much more plastic, resulting in higher critical loads and a much more "smooth" crack propogation response. This phenomenon can be seen by the smaller variations in the peaks and valleys of critical loads, as shown in Figure 5.27 (Phenolic FRP-wood/wet) compared to those of Figure 5.23 (Phenolic FRP-wood/dry).

Following the discussion of Brittleness Index given for Wood-Wood samples, the values shown in Table 5.13 indicate that the crack propagation was relatively stable.

Table 5.12. Critical initiation and arrest loads for Phenolic FRP-wood interface bonds

	P_c^i (lb)	P_c^a (lb)
Phenolic FRP-wood/Dry	109.5 (COV = 15.4%)	100.0 (COV = 17.0%)
Phenolic FRP-wood/Wet	157.50 (COV = 13.1%)	146.87 (COV = 15.1%)

Table 5.13. Fracture toughness of Phenolic FRP-wood interface bonds

	G_{Ic}^i (lb/in)	G_{Ic}^a (lb/in)	*Brittleness Index*
Phenolic FRP-wood/Dry	1.28	1.06	0.17
Phenolic FRP-wood/Wet	2.57	2.23	0.13

5.6.6 Mode-I fracture toughness for Epoxy FRP-wood bonded interface

5.6.6.1 Epoxy FRP-wood dry condition

The linear-slope CDCB specimen shown in Figure 5.13(a) was used for the Mode-I fracture tests of Epoxy FRP-wood bonded interfaces under dry conditions. Seven specimens were fabricated for each coupling agent type (HMR and RF), and the specimens were tested to obtain the critical loads for crack initiation and arrest.

5.6.6.1.1 HMR coupling agent for dry condition

The fractured surfaces of a typical specimen (HMR-DRY 7) are shown in Figure 5.28. A representative test result is given in Figure 5.29 for specimen HMR-DRY 4. Specimens HMR-DRY 2 and HMR-DRY 3 were both omitted because of material failures within the contour of the samples. The critical loads for crack initiation and crack arrest were obtained for the remaining five specimens, and the results are given in Table 5.14. An analysis of the critical loads yields a mean crack-initiation load value of 225.6 lb. with a COV of 4.4 %, and a mean crack-arrest load value of 222.4 lb. with a COV of 4.5 %. The critical strain energy release rates (fracture toughness) given by Equation 4.1 are computed using the mean values of the critical loads and the compliance rate change, *dC/da*, obtained by the Rayleigh-Ritz (RR) method (see Table 5.5). Using Equation 4.1, the fracture toughness under mode-I fracture for crack initiation (G_{Ic}^{i}) and crack arrest (G_{Ic}^{a}) are 2.54 lb/in and 2.47 lb/in, respectively.

Figure 5.28. Fractured faces of Epoxy FRP-wood/HMR/dry specimen (HMR-DRY 7)

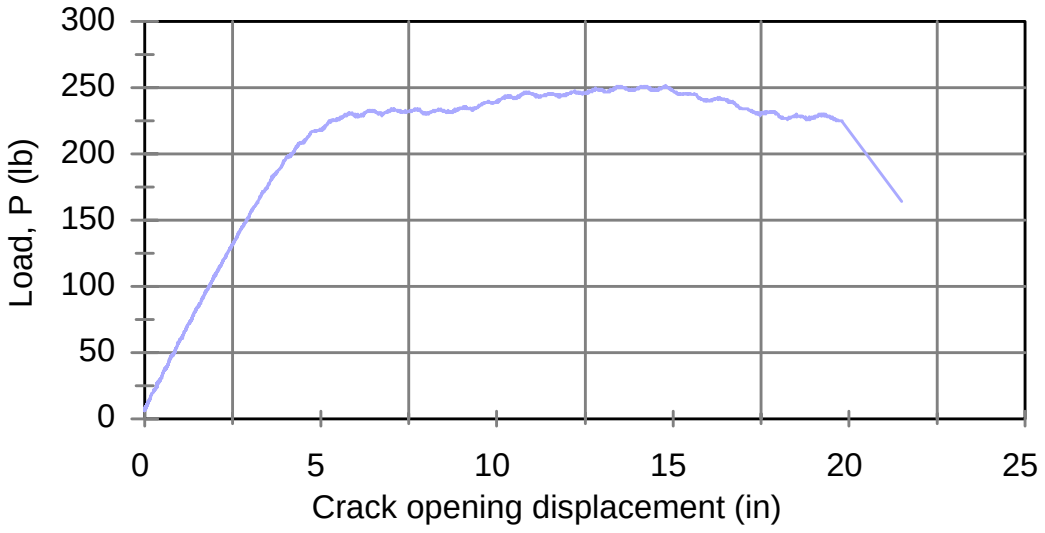

Figure 5.29. Load vs. crack opening displacement for specimen HMR-DRY 4

Table 5.14. Crack loads of CDCB specimens with Epoxy FRP-wood/HMR/Dry interface

Specimen No.	Critical loads (lb)	
	Crack initiation (P_{Ic}^{i})	Crack arrest (P_{Ic}^{a})
HMR-DRY 1	221	218
	223	220
	224	220
	223	219
	221	218
	222	217
	223	221
	227	224
	230	225
HMR-DRY 4	231	228
	233	229
	234	231
	234	230
	234	231
	236	233
	240	238
	244	242
	247	243
	246	243
HMR-DRY 5	211	209
	214	212
	217	215
	222	221
	232	229
	234	228
HMR-DRY 6	212	210
	215	214

HMR-DRY 6 (Continued)	216	213
	214	212
	215	213
	216	214
	217	214
	217	214
	215	210
	214	211
	213	210
HMR-DRY 7	220	218
	221	213
	222	213
	232	230
	234	232
	238	234
	237	234
	235	232
Average (COV)	225.6 lb (COV = 4.4%)	222.4 lb (COV = 4.5%)

5.6.6.1.2 RF coupling agent for dry condition

A typical specimen, and its corresponding fractured surfaces, (RF-DRY 1) is shown in Figure 5.30. A representative test result is given in Figure 5.31 for specimen (RF-DRY 7). The critical loads for crack initiation and crack arrest were obtained for all seven specimens, and the results are given in Table 5.15. An analysis of the critical loads yields a mean crack-initiation load value of 106.3 lb. with a COV of 31.8%, and a mean crack-arrest load value of 97.5 lb. with a COV of 33.3%. The critical strain energy release rates (fracture toughness) given by Equation 4.1 are computed using the mean value of the critical loads and the compliance rate change, *dC/da*, obtained by the Rayleigh-Ritz (RR) method (see Table 5.5). Using Equation 4.1, the fracture toughness under mode-I fracture for crack initiation (G_{Ic}^{i}) and crack arrest (G_{Ic}^{a}) are 0.57 lb/in and 0.48 lb/in, respectively.

Figure 5.30. Fractured faces of Epoxy FRP-wood/RF/dry specimen (RF-DRY 1)

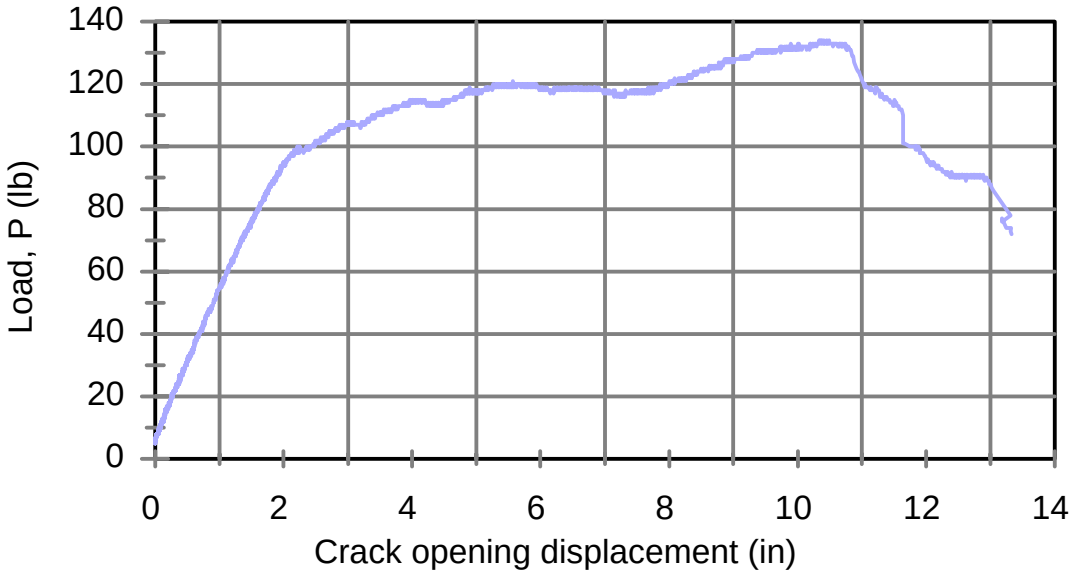

Figure 5.31. Load vs. crack opening displacement for specimen (RF-DRY 7)

Table 5.15. Crack loads of CDCB specimens with Epoxy FRP-wood/RF/Dry interface

Specimen No.	Critical loads (lb)	
	Crack initiation (P_{Ic}^{i})	Crack arrest (P_{Ic}^{a})
RF-DRY 1	144	135
	141	138
	140	133
	134	128
RF-DRY 2	65	48
	67	62
	74	60
	78	70
RF-DRY 3	64	62
	67	64
	67	64
	71	68
RF-DRY 4	163	145
	162	148
	148	125
RF-DRY 5	112	97
	115	87
RF-DRY 6	70	58
	73	69
	81	73
RF-DRY 7	117	113
	119	117
	121	119
	120	118
	119	116
	133	118
Average (COV)	106.3 lb (COV = 31.8%)	97.5 lb (COV = 33.3%)

5.6.6.1.3 Discussion for Epoxy FRP-wood Dry samples

The experimental results of the critical strain energy release rates (G_{Ic}; fracture toughness) for the Epoxy FRP-wood/HMR/dry and Epoxy FRP-wood/RF/dry samples are summarized and discussed in this section. As indicated in Table 5.16, the mean critical load values for Epoxy FRP-wood/HMR/dry interface bonds are much higher than the corresponding values for Epoxy FRP-wood/RF/dry interface bonds. The variability of the load data, as measured by the COV (%), is four times larger for the Epoxy FRP-wood/RF/dry samples than for the HMR-treated samples. The fracture toughness values for the Epoxy FRP-wood/dry interface bonds are given in Table 5.17. The fracture toughness of the RF/dry samples is only 22% of the value for the HMR/dry samples. This is a clear indication of the enhanced bonding obtained by the HMR coupling agent over the RF. The Brittleness Index for both types of samples indicates a stable crack propagation.

Table 5.16. Critical initiation and arrest loads for Epoxy FRP-wood/dry interface bonds

	P_c^i (lb)	P_c^a (lb)
Epoxy FRP-wood/HMR	218.6 (COV = 8.0%)	214.5 (COV = 8.8%)
Epoxy FRP-wood/RF	106.3 (COV = 31.8%)	97.5 (COV = 33.3%)

Table 5.17. Fracture toughness of Epoxy FRP-wood/dry interface bonds

	G_{Ic}^i (lb/in)	G_{Ic}^a (lb/in)	*Brittleness Index*
Epoxy FRP-wood/HMR	2.54	2.47	0.03
Epoxy FRP-wood/RF	0.57	0.48	0.16

5.6.6.2 Epoxy FRP-wood wet condition

The linear-slope CDCB specimen shown in Figure 5.13(b) was used for the Mode-I fracture test of Epoxy FRP-wood bonded interface under wet conditions. Seven specimens were fabricated for each coupling agent (HMR and RF) and tested to obtain the critical loads for crack initiation and arrest.

5.6.6.2.1 HMR coupling agent for wet condition

The fractured surfaces of a typical specimen (HMR-WET 7) are shown in Figure 5.32. A representative test result is given in Figure 5.33 for specimen HMR-WET 4. Two samples, HMR-WET 2 and HMR-WET 3, were omitted from the results because of contour material failures around the loading pins. The critical loads for crack initiation and crack arrest were obtained for the remaining five specimens, and the results are given in Table 5.18. An analysis of the critical loads yields a mean crack-initiation load value of 284.0 lb. with a COV of 6.4%, and a mean crack-arrest load value of 280.9 lb. with a COV of 6.5%. The critical strain energy release rates (fracture toughness) given by Equation 4.1 are computed using the mean value of the critical loads and the compliance rate change, *dC/da*, obtained by the Rayleigh-Ritz (RR) method (see Table 5.5). Using Equation 4.1, the fracture toughness under mode-I fracture for crack initiation (G_{Ic}^{i}) and crack arrest (G_{Ic}^{a}) are 4.03 lb/in and 3.94 lb/in, respectively.

Figure 5.32. Fractured faces of Epoxy FRP-wood/HMR/wet specimen (HMR-WET 7)

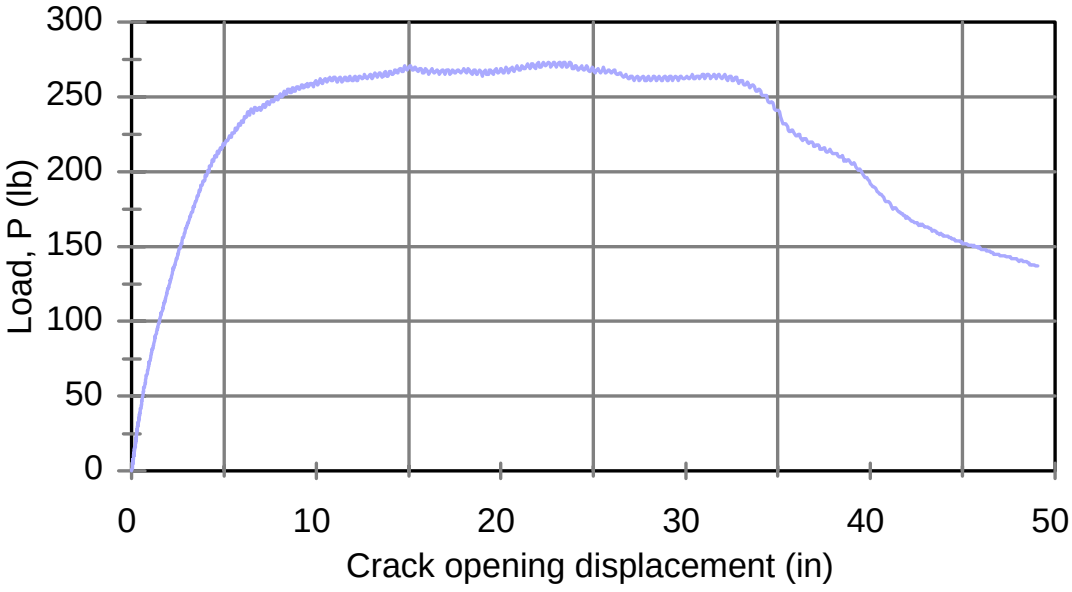

Figure 5.33. Load vs. crack opening displacement for specimen HMR-WET 4

Table 5.18. Crack loads of CDCB specimens with Epoxy FRP-wood/HMR/wet interface

Specimen No.	Critical loads (lb)	
	Crack initiation (P_{Ic}^{i})	Crack arrest (P_{Ic}^{a})
HMR-WET 1	278	257
	282	280
	288	285
	291	288
	294	291
	298	295
	300	297
	301	299
	301	299
	302	299
	304	300
	303	299
	302	298
	301	297
	300	295
	298	294
	296	292
	292	288
HMR-WET 4	264	261
	264	261
	265	262
	265	262
	266	263
	266	263
	267	264
	268	266
	269	267

HMR-WET 4 (Continued)	271	268
	271	268
	270	267
	269	266
	269	266
	268	265
HMR-WET 5	248	245
	250	248
	254	252
	255	253
	257	254
	257	254
	257	254
	257	254
	256	253
	256	252
	255	253
	256	254
	257	254
	259	256
	260	257
	259	257
	257	254
	256	253
HMR-WET 6	297	293
	295	292
	296	293
	297	294
	298	295
	299	296
	298	296

HMR-WET 6 (Continued)	298	296
	299	296
	299	295
	298	295
	298	295
	299	296
	300	297
	300	298
	300	297
	301	298
	302	300
	303	300
	303	300
	304	302
	305	302
	305	302
	306	303
	307	304
	307	304
	307	304
	306	303
	305	302
	305	302
	304	301
	304	301
	303	300
	302	298
HMR-WET 7	274	272
	276	274
	278	275
	279	277

HMR-WET 7 (Continued)	281 282 282 282 281 281 282 283 282 282 282 282 282	279 279 279 278 278 278 279 279 278 278 279 279 278
Average (COV)	284.0 lb (COV = 6.4%)	280.9 lb (COV = 6.5%)

5.6.6.2.2 RF coupling agent for wet condition

The fractured surfaces of a typical specimen (RF-WET 2) are shown in Figure 5.34. A representative test result is given in Figure 5.35 for specimen RF-WET 7. The critical loads for crack initiation and crack arrest were obtained for all seven specimens, and the results are given in Table 5.19. An analysis of the critical loads yields a mean crack-initiation load value of 62.7 lb. with a COV of 78.0%, and a mean crack-arrest load value of 60.8 lb. with a COV of 80.3%. The critical strain energy release rates (fracture toughness) given by Equation 4.1 are computed using the mean value of the critical loads and the compliance rate change, *dC/da*, obtained by the Rayleigh-Ritz (RR) method (see Table 5.5). Using Equation 4.1, the fracture toughness under mode-I fracture for crack initiation (G_{Ic}^{i}) and crack arrest (G_{Ic}^{a}) are 0.20 lb/in and 0.18 lb/in, respectively.

Figure 5.34. Fractured faces of Epoxy FRP-wood/RF/wet specimen (RF-WET 2)

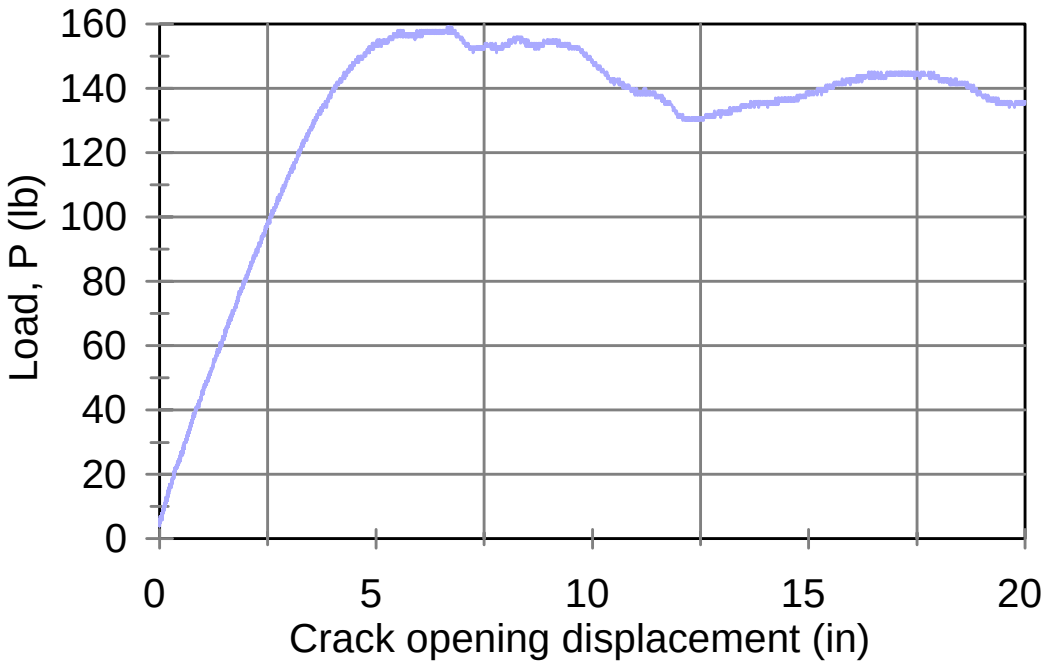

Figure 5.35. Load vs. crack opening displacement for specimen RF-WET 7

Table 5.19. Crack loads of CDCB specimens with Epoxy FRP-wood/RF/wet interface

Specimen No.	Critical loads (lb)	
	Crack initiation (P_{Ic}^{i})	Crack arrest (P_{Ic}^{a})
RF-WET 1	19	17
	19	17
	19	17
	19	18
	19	18
	19	18
	20	18
	20	19
	20	19
	20	19
	20	19
	20	18
	19	18
	20	19
	21	19
	21	19
	21	19
	21	19
	20	18
	20	18
	20	18
	20	18
	20	18
	20	18
	21	19
	22	20
RF-WET 2	105	103
	105	103

RF-WET 2 (Continued)	106	104
	107	105
	107	105
	107	105
	107	105
	107	105
	108	106
	108	106
	109	107
	108	106
	108	106
	108	106
	107	105
	106	104
	105	103
RF-WET 3	18	16
	17	15
RF-WET 4	18	16
	18	16
	17	15
	17	15
	17	15
	16	14
	16	14
	15	13
RF-WET 5	11	9
	11	9
	11	9
	11	9
	10	8
	9	7

RF-WET 6	78	76
	76	74
	75	72
	74	72
	73	71
	72	69
	70	68
	71	69
	71	69
	70	68
	70	68
	69	67
RF-WET 7	136	134
	137	135
	138	136
	140	138
	141	139
	144	142
	145	143
	145	143
	145	143
	143	141
	141	139
	138	136
	136	134
Average (COV)	62.7 (COV = 78.0%)	60.8 (COV = 80.3%)

5.6.6.2.3 Discussion for Epoxy FRP-wood Wet samples

The experimental results of the critical strain energy release rates (G_{Ic}; fracture toughness) for the Epoxy FRP-wood/HMR/wet and Epoxy FRP-wood/RF/wet samples are summarized and discussed in this section. As indicated in Table 5.20, the mean critical load values for Epoxy FRP-wood/HMR/wet interface bonds are much higher than the corresponding values for Epoxy FRP-wood/RF/wet interface bonds. The variability of critical loads for the RF-treated samples was significant (COV = 80.3%), with values ranging from about 10 lbs to 130 lbs (see Table 5.19). The fracture toughness values for the Epoxy FRP-wood interface bonds are given in Table 5.21. The RF/wet samples achieved only about 5% of the fracture toughness values of the HMR/wet samples. This big difference in values gives a definite indication of the enhanced bonding provided by the HMR coupling agent over the RF coupling agent. The Brittleness Index indicates stable crack growth for both types of laminates.

Table 5.20. Critical initiation and arrest loads for Epoxy FRP-wood/wet interface bonds

	P_c^i (lb)	P_c^a (lb)
Epoxy FRP-wood/HMR	284.0 (COV = 6.4%)	280.9 (COV = 6.5%)
Epoxy FRP-wood/RF	62.7 (COV = 78.0%)	60.8 (COV = 80.3%)

Table 5.21. Fracture toughness of Epoxy FRP-wood/wet interface bonds

	G_{Ic}^i (lb/in)	G_{Ic}^a (lb/in)	*Brittleness Index*
Epoxy FRP-wood/HMR	4.03	3.94	0.02
Epoxy FRP-wood/RF	0.20	0.18	0.10

5.6.7 Review and comparison of critical loads and fracture toughness

This section presents a compilation of the critical loads and fracture toughness data that were obtained for all of the tested samples discussed in this chapter. See Table 5.22 and Table 5.23 for a comparison of the critical loads and fracture toughness, respectively.

Table 5.22. Comparison of critical initiation and arrest loads

	P_c^i (lb)	P_c^a (lb)
Wood-Wood/Dry	175.7 (COV = 14.1%)	131.7 (COV = 20.3%)
Wood-Wood/Wet	198.9 (COV = 12.9%)	183.2 (COV = 14.8%)
Phenolic FRP-wood/Dry	109.5 (COV = 15.4%)	100.0 (COV = 17.0%)
Phenolic FRP-wood/Wet	157.5 (COV = 13.1%)	146.9 (COV = 15.1%)
Epoxy FRP-wood/HMR/Dry	218.6 (COV = 8.0%)	214.5 (COV = 8.8%)
Epoxy FRP-wood/HMR/Wet	284.0 (COV = 6.4%)	280.9 (COV = 6.5%)
Epoxy FRP-wood/RF/Dry	106.3 (COV = 31.8%)	97.5 (COV = 33.3%)
Epoxy FRP-wood/RF/Wet	62.7 (COV = 78.0%)	60.8 (COV = 80.3%)

Table 5.23. Comparison of fracture toughness

	G_{Ic}^i (lb/in)	G_{Ic}^a (lb/in)	*Brittleness Index*
Wood-Wood/Dry	3.35	1.88	0.44
Wood-Wood/Wet	3.63	3.08	0.14
Phenolic FRP-wood/Dry	1.28	1.06	0.17
Phenolic FRP-wood/Wet	2.57	2.23	0.13
Epoxy FRP-wood/HMR/Dry	2.54	2.47	0.03
Epoxy FRP-wood/HMR/Wet	4.03	3.94	0.02
Epoxy FRP-wood/RF/Dry	0.57	0.48	0.16
Epoxy FRP-wood/RF/Wet	0.20	0.18	0.10

5.6.8 Fracture Toughness Predictions by the Jacobian Derivative Method (JDM)

The Jacobian Derivative Method (JDM), a Finite Element post-processing algorithm, can be used to predict the strain energy release rate, or fracture toughness, of the CDCB specimens (Davalos, Raman, and Qiao 1997). The FE model of the specimens in Section 5.5 was used to simulate the interface of all the designed and tested specimens, and from these analyses, the displacement fields around the crack tips can be obtained and applied in the JDM. The mode-I critical strain energy release rates (G_{Ic}) can then be obtained for the experimentally measured critical loads. The details can be found in Davalos, Raman, and Qiao (1997).

5.7 Conclusions

The fracture toughness of wood-wood, Phenolic FRP-wood, and Epoxy FRP-wood bonded interfaces under mode-I fracture was evaluated using contoured double cantilever beam (CDCB) specimens. The best bonding process parameters (pressure and assembly time) obtained from the modified ASTM D 2559 tests were applied to manufacture the wood-wood and Phenolic FRP-wood specimens, and an RF adhesive (G-1311) was used. The composite-to-wood bonding process of the Epoxy FRP-wood specimens was accomplished during the filament winding process, and HMR and RF coupling agents were used to promote bonding. The linearity of the compliance crack-length relationship of linear-slope specimens was theoretically verified using Rayleigh-Ritz (RR), Modified Rayleigh-Ritz (MRR), and finite element models. A close correlation was achieved between the MRR method and finite element model, and the improved MRR method can be used with confidence to design the specimens and predict the compliance rate change. Through an experimental study of the compliance crack-length relationship of linear-slope specimens for wood-wood, Phenolic FRP-Phenolic FRP, and Epoxy FRP-wood bonded interfaces under dry and wet conditions, it is shown that the linearlized specimen can be used for Mode-I fracture tests with reasonable confidence on the linearity of the compliance rate change. The fracture toughness values of wood-wood, Phenolic FRP-

wood, and Epoxy FRP-wood bonded interfaces under dry and wet conditions were experimentally determined, and an increase in interface fracture toughness due to moisture absorption was obtained for the wet wood-wood, Phenolic FRP-wood, and Epoxy FRP-wood samples. Also, the effect of coupling agent on fracture toughness of Epoxy FRP-wood interfaces under both dry and wet conditions were investigated; the fracture toughness of interfaces with HMR coupling is much higher than those treated with RF. The toughening of the interface under exposure to moisture is mainly due to a much more plastic fracture failure mode.

CHAPTER 6

FRACTURE TOUGHNESS OF AGED PHENOLIC FRP-WOOD BONDED INTERFACE

6.1 Introduction

Once the Mode-I fracture toughness data was obtained for the dry and wet samples in chapter 5, Contoured Double Cantilevered Beam (CDCB) specimens were designed to conduct Mode-I fracture tests and obtain fracture toughness data for aged Phenolic FRP-wood interface bonds. In this chapter, bi-layer CDCB specimens are designed by the Rayleigh-Ritz method and used for fracture toughness tests of bonded Phenolic FRP-wood interfaces subjected to repeating cycles of wetting and drying. Using linear-slope CDCB specimen, fracture tests are performed for aged specimens to determine critical loads for crack initiation and crack arrest, from which the critical strain energy release rates (G_{Ic}) are evaluated by using the designed constant compliance rate changes over defined crack lengths.

The CDCB specimens were aged (conditioned) in accordance with the three conditioning cycles of the ASTM D 2559 (Section 2.4). A set of 7 samples for each cycle of the cyclic test was manufactured and tested, which resulted in a total number of 21 Phenolic FRP-wood samples.

6.2 Materials

6.2.1 Wood materials

The wood materials used for the production of the Mode-I fracture samples were Red Maple (Section 2.2.1) and Yellow Poplar Laminated Veneer Lumber (LVL: Section 5.2.1). Red Maple was used for the adherend bonded to the Phenolic FRP composite, and the LVL was used for the designed contours of both the Red Maple and Phenolic FRP adherends.

6.2.2 FRP material

The FRP material consisted of E-glass fiber rovings embedded in a Phenolic resin Matrix (Figure 2.3, Chapter 2). The Phenolic fiber reinforced plastic (Phenolic FRP) composite material was produced by the pultrusion process, which is a well controlled and relatively low cost manufacturing process for FRP composites.

The Phenolic FRP composite contains Continuous Strand Mat (CSM) layers on both outside surfaces, which provide desirable surface texture for obtaining a good adhesive bond interface. The lay-up of the Phenolic FRP laminate is shown in Figure 2.4. The Phenolic FRP surfaces were sanded and cleaned, before bonding, as explained in Section 2.2.2.

6.2.3 Material characterization

To design CDCB specimens for aged conditions, the stiffness properties of the wood and Phenolic FRP materials under the required aging conditions must be obtained. The contoured shapes for each aging cycle should be designed accounting for the degraded stiffness properties of the materials due to the aging effects. The change in properties for

the Phenolic FRP laminate was neglected in this study, and the properties of the Phenolic FRP/dry samples are used for the design of all the conditioned samples.

Initially, small coupon samples were conditioned and tested to obtain degraded values of E and G; these values were then used to design the CDCB specimens. Later, and after the CDCB specimens were tested for Fracture Toughness, larger and more representative samples were cut from the CDCB specimens to re-evaluate the material properties, as explained in the following two sections.

6.2.3.1 Testing of small coupon samples

The wood stiffness properties were initially evaluated by testing small samples, which were tested after each of the three cycles specified in ATSM D 2559.

The longitudinal-tensile and shear moduli of the Red Maple and LVL were obtained from tension and torsion coupon tests, respectively. For the tension tests, 14 specimens (Red Maple: 1” x ½” x 17”; LVL: 1” x 0.4” x 17”) for each cycle of the ASTM D 2559 test were conditioned and tested. Similarly, six specimens (Red Maple: 1” x 1” x 17”; LVL: 1” x 1.5” x 17”) for each cycle of the ASTM D 2559 were prepared, conditioned and tested in torsion to obtain shear moduli data.

Six Phenolic FRP strips (see Figure 2.4) were also tested under tension. The tensile madulus was compared with the Micro/Macromechanics model prediction (Davalos et al. 1996). The Phenolic FRP strips were too flexible to be tested in torsion; therefore, the shear modulus predictions by the Micro/Macromechanics model were used in the design.

The stiffness properties reported in Tables 6.1 through 6.3 were used to design the contour shapes of the conditioned Phenolic FRP-wood CDCB specimens.

Table 6.1 Material properties of Red Maple under cyclic conditioning

	E (10^6 psi)	G (10^6 psi)
Cycle 1	1.646 (COV = 12.36%)	0.150 (COV = 9.71%)
Cycle 2	0.7249 (COV = 13.56%)	0.1413 (COV = 11.78%)
Cycle 3	0.7211 (COV = 13.22%)	0.1240 (COV = 13.57%)

Table 6.2 Material properties of LVL under cyclic conditioning

	E (10^6 psi)	G (10^6 psi)
Cycle 1	1.790 (COV = 11.99%)	0.0531 (COV = 4.80%)
Cycle 2	0.8685 (COV = 12.40%)	0.0529 (COV = 2.93%)
Cycle 3	0.8561 (COV = 8.20%)	0.0418 (COV = 1.09%)

Table 6.3 Material properties of Phenolic FRP under normal conditions

	E (10^6 psi)	G (10^6 psi)
Experiment	4.410 (COV = 0.55%)	--
Micro/Macromechanics	4.378	0.650

6.2.3.2 Testing of samples cut from CDCB specimens

Following the Mode-I fracture toughness tests of the conditioned Phenolic FRP-wood specimens, samples were cut from the LVL contours of the CDCB specimens to re-evaluate the Modulus of Elasticity of the conditioned LVL. This re-evaluation was conducted because it was observed that the actual CDCB specimens were not fully dried to the expected 12% MC during the 22 hours of oven drying specified by the ASTM D 2559. The CDCB samples were designed using the stiffness properties from the small samples, which were fully dried during the 22 hours of oven drying after each moisture conditioning cycle.

The re-evaluated longitudinal-tensile modulus of the LVL was obtained from tension coupon tests. After testing CDCB specimens for Fracture Toughness, LVL coupons were cut from the middle portions of the contours to obtain a more representative longitudinal-tensile modulus after conditioning. Fourteen LVL samples (1.25" x 1/2" x 12") for each conditioning cycle were tested, and the results showed that for all three conditioning cycles the Modulus of Elasticity was nearly constant and approximately equal to 1.03 E^6 psi (COV = 23.9%).

This apparent and more representative Modulus of Elasticity value along with the stiffness properties obtained initially from coupon samples were then used to re-evaluate the dC/da of the tested CDCB specimens.

6.3 Contour Shapes of the Designed CDCB Specimens

Based on the design procedure of section 4.3 and the coupon material properties described in section 6.2.3.1, the slopes of the CDCB specimens were designed using the simplified Raleigh-Ritz method for a target dC/da = 6.25 x 10^{-5} lb^{-1}. The slopes for each cycle are given in Table 6.4, and the as-manufactured specimens are shown in Figure 6.1. These specimens were re-analyzed to obtain their predicted "Initial" *dC/da* values (Table 6.4), which are within 3% (average = 6.15 x 10^{-5} lb^{-1}) of the target value. Later, the specimens shown in Figure 6.1 were analyzed again to obtain the "Final" *dC/da* values, based on as-conditioned value of E = 1.03 x 10^6 psi for the LVL contours (Table 6.4).

Table 6.4 Compliance rate change of linear tapered specimens

Cycle	Specimen	Slope [a] (in/in)	dC/da (10^{-5} lb^{-1})	
			Initial RR[a]	Final RR[b]
Cycle 1	Phenolic FRP	0.1344	6.22	8.89
	Wood	0.1411	6.19	8.81
Cycle 2	Phenolic FRP	0.1729	6.17	5.53
	Wood	0.1968	6.07	4.87
Cycle 3	Phenolic FRP	0.1754	6.17	5.39
	Wood	0.2011	6.07	4.65

(a) Based on material properties for small coupon samples
(b) Based on material properties for coupon samples cut from conditioned CDCB

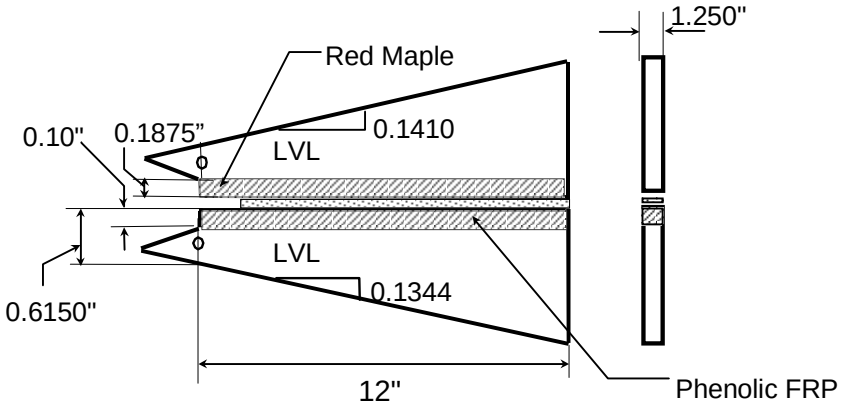

(a) Geometry of Phenolic FRP-wood/Cycle 1 Specimen

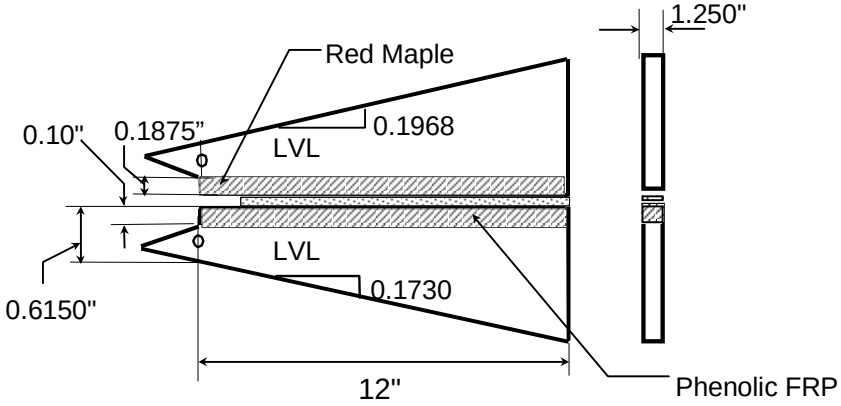

(b) Geometry of Phenolic FRP-wood/Cycle 2 Specimen

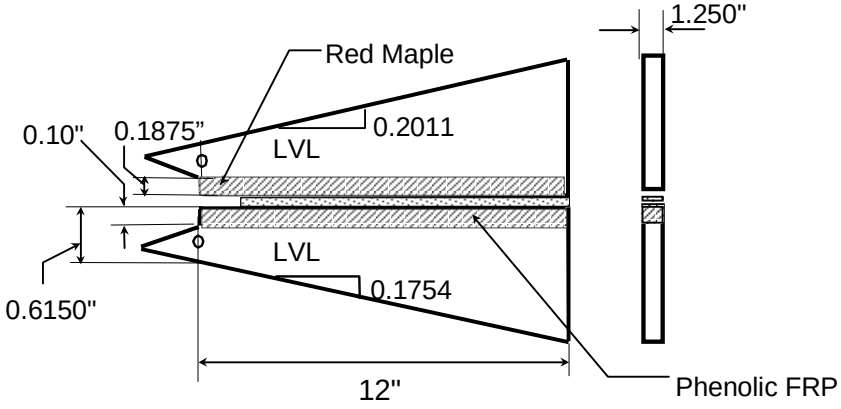

(c) Geometry of Phenolic FRP-wood/Cycle 3 Specimen

Figure 6.1. Contour shapes for CDCB Phenolic FRP-wood aged specimens

6.4 Experimental Evaluation of Fracture Toughness

Based on the most favorable assembly conditions evaluated from the modified ASTM D 2559 (pressure p = 210 psi and open/closed assembly times t = 5/30 min), Phenolic FRP-wood samples were manufactured, aged, and tested for each cycle of the 3-cycle aging conditions. The adhesive used to bond wood to wood and Phenolic FRP to wood was resorcinol formaldehyde (RF, G-1131) resin as described in section 2.2.5. A set of seven samples for each cycle of the aging process was manufactured and tested, which resulted in a total number of 21 samples.

6.4.1 Testing procedure

The experiments were performed on an MTS servo hydraulic testing machine. The load was applied using a loading fixture made of aluminum (Figure 5.5). For testing, the tip of the specimen was connected to the loading fixture, while the specimen was supported vertically by a plastic thread attached to the upper frame of the testing machine (Figure 5.5). The experiment was conducted under displacement-controlled mode with a displacement rate of 0.002 in/s. Under displacement control, the crack propagation is stable, since the energy required for crack extension is obtained from the release of elastic strain energy (Anderson 1995). The load was applied continuously to initiate and sustain the crack propagation in the specimen. Since the compliance rate change (dC/da) was previously established, it was required to measure only the critical loads from which the fracture toughness could be evaluated (see Equation 4.1). To monitor the crack propagation, the critical loads versus crack opening displacements were plotted. An accurate measurement of the crack opening displacement is not essential, and therefore, the load grip displacements were recorded and used to interpret the test results. Following testing, the mode-I fracture toughness of the interface was evaluated.

6.4.2 Mode-I fracture toughness for Phenolic FRP-wood aged bonded interface

6.4.2.1 Cycle 1 conditioning

The linear-slope CDCB specimen shown in Figure 6.1(a) was used for the Mode-I fracture test of the cycle 1 aged Phenolic FRP-wood specimens. The specimen was designed by the method described in Section 6.3. Seven specimens were fabricated (see Figure 6.1a) and then tested to obtain the critical loads for crack initiation and arrest. The fractured surfaces for a typical specimen [Phenolic FRP-wood sample #2, day 1 cycle (Day 1-2)] are shown in Figure 6.2. A representative test result is given in Figure 6.3 for day 1 cycle of specimen #7, Phenolic FRP-Day 1-7. The critical loads for crack initiation and crack arrest were obtained for all seven specimens, and the results are given in Table 6.5. An analysis of the critical loads yields a mean crack-initiation load value of 174.9 lb. with a COV of 15.2%, and a mean crack-arrest load value of 166.0 lb. with a COV of 17.8%. The critical strain energy release rates (fracture toughness) given by Equation 4.1 are computed using the mean values of the critical loads and the "Final" compliance rate change, *dC/da*, obtained by the Final Rayleigh-Ritz (RR) method (see Table 6.4). Using Equation 4.1, the fracture toughness under mode-I fracture for crack initiation (G_{Ic}^{i}) and crack arrest (G_{Ic}^{a}) are 2.17 lb/in and 1.95 lb/in, respectively.

Figure 6.2. Fractured faces of Phenolic FRP-wood cycle 1 specimen #2 (Day 1-2)

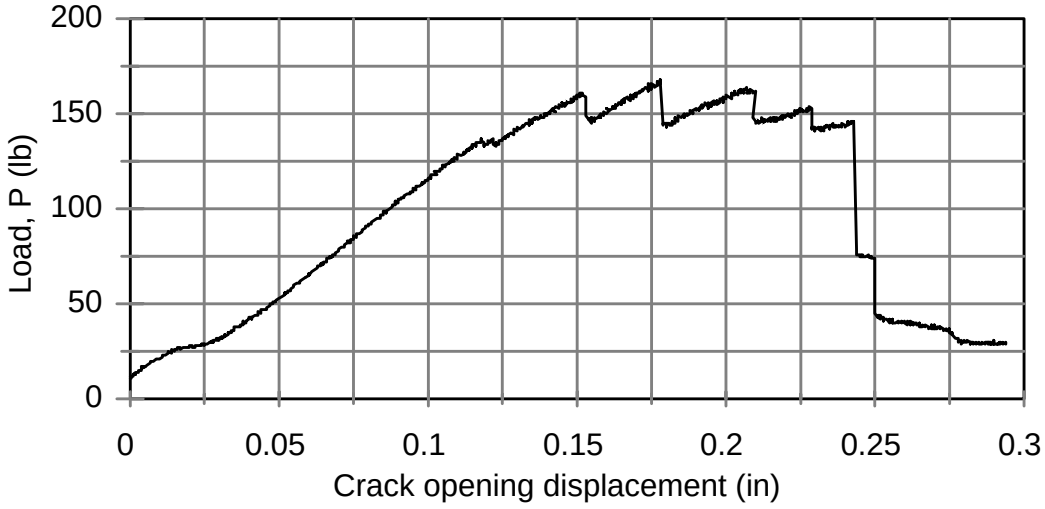

Figure 6.3. Load vs. crack opening displacement for specimen Day 1-7

Table 6.5. Crack loads of CDCB specimens with cycle 1 aged Phenolic FRP-wood interface

Specimen No.	Critical loads (lb)	
	Crack initiation (P_{Ic}^{i})	Crack arrest (P_{Ic}^{a})
Phenolic Day 1-1	182 173 175 171 180 180	165 167 166 166 174 175
Phenolic Day 1-2	144 149 142 142	131 137 136 139
Phenolic Day 1-3	150 160 156 145	144 143 130
Phenolic Day 1-4	159 161 156	149 152 152
Phenolic Day 1-5	187 181 184	167 177 171
Phenolic Day 1-6	214 221 221 221 224 222	211 218 218 219 214 219
Phenolic Day 1-7	161 168 163 154	146 143 145 141
Average (COV)	174.8 lb. (COV = 15.2%)	166.0 lb. (COV = 17.8%)

6.4.2.2 Cycle 2 conditioning

The linear-slope CDCB specimen shown in Figure 6.1(b) was used for the Mode-I fracture test of the cycle 2 aged Phenolic FRP-wood specimens. The specimen was designed by the method described in Section 6.3. Seven specimens were fabricated (see Figure 6.1b) and then tested to obtain the critical loads for crack initiation and crack arrest. The fractured surfaces of a typical specimen, [Phenolic FRP-wood sample #2, Day 2 cycle (Day 2-2)] are shown in Figure 6.4. A representative test result is given in Figure 6.5 for the specimen Phenolic FRP Day 2-4. The critical loads for crack initiation and crack arrest were obtained for all seven specimens, and the results are given in Table 6.6. An analysis of the critical loads yields a mean crack-initiation load value of 199.1 lb. with a COV of 8.5%, and a mean crack-arrest load value of 188.7 lb. with a COV of 11.0%. The critical strain energy release rates (fracture toughness) given by Equation 4.1 are computed using the mean values of the critical loads and the "Final" compliance rate change, *dC/da*, obtained by the Final Rayleigh-Ritz (RR) method (see Table 6.4). Using Equation 4.1, the fracture toughness under mode-I fracture for crack initiation (G_{Ic}^{i}) and crack arrest (G_{Ic}^{a}) are 1.65 lb/in and 1.48 lb/in, respectively.

Figure 6.4. Fractured faces of Phenolic FRP-wood cycle 2 specimen #2 (Day 2-2)

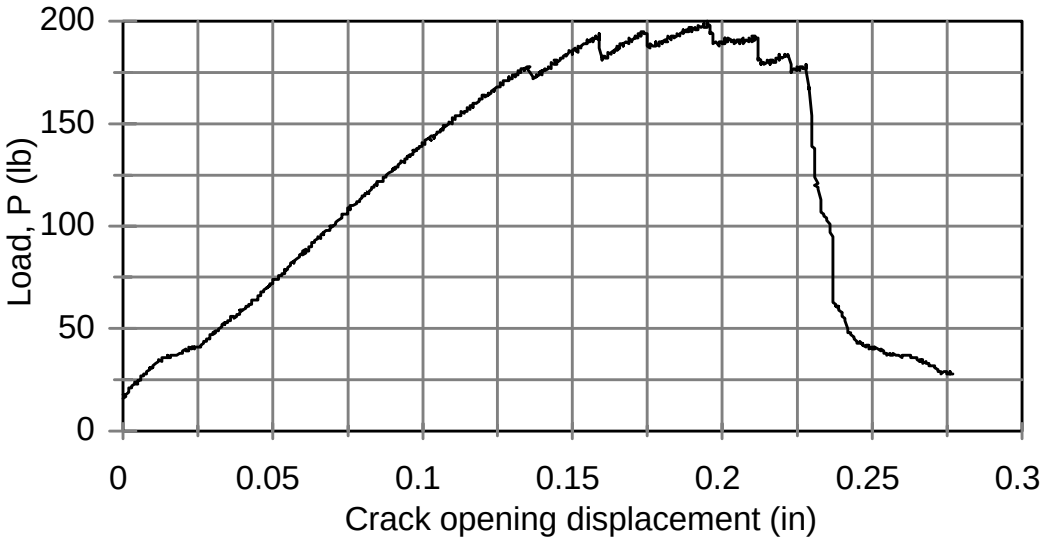

Figure 6.5. Load vs. crack opening displacement for specimen Day 2-4

Table 6.6. Crack loads of CDCB specimens with cycle 2 aged Phenolic FRP-wood interface

Specimen No.	Critical loads (lb)	
	Crack initiation (P_{Ic}^{i})	Crack arrest (P_{Ic}^{a})
Phenolic Day 2-1	201 202 199 199 201 201 202 203	199 198 197 197 198 199 200 201
Phenolic Day 2-2	180 184 175	173 166 146
Phenolic Day 2-3	193 196 183 180	186 177 177 153
Phenolic Day 2-4	194 195 200 192 193	181 187 188 189 179
Phenolic Day 2-5	174 191 197 191	169 175 180 169
Phenolic Day 2-6	217 221 206 186	206 196 184 175
Phenolic Day 2-7	237 240 240	231 236 236
Average (COV)	199.1 lb. (COV = 8.5%)	188.7 lb. (COV = 11.0%)

6.4.2.3 Cycle 3 conditioning

The linear-slope CDCB specimen shown in Figure 6.1(c) was used for the Mode-I fracture test of the cycle 3 aged Phenolic FRP-wood specimens. The specimen was designed by the method described in Section 6.3. Seven specimens were fabricated (see Figure 6.1c) and then tested to obtain the critical loads for crack initiation and arrest. The fractured surfaces for a typical specimen [Phenolic FRP-wood sample #1, Day 3 cycle (Day 3-1)] are shown in Figure 6.6. A representative test result is given in Figure 6.7 for day 3 cycle of specimen #1, Phenolic FRP Day 3-4. The critical loads for crack initiation and crack arrest were obtained for all seven specimens, and the results are given in Table 6.7. An analysis of the critical loads yields a mean crack-initiation load value of 207.7 lb. with a COV of 9.3%, and a mean crack-arrest load value of 199.7 lb. with a COV of 10.5%. The critical strain energy release rates (fracture toughness) given by Equation 4.1 are computed using the mean values of the critical loads and the "Final" compliance rate change, *dC/da*, obtained by the Final Rayleigh-Ritz (RR) method (see Table 6.4). Using Equation 4.1, the fracture toughness under mode-I fracture for crack initiation (G_{Ic}^{i}) and crack arrest (G_{Ic}^{a}) are 1.73 lb/in and 1.60 lb/in, respectively.

Figure 6.6. Fractured faces of Phenolic FRP-wood cycle 3 specimen #1 (Day 3-1)

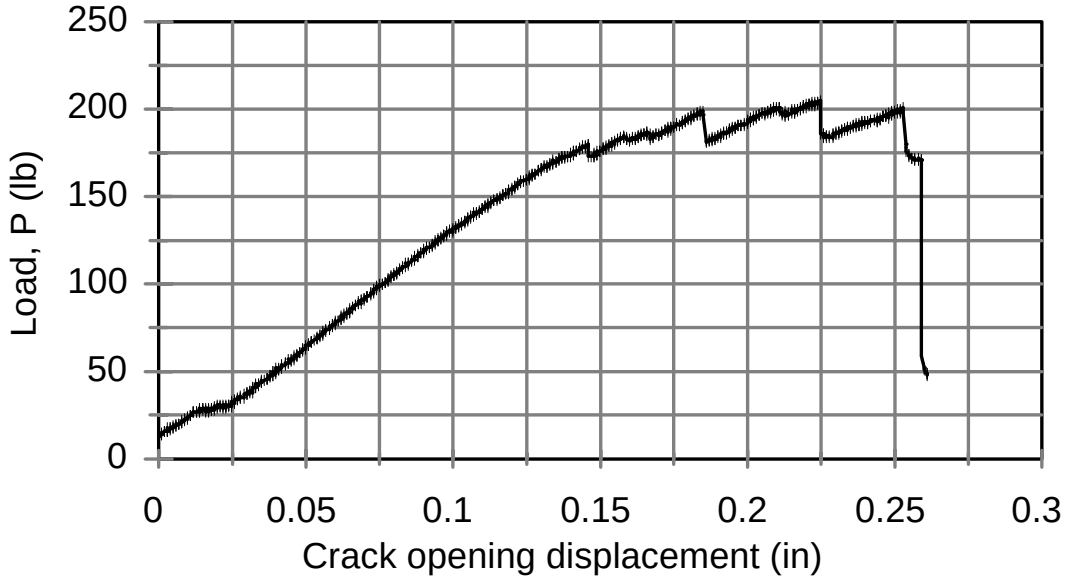

Figure 6.7. Load vs. crack opening displacement for specimen Day 3-4

Table 6.7. Crack loads of CDCB specimens with cycle 3 aged Phenolic FRP-wood interface

Specimen No.	Critical loads (lb)	
	Crack initiation (P_{Ic}^{i})	Crack arrest (P_{Ic}^{a})
Phenolic Day 3-1	190	183
	197	194
	200	193
	200	190
	198	190
	194	191
Phenolic Day 3-2	195	181
	193	187
	223	216
	220	194
Phenolic Day 3-3	211	199
	235	222
	240	212
	218	211
Phenolic Day 3-4	199	181
	201	196
	205	184
	201	180
Phenolic Day 3-5	173	162
	189	184
	193	189
	193	170
	176	161
Phenolic Day 3-6	212	210
	216	214
	220	217
	221	219

Phenolic Day 3-6 (Continued)	225	223
	227	224
	232	229
	236	233
	237	234
	238	235
	239	235
	237	232
	232	228
Phenolic Day 3-7	184	179
	184	181
	188	185
	198	195
	198	190
	194	191
	192	186
	185	176
Average (COV)	207.7 lb. (COV = 9.3%)	199.7 lb. (COV = 10.5%)

6.4.2.4 Discussion for Phenolic FRP-wood aged samples

The experimental results of the critical strain energy release rates (G_{Ic}; fracture toughness) for the Phenolic FRP-wood aged samples are summarized and discussed in this section. As indicated in Table 6.8, the mean critical load values for the interface bonds are highest with the cycle 3 and lowest with the cycle 1 interface bonds; this is due primarily to the larger *dC/da* values (Table 6.4) of the cycle 1 specimens compared to the cycle 2 and cycle 3 specimens. Note that the specimen slopes for the three cycles are substantially different, while the modulus of elasticity of the LVL contours remains nearly constant through the three cycles (see Section 6.3). In general, the G_{IC} value decreases substantially after the first cycle and remains stable for cycles 2 and 3. In addition to fracture toughness data, a "Brittleness Index *I*," (River and Okkonen 1993) which is the ratio of energy lost during crack growth to the energy required to initiate crack growth, can also be used to indicate stability of the crack growth (See Equation 5.1 and Section 5.6.8). Based on the fracture toughness data obtained, the corresponding I values for all the aged Phenolic FRP-wood specimens are given in Table 6.9. It is shown that a relatively stable crack propagation was observed for all three cycles of the aged specimens. This is consistent with the observed failure type: In all 21 aged Phenolic FRP-wood samples the fracture plane was within the CSM layer of the Phenolic FRP, with visible fiber bridging of the CSM layer.

Table 6.8. Critical initiation and arrest loads for aged Phenolic FRP-wood interface bonds

	P_c^i (lb)	P_c^a (lb)
Phenolic FRP-wood Cycle 1	174.9 (COV = 15.2%)	166.0 (COV = 17.8%)
Phenolic FRP-wood Cycle 2	199.1 (COV = 8.5%)	188.7 (COV = 11.0%)
Phenolic FRP-wood Cycle 3	207.7 (COV = 9.3%)	199.7 (COV = 10.5%)

Table 6.9. Fracture toughness of aged Phenolic FRP-wood interface bonds

	G_{Ic}^{i} (lb/in)	G_{Ic}^{a} (lb/in)	*Brittleness Index*
Phenolic FRP-wood Cycle 1	2.17	1.95	0.10
Phenolic FRP-wood Cycle 2	1.65	1.48	0.10
Phenolic FRP-wood Cycle 3	1.73	1.60	0.08

6.5 Conclusions

The fracture toughness of aged Phenolic FRP-wood bonded interfaces under mode-I fracture was evaluated using contoured double cantilever beam (CDCB) specimens. The best bonding process parameters (pressure and assembly time) obtained from the modified ASTM D 2559 tests were applied to the manufacture the Phenolic FRP-wood specimens, and an RF adhesive (G-1131) was used. The linearity of the compliance crack-length relationship of linear-slope specimens was theoretically verified using the simplified Rayleigh-Ritz (RR) method; therefore, the RR method can be used with confidence to design the specimens and predict the compliance rate change. The fracture toughness values of aged Phenolic FRP-wood bonded interfaces were experimentally determined, and a decrease of interface fracture toughness was obtained from the cycle 1 specimens to the cycle 2 and cycle 3 specimens.

Because of the difficulties we faced with "representative" material properties to design the CDCB specimens the conclusions of this study for aged samples are not definite, and the G_{IC} values given in Table 6.9 can not be used with certainty. A better way to design the contour samples for aging conditioning is needed, and we suggest the following two alternatives:

(1) Obtain contour material properties from larger specimens, where the depth can be about the mid-height of the tapered section.

(2) Condition only the constant thickness FRP-wood laminate, and after oven-drying attach dry (12% MC) contour portions to the bi-layer laminate and test for compliance calibration and Fracture Toughness.

CHAPTER 7

CONCLUSIONS AND RECOMMENDATIONS

7.1 Importance of FRP-Wood Bonded Interface Performance

Fiber-reinforced plastic (FRP) composites are being used for reinforcement of wood, concrete, and steel. The significant attention devoted to rehabilitation of industrial and public works has presented a unique opportunity for development of combined fiber-reinforced plastic (FRP) and wood materials, which can provide longer service-life and lower life-cycle costs than conventional materials. Current research on wood reinforcement has focused on the use of fiber-reinforced plastic (FRP) composites bonded to wood members. Although significant increases in stiffness and strength have been achieved by this reinforcing technique, there is a concern about the reliable performance of the wood-FRP interface bond, which can be susceptible to delamination (Hernandez et al. 1997). Several adhesive systems have been used to reinforce conventional materials with composites; however, there are no long-term performance qualification methods for bonded interfaces of hybrid composites. In particular, the service performance of FRP-wood interface bonds is critical in the design and durability of reinforced wood products, and the delamination of the interface can lead to premature failure of hybrid FRP-wood composites. Moreover, fracture toughness data of the interface is needed to properly evaluate the potential propagation of an existing delamination.

7.2 Guidelines for FRP-Wood Bonded Interface Performance Evaluations

In this study, a comprehensive program to evaluate the durability of and obtain shear strength and fracture toughness data for FRP-wood bonded interfaces is presented.

The potential in-service delamination of bonded interfaces is evaluated by a 3-cycle test of repeated wetting and drying. Also, wet and dry interface strengths are evaluated through block-shear tests. The fracture toughness of the interface is measured by an innovative fracture mechanics test. Several key parameters on the durability of interface are investigated, such as coupling agent (primer) to promote bonding, open/closed assembly time, and clamping pressure. The present bond-interface characterization study can be used to qualify adhesives, establish service performance, and obtain apparent bond strength and fracture toughness values for interfaces of FRP bonded to wood materials.

To evaluate the in-service performance of bonded FRP-wood hybrid products and to qualify adhesive systems for FRP-wood bonding, the following general guidelines for interface bond characterization are suggested:

- The ASTM D 2559 wetting-and-drying cyclic delamination test appears to be sensitive enough to investigate key performance parameters, such as coupling agent (primer) to promote bonding, open/closed assembly time, clamping pressure, bonding surface preparation, etc, and it can be first used as a screening test to evaluate the delamination of bonded interfaces.

- Once the best combination of parameters is obtained from the ASTM D 2559 tests, standard block-shear tests (ASTM D 905) can then be used to evaluate average bond "shear" strength, which can be applied in design with an appropriate factor of safety. Also, the bond strength under various moisture contents (conditions) can be obtained.

- Finally, the Contoured Double Cantilever Beam (CDCB) specimen (Davalos, Raman and Qiao 1997) described in this study can be effectively used to obtain interface Mode-I fracture toughness values; these data can be implemented in practical applications to assess the potential growth of a delamination crack at the FRP-wood interface.

7.3 Overall Conclusions of This Research

This research presents a combined experimental and analytical program to evaluate the potential in-service performance and the fracture toughness of FRP-wood interface bonds. It was shown that the ASTM D 2559 standard test could be effectively used to study the effect of several bonding parameters. Then for the best combination of bonding parameters, the average interface shear strengths were obtained by block-shear tests of ASTM D 905 for hybrid laminates under dry and wet conditions. However, performance evaluation tests are not sufficient to predict whether or not a bonded interface will delaminate under general moisture, temperature, and service loads conditions. Therefore, the fracture toughness of interfaces were obtained to evaluate the potential "crack" initiation and arrest of a present delamination. The contoured double cantilever beam (CDCB) specimen discussed in this study was an efficient tool to evaluate Mode-I fracture toughness of hybrid interfaces, such as FRP-wood. The guidelines presented in this study are useful for designing bonded joints, evaluating the in-service durability of bonded interfaces, and obtaining fracture toughness data for FRP-wood material combinations.

7.4 Specific Findings of this Research

Although the objective of this research was not to develop or recommend any specific reinforcing FRP product, adhesive/primer system, or bonding process, an overview is presented of some specific results obtained with the materials used in this study.

7.4.1 Results of each test method

7.4.1.1 Delamination tests

The ASTM D 2559 standard test was shown to be very useful in studying several bonding parameters.

- The measured end-grain delamination was within acceptable limits for the Phenolic FRP composite, with continuous strand mat (CSM) exterior layers and sanded surfaces bonded to Red Maple with an RF adhesive without the need of a coupling agent such as HMR.

- The Epoxy FRP composite samples filament wound to Red Maple primed with HMR coupling agent performed within acceptable end grain delamination limits given for hardwoods, such as Red Maple.

- The Epoxy FRP composite samples primed with RF coupling agent, performed out of the acceptable end grain delamination limits given for hardwoods, such as Red Maple; therefore, it is shown that the RF primer should not be used for filament winding with an Epoxy composite.

7.4.1.2 Block-Shear tests

The ASTM D 905 standard test method, commonly used to evaluate bond shear strength and percent material failure, was reasonably effective for FRP-wood assemblies. The following observations are reported:

- For wood-wood bonds, the shear strength of dry (12% MC) samples was about twice that of wet (moisture saturated) samples. Also, the percent wood failure (cohesive failure) was 81% for dry and 58% for wet samples.

- For Phenolic FRP-wood bonds, the strengths of dry and wet samples were nearly the same and coincidentally approximately equal to the wood-wood wet bond strength. The failure occurred mainly within the CSM layer of the Phenolic FRP, about 100% cohesive failure for dry and 76% for wet samples. Thus, the Phenolic FRP-wood bond strength was controlled by the CSM's relatively week shear strength, which was only about one half of the wood-wood dry shear strength. While it appears that a sanded CSM layer bonds well to wood, the CSM shear strength may control the bond performance, and therefore, this failure mode must be considered when using this product. However, the

fiber architecture of the composite can always be optimized to prevent or avoid this type of failure.

- For Epoxy FRP-wood bonds, produced by Filament Winding and direct cure of the resin over the wood core, the strengths of dry and wet samples with HMR primer exhibited high shear strength values and percent cohesive (wood) failures. This was due to the HMR bond enhancement at the interface. The RF primed samples showed a larger variation in shear strength and a relatively lower percent cohesive (wood) failure, which showed that RF should not be used as a primer for Filament Wound Epoxy composites.

7.4.1.3 Fracture mechanics tests

The specimens and test methods described in this study can be used to evaluate the potential crack extension of an existing delamination at the bond interface. The fracture toughness of the interface is necessary for such studies. Although its application in design is not readily apparent, the strain energy release rate, or fracture toughness, concept is typically used in numerical and explicit analyses concern with the delamination of laminates, such as the analysis of FRP-reinforced Glulam beams; see for example the delamination buckling studies of FRP-Glulam beams by Kim et al. (1997). For the wood-wood, Phenolic FRP-wood, and Epoxy FRP-wood samples tested under dry, wet and cyclic wet/dry conditioning in this study, the following specific observations are summarized:

- For the dry wood-wood samples, the difference between the fracture energies for crack initiation and arrest indicates a relatively unstable crack propagation, which is consistent with the crack propagation into the wood substrate in the test samples (60% wood failure). In contrast, for the wet wood-wood samples this difference is much less, and correspondingly the crack propagation was much more stable and primarily along the bond interface (40% wood failure).

- For the dry and wet Phenolic FRP-wood samples, the crack extension was very much stable, but the failure occur almost entirely in the CSM layer.

- For the dry and wet Epoxy FRP-wood samples with HMR primer, the crack extension was stable, and the corresponding fracture toughness values were approximately 95% and 80% higher than those obtained for dry and wet Epoxy FRP-wood with RF primer.

- For wet specimens, increases in fracture energy occurred because of the plastification of the bond and the adherends. This increase is negligible for wood-wood samples, but about 100% for wet Phenolic FRP-wood samples and 65% for Epoxy FRP-wood samples with HMR primer.

- For Filament Wound samples produced with the Epoxy based composite, the HMR primer showed promising Fracture Toughness results, whereas the RF primer produced consistently bad results, showing that it should not be used as a coupling agent with Epoxy composites.

- For the cyclic conditioning Phenolic FRP-wood specimens, the crack extension was stable in all of the samples, but the fracture occurred entirely in the CSM layer. The Fracture Toughness decreased substantially from Cycle 1 conditioning to Cycles 2 and 3. A better way to design the test-specimen is needed, as discussed in Section 6.5.

7.4.2 Correlation of test methods

In this research, no attempt was made to establish correlations among the delamination (ASTM D 2559), block-shear (ASTM D 905), and fracture mechanics tests. However, a complementary and sequential process to effectively combine these three tests in the evaluation of FRP-wood bonded joints is presented. Both the delamination and block-shear tests for wood-wood assemblies are specified by ASTM, while the Mode-I fracture tests proposed in this study for bonded hybrid interfaces is a new development. Similar ASTM specifications exist for fracture toughness of interfaces for bonded metals and interlaminar fracture toughness for composite materials. The following combined tests are suggested for the evaluation of FRP-wood bonded interfaces:

- Use the delamination test for development, qualification, and evaluation of bonded joints, including adhesive/primer systems, surface texture of adherends, clamping pressure, and other parameters. The sensitivity and ease of implementation and interpretation of this test are favorable attributes for this application.

- Next, use the block-shear test to obtain apparent average interface shear strengths and percent material failures for the specimens under the required environmental conditions. The strength values can be used in design with the appropriate adjustment factors as described by Soltis et al. ???

- Finally, use the CDCB specimens to obtain the fracture toughness of interfaces to use in explicit and numerical models to study interface delamination of existing cracks (e.g., Kim et al. 1997) and design applications.

7.5 Recommendations for Future Work

For the delamination test, further work is needed to define the appropriate size of the specimen, accounting for the material lay-up and thickness of the composite in relation to the characteristics of the core wood laminate.

For the block-shear test, new guidelines are needed to define the test specimen accounting for the relatively thin layer of composite bonded to the 3/4" wood layer. For standard wood-wood samples, the stress concentration factor at the re-entry corner is about 2.5, and the contour of the interface shear stress is highly nonlinear (and not constant as assumed). The possibility exists to optimize the wood-FRP specimen to achieve a relatively constant shear stress distribution at the interface. Moreover, new guidelines are needed to test moisture saturated specimens.

For the CDCB specimens for fracture toughness, there is a need to simplify and standardize this test method. Also, an in-depth study of the delamination specimen (ASTM D

2559) using fracture toughness data to predict interface crack propagation can lead to useful correlation of these two test methods, whereby approximate fracture toughness data may be predicted with specialized delamination specimens subjected to prescribed test procedures.

At a larger scale, the results of these three test methods can be extended to applications in product design, such as FRP-Glulam and FRP-wood-composite joists and beams.

REFERENCES

ANSYS Theoretical Manual. (1991). Swanson Analysis Systems, Houston, PA.

Abdel-Magid, B., Scholsky, K., Shaler, S., Dagher, H., Kimball, T. (1996), "Interfacial Bonding Between Phenolic Matrix Composites and Wood", Proceedings of the First International Conference on Composites in Infrastructure (ICCI'98), Tucson, AZ, January 5-7, 1996, 54-58.

American Society for Testing and Materials, (1985), Standard Practice for Fracture Strength in Cleavage of Adhesives in Bonded Joints, ASTM D 3433-75 (Reapproved 1985), Philadelphia, PA.

American Society for Testing and Materials, (1989), Standard Test Method for Strength Properties of Adhesive Bonds in Shear by Compression Loading, ASTM D 905-89, Philadelphia, PA.

American Society for Testing and Materials, (1992), Standard Test Methods for Integrity of Glue Joints in Structural Laminated Wood Products for Exterior Use, ASTM D 1101-92, Philadelphia, PA.

American Society for Testing and Materials, (1992), Standard Specification for Adhesives for Structural Laminated Wood Products for Use Under Exterior (Wet Use) Exposure Conditions, ASTM D 2559-92, Philadelphia, PA.

American Society for Testing and Materials, (1992), Standard Test Method for Plane-Strain Fracture Toughness of Metallic Materials, ASTM E 399-90, Philadelphia, PA.

Barbero, E. J., Davalos, J. F. and Munipalle, U. M. (1994). "Bond strength of FRP-wood interface." *J. of Reinforced Plastics and Composites*, 13 (9), 835-854.

Cagle, C.V., (1968), *Adhesive Bonding: Techniques and Applications*, McGraw-Hill Book Company, 1968.

Chajes, M.J., Thomson Jr., T.A., Farschman, C.A., (1995), "Durability of concrete beams externally reinforced with composite fabrics", Construction of Building Materials, 9(3), 141-148.

Davalos, J.F., Madabhusi-Raman, P., Qiao, P., (1997), "Characterization of Mode-I Fracture of Hybrid Material Interface Bonds By Contoured DCB Specimens", Engineering Fracture Mechanics, 58(3), 173-192.

Davidson, B. D., Kruger, R., Konig, M., (1996), “Effect of Stacking Sequence on Energy Release Rate Distributions in Multidirectional DCB and ENF Specimens”, Engineering Fracture Mechanics, Vol. 55, No. 4, 1996, 557-569.

Devalapura, R.K., Greenwood, M.E., Gauchel, J.V., Humphrey, T.J., (1998), “Evaluation of GFRP Performance Using Accelerated Test Methods”, Durability of Fiber Reinforced Polymer (FRP) Composites for Construction: Proceedings of the First International Conference (CDCC’98), Sherbrooke (Quebec), Canada, August 5-7, 1998, 107-116.

Dewimille, B., Bunsell, A.R., (1983), “Accelerated ageing of a glass fibre-reinforced epoxyresin in water”, Composites, January 1983, 35-40.

Elewele, R., River, B.H., and Koutsky, J.A., "Tapered Double Cantilever Beam Fracture Tests of Phenolic-Wood Adhesive Joints," Wood and Fiber, 1979, 11(3), pp.197-213.

Fonselius, M., Riipola, K. (1992), “Determination of Fracture Toughness for Wood”, Journal of Structural Engineering, Vol. 118, No. 7, July, 1992, 1727-1740.

Gallagher, J. P. (1971), “Experimentally Determined Stress Intensity Factors for Several Contoured Double Cantilevered Beam Specimens”, Engineering Fracture Mechanics, Vol. 3, 1971, 27-43.

GangaRao, H. V. S. (1997), “Sawn and Laminated Wood Beams Wrapped with Fiber Reinforced Plastic Composites”, Wood Design Focus, Fall 1997, 13-18.

Gardner, D.J., Davalos, J.F., Munipalle, U.M. (1994),”Adhesive Bonding of Pultruded Fiber-Reinforced Plastic to Wood”, Forest Products Journal, 44(5), 62-66.

Ghasemzadeh, S., Kajorncheappunngam, S., Gupta, R.K., Gangarao, H. V.S., (1998), “Durability of Glass-Epoxy-Wood Hybrid Composites For Rehabilitation of Railroad Crossties”, Durability of Fiber Reinforced Polymer (FRP) Composites for Construction: Proceedings of the First International Conference (CDCC’98), Sherbrooke (Quebec), Canada, August 5-7, 1998, 81-93..

“Inspection Manual: For Structural Glued Laminated Timber”, AITC 200-92, American Institute of Timber Construction, Englewood, CO, 1996.

Janowiak, J.J., Manbeck, H.B., Blankenhorn, P.R., Kessler, Kevin R. (1992), “Strength Properties of Exterior Adhesives on Preservative-Treated Hardwoods”, Forest Products Journal, 42(10), 68-76.

Kshirsagar, S., Lopez-Anido, R., Gupta, R.K., (1998), “Durability of Fiber-Reinforced Composite Wrapping For The Rehabilitation of Concrete Piers”, Durability of Fiber Reinforced Polymer (FRP) Composites for Construction: Proceedings of the First International Conference (CDCC’98), Sherbrooke (Quebec), Canada, August 5-7, 1998, 117-128.

Marcus, H. L. and Sih, G.C. (1969), “A Crackline-Loaded Edge-Crack Stress Corrosion Specimen”, Engineering Fracture Mechanics, 1971, Vol 3, 453-461.

Martin, R.H., (1997), “Delamination Characterization of Woven Glass/Polyester Composites”, Journal of Composites Technology & Research, JCTRER, Vol. 19, No. 1, 1997, 20-28.

Mostovoy, S., Crosley, P.B., Ripling, E.J., (1967), “Use of Crack-Lined-Loaded Specimens for Measuring Plane-Strain Fracture Toughness”, Journal of Materials, 2(3), September 1967, 661-681.

Nanni, A., Bakis, C.E., Mathew, J.A., (1998), “Acceleration of FRP Bond Degradation”, Durability of Fiber Reinforced Polymer (FRP) Composites for Construction: Proceedings of the First International Conference (CDCC’98), Sherbrooke (Quebec), Canada, August 5-7, 1998, 45-56.

Okkonen, E.A. and River, B.H. (1988), “Factors Affecting the Strength of Block-Shear Specimens”, Forest Products Journal, 39(1), 43-50.
Penado, F. E. (1993), “A Closed Form Solution for the Energy Release Rate of the Double Cantilever Beam Specimen with an Adhesive Layer”, Journal of Composite Materials, Vol. 27, No. 4, 1993, 383-407.

Ozdil, F., Carlsson, L. A., (1999), “Beam Analysis of angle-ply laminate DCB Specimens”, Composites Science and Technology, 59, 1999, 305-315.

"Penacolite Adhesive G-1131", Technical Bulletin, Indspec Chemical Corporation, Pittsburgh, PA, 1989.

Penado, F.E., (1993), “A closed form solution for the energy release rate of the double cantilever beam specimen with an adhesive layer”, Journal of Composite Materials, 27(4), 1993, 383-407.

Prokopski, G. (1996), “Influence of Moisture Content on Fracture Toughness of Wood”, International Journal of Fracture 79, R73-R77.

River, B.H., Okkonen, E.A., (1993), “Contoured Wood Double Cantilever Beam Specimen for Adhesive Joint Fracture Tests”, Journal of Testing and Evaluation, JTEVA, 21(1), January 1993, 21-28.

Russell, A.J., "Factors Affecting the Opening Mode Delamination of Graphite/Epoxy Laminates," DREP Materials Report 82-Q, Victoria, B.C., Canada, 1982.

Russell, A.J., Street, K.N., (1985), “Moisture and Temperature Effects on the Mixed-Mode Delamination Fracture of Unidirectional Graphite/Epoxy”, Delamination and Debonding of Materials, ASTM STP 876, American Society for Testing and Materials, Philadelphia, PA, 1985, 349-370.

Scott, T., River, B.H., Koutsky, J.A., (1991), “Fracture Testing Wood Adhesives with Composite Cantilever Beams”, Journal of Testing and Evaluation, JTEVA, 20(4), July 1992, 259-264.

Sellers Jr., T. and Miller Jr., G.D. (1997), “Evaluations of Three Adhesive Systems for CCA-Treated Lumber”, Forest Products Journal, 47(10), 73-76.

Soltis, L.A. and Rammer, D.R., "Shear Strength of Unchecked Glued-Laminated Beams," Forest Products Journal, Vol. 44, No.1, 1994, pp.51-57.

Soudki, K.A., Zeng, J.S., Meise, B., Sherwood, E.G., (1998), “Durability of Repaired Concrete Beams With Carbon Fibre Reinforced Polymer Laminates Subjected To Wet/Dry Cycles”, Durability of Fiber Reinforced Polymer (FRP) Composites for Construction: Proceedings of the First International Conference (CDCC’98), Sherbrooke (Quebec), Canada, August 5-7, 1998, 499-512.

Vick, C.B. (1996), “Hydroxymethylated Resorcinol Coupling Agent for Enhanced Adhesion of Epoxy and Other Thermosetting Adhesives to Wood”, Proceedings of the 1996 symposium by U.S. Department of Agriculture Forest Service, Forest Products Laboratory and the Forest Products Society, Portland, OR, June 29-30, 1995, 47-55.

APPENDIX A

Maple Code for Simplified Design of Contoured Portion of CDCB Specimen: Solve for Slope of the Contour

```
# MAPLE CODE: Design of Contoured Portion by Rayleigh-Ritz CDCB

restart;

with(linalg);

# 'ii' represtents the total number of algebraic functions used in the
#displacement vector, a quadratic function is used

ii:=2;
SF:=vector(ii);
VI:=vector(2*ii);
RR:=vector(2*ii);
AA:=matrix(ii,ii);
BB:=matrix(ii,ii);
CC:=matrix(ii,ii);
KI:=matrix(2*ii,2*ii);

#material and geometric parameters
#material property definition:  the first letter stands for the type of material property
#the second letter denotes the portion of the cross-section. (b- for base, c- contour)

Ec:=1311000.0;
Gc:=85015.0;
Eb:=4410000.0;
Gb:=650000.0;
Bb:=1.375;
scf:=0.83333;
hb:=0.1000;
mr:=Eb/Ec;

# Define the initial height of contoured portion

h0:=0.5150;

for j1 from 1 to ii do
for j2 from 1 to ii do
```

```
AA[j1, j2]:=0.0;
BB[j1,j2]:=0.0;
CC[j1,j2]:=0.0;

od;
od;

print(AA);
print(BB);
print(CC);

# define crack lengths
# the final position of the crack length is a variable.  'll' is not a constant
# definition of approximating functions

for j from 1 to ii do

SF[j]:=(a-x)^j;

od;

print(SF);
vdisp:=0;

for j from 1 to ii do

vdisp:=vdisp+SF[j]*VI[j+ii];

od;

print(vdisp);

# LOOP FOR DIFFERENT CRACK LENGTHS
# contour definition: a linear tapered contour with slope k

hc:=h0+k*x;
De:=Bb*Ec/12*(3*mr*hb*hc*(hc+hb)^2/(hc+mr*hb)+hc^3+mr*hb^3);
Fs:=Bb*scf*(Gb*hb+Gc*hc);

for j1 from 1 to ii do
for j2 from 1 to ii do


A1ij:=int(simplify(De*diff(SF[j1],x)*diff(SF[j2],x)),x=0..a);
A2ij:=int(simplify(Fs*SF[j1]*diff(SF[j2],x)),x=0..a);
```

```
A3ij:=int(simplify(Fs*SF[j1]*SF[j2]),x=0..a);
A4ij:=int(simplify(Fs*diff(SF[j1],x)*diff(SF[j2],x)),x=0..a);

AA[j1,j2]:=AA[j1,j2]+A1ij+A3ij;
BB[j1,j2]:=BB[j1,j2]+A2ij;
CC[j1,j2]:=CC[j1,j2]+A4ij;

od;
od;

x:=0;

for j1 from 1 to ii do

RR[j1]:=0;
RR[j1+ii]:=SF[j1];

od;

x:='x';

for j1 from 1 to ii do
for j2 from 1 to ii do

KI[j1,j2]:=AA[j1,j2];
KI[j1,j2+ii]:=-BB[j1,j2];
KI[j1+ii,j2]:=-BB[j2,j1];
KI[j1+ii,j2+ii]:=CC[j1,j2];

od;
od;

print(KI);

VI:=multiply(inverse(KI),RR);

# Displacement at x=0 for a unit tip-load is same as the Compliance of the canilever
# beam

x:=0;
CP:=vdisp;
CP:=collect(CP,a);

#d(C)/da

dCda:=diff(CP,a);
```

```
dcnum:=collect(numer(dCda),a);
dcdnm:=collect(denom(dCda),a);

# define the numerical value of ll.  'll'=CL, to compute dC/da at x=a

a:=8.0;

# the numerical value used in the next statement is the constant value of dC/da, K,
# assumed in the design procedure.  'K' should be equal to one half the actual valie,
# since the design is obtained for one half of the CDCB specimen

dcda:=dcnum/dcdnm-0.0000625;

# dcda is a function of the slope and the crack length
# for every given crack length, we can solve a linear slope value

const:=fsolve(dcda=0,k,k=0.0..0.30);

# The end
```

APPENDIX B

Maple Code for the Design of Contoured Portion of CDCB Specimen: Solve for *dC/da* of a Linear Tapered Contour

```
# MAPLE CODE: Design of Contoured Portion by Rayleigh-Ritz CDCB

restart;

with(linalg);

# 'ii' represtents the total number of algebraic functions used in the displacement vector,
# a quadratic function is used

ii:=2;
SF:=vector(ii);
VI:=vector(2*ii);
RR:=vector(2*ii);
AA:=matrix(ii,ii);
BB:=matrix(ii,ii);
CC:=matrix(ii,ii);
KI:=matrix(2*ii,2*ii);

#material and geometric parameters
#material property definition:  the first letter stands for the type of material property
#the second letter denotes the portion of the cross-section. (b- for base, c- contour)

Ec:=1221100;
Gc:=28700.0;
Eb:=1311200.0;
Gb:=85000.0;
Bb:=1.250;
scf:=0.83333;
hb:=0.1875;
mr:=Eb/Ec;

#  Define a initial height for con tour portion, h0
# Input the slope of a linear tapered contour, k

h0:=0.5150;
k:=0.1764070805;

for j1 from 1 to ii do
```

```
for j2 from 1 to ii do

AA[j1, j2]:=0.0;
BB[j1,j2]:=0.0;
CC[j1,j2]:=0.0;

od;
od;

print(AA);
print(BB);
print(CC);

# define crack lengths
# the final position of the crack length is a variable.  'll' is not a constant
# definition of approximating functions

for j from 1 to ii do

SF[j]:=(a-x)^j;

od;

print(SF);
vdisp:=0;
for j from 1 to ii do

vdisp:=vdisp+SF[j]*VI[j+ii];

od;

print(vdisp);

# LOOP FOR DIFFERENT CRACK LENGTHS
# contour definition in which the contour is in a linear function

hc:=h0+k*x;
De:=Bb*Ec/12*(3*mr*hb*hc*(hc+hb)^2/(hc+mr*hb)+hc^3+mr*hb^3);
Fs:=Bb*scf*(Gb*hb+Gc*hc);

for j1 from 1 to ii do
for j2 from 1 to ii do

A1ij:=int(simplify(De*diff(SF[j1],x)*diff(SF[j2],x)),x=0..a);
A2ij:=int(simplify(Fs*SF[j1]*diff(SF[j2],x)),x=0..a);
A3ij:=int(simplify(Fs*SF[j1]*SF[j2]),x=0..a);
```

```
A4ij:=int(simplify(Fs*diff(SF[j1],x)*diff(SF[j2],x)),x=0..a);

AA[j1,j2]:=AA[j1,j2]+A1ij+A3ij;
BB[j1,j2]:=BB[j1,j2]+A2ij;
CC[j1,j2]:=CC[j1,j2]+A4ij;

od;
od;

x:=0;
for j1 from 1 to ii do

RR[j1]:=0;
RR[j1+ii]:=SF[j1];

od;
x:='x';

for j1 from 1 to ii do
for j2 from 1 to ii do

KI[j1,j2]:=AA[j1,j2];
KI[j1,j2+ii]:=-BB[j1,j2];
KI[j1+ii,j2]:=-BB[j2,j1];
KI[j1+ii,j2+ii]:=CC[j1,j2];

od;
od;

print(KI);
VI:=multiply(inverse(KI),RR);

# Displacement at x=0 for a unit tip-load is same as the Compliance of the canilever beam

x:=0;
CP:=vdisp;
CP:=collect(CP,a);

#d(C)/da

dCda:=diff(CP,a);

dcnum:=collect(numer(dCda),a);
dcdnm:=collect(denom(dCda),a);

# dCda is a function in terms of crack length (a) and linear slope (k)
```

```
# For a given linear slope and a crack length, dCda can be determined.

a:=12.0;

# The numerical value of dCda

print(dCda);

# The end!
```

VITA

Brent Stephen Trimble was born on July 9, 1974 in Parkersburg, West Virginia. He was raised in northwest West Virginia and graduated from Parkersburg South High School in May 1992. He earned his Bachelor of Science in Civil Engineering from West Virginia University in May 1997 and passed the Fundamentals of Engineering Exam in the Spring of 1998. He joined the graduate program in Structural Engineering at West Virginia University in May 1997 as a Graduate Teaching Assistant of Structural Analysis I (CE 161); he expects to complete his Master of Science degree in Civil Engineering in August 1999. He is a member of the following organizations: American Society of Civil Engineers (ASCE), Tau Beta Pi, and Chi Epsilon.